

KNOOP, JAMES EUGENE, M.S. Synthesis of Novel Lanthanide Paramagnetic Ionic Liquids. (2019)
Directed by Dr. Daniel J. C. Herr. 95 pp.

Room temperature ionic liquids (RTILs) are bulky and asymmetric organic salts, such as those presented in this work in the form, 1-alkyl-3-methylimidazolium. Typically, RTIL refers to those salts whose melting point is below 100 °C. RTILs can be paired with a wide range of anions, from simple halides to inorganic anions such as hexafluorophosphate, large organic anions like triflates or tosylates, or as in this work, we demonstrate a more exotic anion pairing, to lanthanide-based anions that induce a strong paramagnetic susceptibility to the ionic liquid.

Ionic liquids (ILs) have been used for battery electrolytes, cellulose solvents, prepolymer monomers, and have been identified as potential candidates for carbon dioxide absorption. Ionic liquids have many advantages for these applications due to their high thermal stability, low vapor pressure, and practically infinite tunable chemistry. This thesis is inspired by a NASA call to investigate ionic liquids to replace silica gel/zeolite mixtures currently used in their atmosphere revitalization system. We have proposed an application taking advantage of magnetocaloric pumping. However, to pump ILs using an applied magnetic field, the ionic liquids must be paramagnetic.

This thesis communicates the synthesis, and characterization of a series of novel paramagnetic ionic liquids paired with lanthanide-based ($M = \text{Dy}, \text{Gd}, \text{Ho}$) metal halide anions. The thermal, physical, and magnetic properties of these new magnetically susceptible imidazolium-based ionic liquids are characterized by FTIR spectroscopy, NMR spectroscopy, thermogravimetric analysis, elemental analysis, and Evan's NMR method.

SYNTHESIS OF NOVEL LANTHANIDE
PARAMAGNETIC IONIC LIQUIDS

by

James Eugene Knoop

A Thesis Submitted to
the Faculty of The Graduate School at
The University of North Carolina at Greensboro
in Partial Fulfillment
of the Requirements for the Degree
Master of Science

Greensboro
2019

Approved by

Dr. Daniel J. C. Herr
Committee Chair

©2019 James Eugene Knoop

To my loving and nurturing parents, born John Harlan Knoop Jr. and Rita Marie Kaokula. I am forever grateful for everything you have provided for me and the wisdom I have received from you both. To my brother-from-another-mother, Michael Patrick Harper. I will be forever thankful for the impact you had in my life as a great friend. May you rest in heavenly peace.

ACKNOWLEDGMENTS

I would like to acknowledge my committee members Dr. Jeffrey R. Alston, Dr. Dennis LaJeunesse, and Dr. Daniel J. C. Herr for their guidance and insight during the duration of my master's project. This work was supported by an Early Career Faculty grant from NASA's Space Technology Research Grants Program (80NSSC18K1513).

TABLE OF CONTENTS

	Page
LIST OF TABLES	vii
LIST OF FIGURES	viii
LIST OF ABBREVIATIONS.....	xii
 CHAPTER	
I. INTRODUCTION	1
1.1. Ionic Liquids	1
1.2. Ionic Liquids and CO ₂ Adsorption	3
1.3. Paramagnetic Ionic Liquids	5
1.4. Project Goals.....	6
1.5. Magnetism.....	8
 II. EXPERIMENTAL.....	 12
2.1. General Considerations.....	12
2.2. Synthesis of [R _n C ₁ Im][Cl]	12
2.2.1. Synthesis of [BmIm][Cl]	12
2.2.2. Synthesis of [HmIm][Cl].....	13
2.2.3. Synthesis of [OmIm][Cl].....	13
2.3. Synthesis of [R _n C ₁ Im][Br]	13
2.3.1. Synthesis of [BmIm][Br].....	13
2.3.2. Synthesis of [HmIm][Br].....	14
2.3.3. Synthesis of [OmIm][Br].....	14
2.4. Synthesis of [R _n C ₁ Im][MXCl ₃].....	14
2.4.1. Synthesis of [BmIm][FeBrCl ₃].....	14
2.4.2. Synthesis of [HmIm][FeBrCl ₃]	15
2.4.3. Synthesis of [OmIm][FeBrCl ₃]	15
2.4.4. Synthesis of [BmIm][DyBrCl ₃].....	15
2.4.5. Synthesis of [HmIm][DyBrCl ₃].....	16
2.4.6. Synthesis of [OmIm][DyBrCl ₃].....	16
2.4.7. Synthesis of [BmIm][GdBrCl ₃].....	16
2.4.8. Synthesis of [HmIm][GdBrCl ₃]	16
2.4.9. Synthesis of [OmIm][GdBrCl ₃].....	17
2.4.10. Synthesis of [BmIm][HoBrCl ₃].....	17
2.4.11. Synthesis of [HmIm][HoBrCl ₃].....	17

2.4.12. Synthesis of [OMIm][HoBrCl ₃]	17
2.5. Synthesis of [R _n C ₁ Im][MCl ₄]	18
2.5.1. Synthesis of [BmIm][FeCl ₄]	18
2.5.2. Synthesis of [HmIm][FeCl ₄]	19
2.5.3. Synthesis of [OMIm][FeCl ₄]	19
2.5.4. Synthesis of [BmIm][DyCl ₄]	19
2.5.5. Synthesis of [HmIm][DyCl ₄]	19
2.5.6. Synthesis of [OMIm][DyCl ₄]	20
2.5.7. Synthesis of [BmIm][GdCl ₄]	20
2.5.8. Synthesis of [HmIm][GdCl ₄]	20
2.5.9. Synthesis of [OMIm][GdCl ₄]	21
2.5.10. Synthesis of [BmIm][HoCl ₄]	21
2.5.11. Synthesis of [HmIm][HoCl ₄]	21
2.5.12. Synthesis of [OMIm][HoCl ₄]	21
III. DATA AND RESULTS	22
3.1. FTIR Data	22
3.1.1. 1-Alkyl-3-Methylimidazolium Halides	22
3.1.2. Paramagnetic Ionic Liquids	25
3.2. TGA Data	37
3.2.1. 1-Alkyl-3-Methylimidazolium Halides	38
3.2.2. Paramagnetic Ionic Liquids	39
3.3. NMR Data	42
3.4. Magnetic Susceptibility Data	49
IV. DISCUSSION AND CONCLUSION	63
4.1. Discussion	63
4.1.1. FTIR	63
4.1.2. TGA	64
4.1.3. NMR	65
4.1.4. Evan's Method	68
4.2. Conclusion	72
4.3. Future Work	74
REFERENCES	75

LIST OF TABLES

	Page
Table 1. 1-Alkyl-3-Methylimidazolium Halide 5 wt% Thermal Degradation38 Temperatures.	38
Table 2. Iron-Based PILs 5 wt% Thermal Degradation Temperatures39	39
Table 3. Dysprosium-Based PILs 5 wt% Thermal Degradation Temperatures.....40	40
Table 4. Holmium-Based PILs 5 wt% Thermal Degradation Temperatures.....41	41
Table 5. Gadolinium-Based PILs 5 wt% Thermal Degradation Temperatures42	42
Table 6. Magnetic Susceptibility Data of all PILs62	62
Table 7. Moles of Hydrate in Lanthanide PILs.....65	65
Table 8. Summary of PILs Physical Properties73	73

LIST OF FIGURES

	Page
Figure 1. Schematic of 1-Alkyl-3-Methylimidazolium Halide Synthesis	7
Figure 2. Schematic of PILs Synthesis	8
Figure 3. A Magnetic Clutch Supports a 117 lb. Woman.....	9
Figure 4. FTIR Spectra of [BMIm][Cl]	22
Figure 5. FTIR Spectra of [HMIm][Cl]	23
Figure 6. FTIR Spectra of [OMIm][Cl]	23
Figure 7. FTIR Spectra of [BMIm][Br]	24
Figure 8. FTIR Spectra of [HMIm][Br].....	24
Figure 9. FTIR Spectra of [OMIm][Br].....	25
Figure 10. FTIR Spectra of [BMIm][FeCl ₄].....	25
Figure 11. FTIR Spectra of [HMIm][FeCl ₄].....	26
Figure 12. FTIR Spectra of [OMIm][FeCl ₄].....	26
Figure 13. FTIR Spectra of [BMIm][FeBrCl ₃].....	27
Figure 14. FTIR Spectra of [HMIm][FeBrCl ₃].....	27
Figure 15. FTIR Spectra of [OMIm][FeBrCl ₃].....	28
Figure 16. FTIR Spectra of [BMIm][DyCl ₄]	28
Figure 17. FTIR Spectra of [HMIm][DyCl ₄]	29
Figure 18. FTIR Spectra of [OMIm][DyCl ₄]	29
Figure 19. FTIR Spectra of [BMIm][DyBrCl ₃]	30
Figure 20. FTIR Spectra of [HMIm][DyBrCl ₃].....	30

Figure 21. FTIR Spectra of [OMIm][DyBrCl ₃]	31
Figure 22. FTIR Spectra of [BMIm][HoCl ₄]	31
Figure 23. FTIR Spectra of [HMIm][HoCl ₄]	32
Figure 24. FTIR Spectra of [OMIm][HoCl ₄]	32
Figure 25. FTIR Spectra of [BMIm][HoBrCl ₃]	33
Figure 26. FTIR Spectra of [HMIm][HoBrCl ₃]	33
Figure 27. FTIR Spectra of [OMIm][HoBrCl ₃]	34
Figure 28. FTIR Spectra of [BMIm][GdCl ₄]	34
Figure 29. FTIR Spectra of [HMIm][GdCl ₄]	35
Figure 30. FTIR Spectra of [OMIm][GdCl ₄]	35
Figure 31. FTIR Spectra of [BMIm][GdBrCl ₃]	36
Figure 32. FTIR Spectra of [HMIm][GdBrCl ₃]	36
Figure 33. FTIR Spectra of [OMIm][GdBrCl ₃]	37
Figure 34. Thermal Curves of 1-Alkyl-3-Methylimidazolium Halide ILs	38
Figure 35. Thermal Curves of Iron-Based PILs	39
Figure 36. Thermal Curves of Dysprosium-Based PILs	40
Figure 37. Thermal Curves of Holmium-Based PILs	41
Figure 38. Thermal Curves of Gadolinium-Based PILs	42
Figure 39. ¹ H NMR Spectra of [BMIm][Cl]	43
Figure 40. ¹³ C NMR Spectra of [BMIm][Cl]	43
Figure 41. ¹ H NMR Spectra of [HMIm][Cl]	44
Figure 42. ¹³ C NMR Spectra of [HMIm][Cl]	44

Figure 43. ^1H NMR Spectra of [OMIm][Cl]	45
Figure 44. ^{13}C NMR Spectra of [OMIm][Cl]	45
Figure 45. ^1H NMR Spectra of [BMIm][Br]	46
Figure 46. ^{13}C NMR Spectra of [BMIm][Br]	46
Figure 47. ^1H NMR Spectra of [HMIm][Br]	47
Figure 48. ^{13}C NMR Spectra of [HMIm][Br]	47
Figure 49. ^1H NMR Spectra of [OMIm][Br]	48
Figure 50. ^{13}C NMR Spectra of [OMIm][Br]	48
Figure 51. ^1H NMR Spectra of [BMIm][FeCl ₄] Standard	49
Figure 52. ^1H NMR Spectra of [BMIm][FeCl ₄]	50
Figure 53. ^1H NMR Spectra of [HMIm][FeCl ₄]	50
Figure 54. ^1H NMR Spectra of [OMIm][FeCl ₄]	51
Figure 55. ^1H NMR Spectra of [BMIm][FeBrCl ₃]	51
Figure 56. ^1H NMR Spectra of [HMIm][FeBrCl ₃]	52
Figure 57. ^1H NMR Spectra of [OMIm][FeBrCl ₃]	52
Figure 58. ^1H NMR Spectra of [BMIm][DyCl ₄]	53
Figure 59. ^1H NMR Spectra of [HMIm][DyCl ₄]	53
Figure 60. ^1H NMR Spectra of [OMIm][DyCl ₄]	54
Figure 61. ^1H NMR Spectra of [BMIm][DyBrCl ₃]	54
Figure 62. ^1H NMR Spectra of [HMIm][DyBrCl ₃]	55
Figure 63. ^1H NMR Spectra of [OMIm][DyBrCl ₃]	55
Figure 64. ^1H NMR Spectra of [BMIm][HoCl ₄]	56

Figure 65. ^1H NMR Spectra of [HMIm][HoCl ₄]	56
Figure 66. ^1H NMR Spectra of [OMIm][HoCl ₄]	57
Figure 67. ^1H NMR Spectra of [BMIm][HoBrCl ₃]	57
Figure 68. ^1H NMR Spectra of [HMIm][HoBrCl ₃]	58
Figure 69. ^1H NMR Spectra of [OMIm][HoBrCl ₃]	58
Figure 70. ^1H NMR Spectra of [BMIm][GdCl ₄]	59
Figure 71. ^1H NMR Spectra of [HMIm][GdCl ₄]	59
Figure 72. ^1H NMR Spectra of [OMIm][GdCl ₄]	60
Figure 73. ^1H NMR Spectra of [BMIm][GdBrCl ₃]	60
Figure 74. ^1H NMR Spectra of [HMIm][GdBrCl ₃]	61
Figure 75. ^1H NMR Spectra of [OMIm][GdBrCl ₃]	61
Figure 76. Elucidation of Solvent Chemical Shift: a) [OMIm][HoBrCl ₃] and b) [OMIm][HoBrCl ₃] with 30 μL anhyd.....	70
Figure 77. Molar Magnetic Susceptibility of Tetrachloro-Halide PILs.....	71
Figure 78. Molar Magnetic Susceptibility of Bromotrichloro-Halide PILs	72

LIST OF ABBREVIATIONS

Anhyd.	anhydrous
Calcd.	calculated
CDCl ₃	deuterated chloroform
CO ₂	carbon dioxide
DEA	diethanolamine
DSC	differential scanning calorimetry
EA	elemental analysis
EtAc	ethyl acetate
FTIR	fourier-transform infrared spectroscopy
FPILs	fluorinated paramagnetic ionic liquids
ILs	ionic liquids
N ₂	nitrogen gas
NMR	nuclear magnetic resonance spectroscopy
MCP	magnetocaloric pumping
MeOH	methanol
MDEA	methyl diethanolamine
MEA	monoethanolamine
CD ₃ OD	deuterated methanol
PILs	paramagnetic ionic liquids
ppm	parts per million

TGA	thermogravimetric analysis
TSILs	task-specific ionic liquids
SQUID	superconducting quantum interference device

CHAPTER I

INTRODUCTION

1.1. Ionic Liquids

Ionic liquids are molten organic salts at room temperature with characteristically low vapor pressure and high thermal stability. Typically, they are described as liquid salts with melting points below 100 °C however, this definition is up for debate as there isn't a significant difference in salts which have melting points of 90 and 110 °C, respectively.¹ They have the potential for infinitely tunable properties due to a wide variety of cationic and anionic combinations. In fact, there are about 10^{18} theoretical ionic liquids due to available chemistry and were coined designer solvents by Michael Freemantle in 1998.^{2,3}

The first ionic liquid, ethylammonium nitrate (m.p. = 12 °C), was discovered by Paul Walden in 1914 while searching for low melting point salts with electrical conductivity.⁴ Despite a few patents in 1934 and 1948 in relation to electroplating, the potential applications of ionic liquids did not become recognized until the 1980s.⁵⁻⁷ This may be attributed to the lack of quickly accessible information that many of us are accustomed to today. Nonetheless, ionic liquids found an early niche in electrochemistry and analytical chemistry due to their unique properties. In the 1970s and early 1980s, nitrogen-heterocyclic chloroaluminate ionic liquids were heavily investigated due to their

liquid phase at room temperature.^{8, 9} However, the chloroaluminate ILs were moisture sensitive and readily reactive to other materials. These early works sparked the use of the imidazolium cation in 1982 and are one of the most popular cations used in ionic liquid systems today. Furthermore, the imidazolium ring lowered melting points of ionic liquids compared to the pyridinium ring.⁹ This started a conversation about the ionic interactions of the imidazolium cation on whether a hydrogen bonding mechanism outcompeted with a stacking mechanism between ions.^{10, 11} Hydrogen bonding mainly occurred between the imidazolium ring protons and a strong hydrogen bond acceptor whereas stacking interactions occurred for a larger anion and weak hydrogen bond acceptor.¹²⁻¹⁴

Since the early days, ionic liquids have become a unique and staple discipline in chemistry and materials research. They have found their way into many applications such as gas chromatography or oil refining.^{15, 16} The idea of TSILs was introduced by Jim Davis in 2000. The purpose of these ionic liquids was different than the designer solvents envisioned by Freemantle, in that, covalently bonded functional groups attached to the cations, anions, or both species would exploit the vast combinations of different ionic liquids for a wide range of applications.¹⁷⁻²²

Using TSILs pivoted ILs for future applications involving green and sustainable chemistry. While the idea of ionic liquids as green solvents was routinely emphasized by Ken Seddon and Robin Rogers, there were those who opposed this idea, mainly because the properties of one ionic liquid was not transferable to ionic liquids with different substituents. Instead, Welton proposed them as materials for sustainable production of chemicals in general.

Aside from green solvents, TSILs have been used for enzyme-catalyzed reactions, extraction of lignin from biomass and cellulose dissolution, lubricants for industry, and various organic, inorganic, and materials synthesis.²³⁻²⁶ One highlight is the role they have played in the synthesis of nanostructures.²⁷

Among the applications of TSILs, Blanchard's group discovered an application for separating non-volatile organic solvents by using an ionic liquid and supercritical CO₂ biphasic system.²⁸ More importantly, they demonstrated high solubility of CO₂ in ionic liquids which launched a colossal series of investigations into the application of ionic liquids for CO₂ sequestration.²⁹⁻⁴²

1.2. Ionic Liquids and CO₂ Adsorption

As of May 2019, the concentration of CO₂ in the atmosphere has reached 415 ppm. The global consensus is that rising levels of CO₂ are causing temperatures around the planet to increase and many governments are taking precautionary measures to reduce CO₂ emissions from anthropogenic sources. The main source of CO₂ emission is due to power plants fueled by the combustion of fossil fuels. To capture CO₂ from industrial waste, SOA amine-based solvents are used.

Primary, secondary, or tertiary amine solvents such as MEA, DEA or MDEA, respectively, are used to capture CO₂ from post-combustion flue gas. However, this SOA technology has many pitfalls such as high corrosiveness, high volatility, and high energy of regeneration. Alternatives, like ionic liquids, could fill the pitfalls in the current technology. During the post-combustion carbon dioxide capture process, the formation of a carbamate zwitterion is formed between CO₂ and the primary or secondary amine.⁴³ The

formation of the carbamate is highly favorable due to a large enthalpy of reaction and requires a large input of energy in the form of heat to regenerate. Moreover, due to the volatility of these solvents, ~30% of the solvent is lost due to evaporation during the regeneration process, increasing the overall process cost.⁴⁴ Furthermore, the operating temperature in these systems is usually restricted to 80-120 °C to prevent solvent evaporation.⁴⁴ The most common solvents used are MEA and DEA due to their reactivity, but they suffer from low adsorption capacities (2 mol amine:1 mol CO₂). To increase the adsorption capacity, MDEA is used and adsorbs CO₂ through base-catalyzed hydration due to a lack of hydrogen on the amine functional groups. Piperazine is added to improve the reactivity and adsorption capacity of MDEA with CO₂ as well as thermal and oxidative stability.⁴⁵

Since the Brennecke group's discovery in 1999, ionic liquids have been identified as a primary alternative to replace SOA amine-based solvents due to high CO₂ solubility and selectivity. Moreover, their inherent properties like low volatility and high thermal stability make them ideal for harsh industrial conditions. Furthermore, depending on the molecular structure and functional groups, ionic liquids have the potential for increased solubility and selectivity of CO₂ over other gases. In fact, a computational investigation has shown a decrease in total energy consumption of ~44% and ~60% for a single-stage and multi-stage CO₂ sequestration process using an ionic liquid compared to MDEA.³¹

To facilitate market penetration of ILs for future CO₂ sequestration technology, there are a few factors that should be addressed, namely: 1) solubility mechanisms of CO₂ in ILs; 2) experimental data and trends regarding CO₂ solubility, selectivity, and diffusivity

in ILs; 3) recent advances of different ionic liquid materials; and 4) structure-property relationships that incorporate real-world factors affecting CO₂ solubility.

Furthermore, there are two main mechanisms for CO₂ adsorption in ILs: physisorption and chemisorption. Physisorption is the weak physical attraction, due to van der Waal forces, between two chemical species; in this case, CO₂ is weakly attracted to the surface interface of ILs and dissolves into them. Chemisorption is the process of adsorption via a chemical reaction with the formation of a covalent bond between chemical species; for instance, CO₂ may form a covalent bond with amine-functionalized ILs to form a carbamate species. In addition, ILs which chemisorb CO₂ is most beneficial in environments with a low partial pressure of CO₂ such as post-combustion flue gas while ILs which physisorb CO₂ are most beneficial in environments with high partial pressures of CO₂ such as the international space station.

1.3. Paramagnetic Ionic Liquids

Paramagnetic ionic liquids are different from ferrofluids and magnetorheological fluids in that they do not contain magnetic nanoparticles or magnetic particles in a carrier fluid. They possess the same characteristics of regular ILs such as high thermal stability, low vapor pressure, and infinite tunability. The first PIL, 1-butyl-3-methylimidazolium tetrachloroferrate(iii), was identified in 2004 by Hayashi *et. al.*^{46,47} Since this period, there have been many reported PILs in literature containing transition and rare-earth metals.⁴⁸⁻⁵³ By far, the most common anion to instill paramagnetism into PILs is the tetrachloroferrate(iii) anion, but other transition metals like cobalt, manganese, copper coordination complexes and rare-earth metals like dysprosium and gadolinium

coordination complexes have been used. The tetrachloroferrate(iii) anion is usually coupled with common IL cations like nitrogen-heterocyclic aromatic rings including imidazolium, pyridinium, pyrrolidinium and quaternary ammonium cations. Moreover, there are few reports of organic non-metal PILs.^{54, 55} Currently, PILs have been widely applied in analytical chemistry as extraction media by use of an external magnet but they have demonstrated success in other applications such as catalysis, templated self-assembly of polymers, cellulose dissolution, and density measurements.⁵⁶⁻⁶³ To implement PILs into broader applications they should be tuned to have high magnetic susceptibility, high hydrophobicity, high thermal stability, and low viscosity.

1.4. Project Goals

The goal of this project is the first part of a three-part process which makes up a grant funded by NASA with the focus to investigate ionic liquids to replace current atmospheric revitalization systems in manned spacecraft. My goal was to synthesize and identify ILs with a good capability of adsorbing carbon dioxide. Next, I would tailor a series of ILs with paramagnetism to form PILs. Using PILs, we may manipulate them in a microgravity environment by taking advantage of a phenomenon called magnetocaloric pumping. Discovered by NASA in the late 1970s by Brown, MCP is a useful phenomenon that allows one to control the movement of paramagnetic fluids without the use of pumps and motors but with a temperature-gradient. The need for this project is based on the low-reliability of the current SOA silica-gel/zeolite technology, which has been used by NASA for decades. Current SOA technology is costly, non-recyclable, presents a potential hazard to electronic equipment/instruments, and long-term human safety in

manned spacecraft by dust generation. Ultimately, the project end goal would result in a new disruptive technology for CO₂ sequestration in space that incorporates a recyclable, robust, and energy-negative system. To achieve this goal, ILs with the ability to absorb carbon dioxide efficiently needed to be identified.

Alkylimidazolium-based ILs are well-known in the literature to selectively adsorb carbon dioxide over other gases such as nitrogen, oxygen, carbon monoxide, hydrogen, and methane. As such, they represented an ideal candidate for this investigation. Alkylimidazolium halide ILs of varying saturated alkyl chains and halide groups were synthesized and characterized.

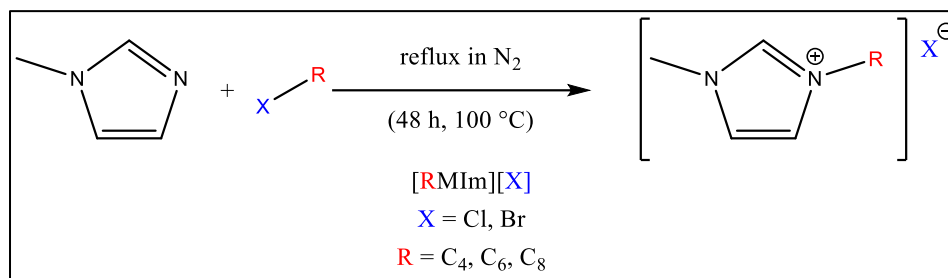


Figure 1. Schematic of 1-Alkyl-3-Methylimidazolium Halide Synthesis

To induce paramagnetic properties into these ionic liquids, lanthanide metal trihalides containing dysprosium, gadolinium, and holmium were used. A series of six PILs were synthesized from 1-alkyl-3-methylimidazolium halides and iron(iii) trichloride hexahydrate as a control. The iron-based imidazolium PILs are known in literature and the molar magnetic susceptibilities of a few have been previously reported.

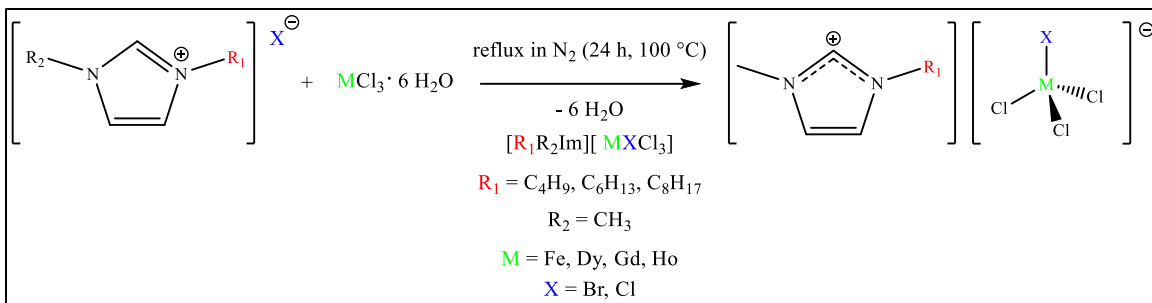


Figure 2. Schematic of PILs Synthesis.

The comparison of the iron-based PILs and dysprosium-based, holmium-based, and gadolinium-based PILs molar magnetic susceptibilities were of main interest. Lanthanide metals in the +3 oxidation state are known to exhibit high magnetic susceptibilities in comparison with transition metal complexes. However, ILs or PILs containing lanthanide metals are scarcely reported. The synthesis of 18 novel PILs containing dysprosium, holmium, and gadolinium was carried out and their molar magnetic susceptibilities determined. We compared these to the six iron-based PILs to determine any advantages of using lanthanide metals to incorporate paramagnetic properties into ILs.

1.5. Magnetism

Humans have observed magnetism in materials since ancient times but until very recently there weren't any definite explanations as to why a material may be magnetic and how magnetism is related to chemical structure on the atomic scale. This changed early in the 20th century when Langevin reported his model in 1905 to describe paramagnetic behavior and was shortly followed by Weiss in 1907 whose model predicted the Curie temperature of ferromagnetic materials.

Perhaps one of the first examples reported of using magnetism in an application, Jacob Rabinow describes the ability of an oil and iron particle mixture (9:1) to act as a magnetic clutch when finely divided by some material.⁶⁴ Rabinow demonstrated how conductive plates dipped in the oil/iron particle mixture, that were separated by a finite distance, would experience increased friction parallel to the surface of the two plates under an induced current. Magnetic attraction caused the two plates to strongly bind and stop the material divider from slipping; they demonstrated this application by allowing the magnetic clutch to support a hanging 117 lb. woman.



Figure 3. A Magnetic Clutch Supports a 117 lb. Woman.

Typically, many people think of ferromagnetism when they think of magnetism. Including ferromagnetism, there are four other types of magnetism: 1) ferrimagnetism; 2) antiferromagnetism; 3) diamagnetism; and 4) paramagnetism.

Ferromagnetism is the type of magnetism that fridge magnets exhibit. Unique properties of ferromagnetism include spontaneous magnetization and permanent magnetization when an induced magnetic field is introduced to a ferromagnetic material. Moreover, the magnetic dipoles are largely polarized, and ferromagnetism represents the strongest form of magnetism. When ferromagnetic materials are heated above their specific Curie temperature, they behave like paramagnetic materials. Ferrimagnetism is similar to ferromagnetism with the exception that the domains of magnetic dipoles are antiparallel and of different magnitudes; if the antiparallel magnetic domains were the same magnitude then the material would have no measurable magnetic susceptibility.

Antiferromagnetic materials are uncommon and only have high magnetization near the Neel temperature. Below and above the Neel temperature, antiferromagnetic materials decrease in magnetic susceptibility exponentially. Diamagnetism is the weakest form of magnetism and causes molecules to be repulsed from an induced magnetic field due to paired electrons in the atoms molecular orbital. Every material is diamagnetic but due to weak magnetization kinetic energy of molecules easily overcomes this force and diamagnetism is not observable.

Lastly, paramagnetism is magnetism as a result of unpaired electrons in an atoms molecular orbital. This form of magnetism is weaker than ferromagnetism but stronger than diamagnetism. Paramagnetic materials are weakly attracted to magnetic fields.

Furthermore, the magnetization of paramagnetic materials is inversely proportional to temperature. Paramagnetic materials have a net magnetization of zero above the Curie temperature. This is due to the kinetic energy of molecules overcoming the magnetization force.

CHAPTER II
EXPERIMENTAL

2.1. General Considerations

All solvents and reagents were used as received by the manufacturer. All reactions were performed under an inert atmosphere containing dry nitrogen gas unless otherwise specified. Due to fluctuations from the A/C unit, the laboratory temperature ranged from 19-24 °C. Using the dean-stark distillation flask, 0.4 - 0.8 mL of water were removed via azeotropic distillation. After synthesis, all compounds were stored under vacuum in an amber vacuum desiccator. All NMR solvents were used as received and stored in a refrigerator. Elemental analysis was performed by Atlantic Microlabs, Inc.

2.2. Synthesis of [R_nC₁Im][Cl]

2.2.1. Synthesis of [BMIm][Cl]

To a 250 mL Schlenk flask with a magnetic stir bar, 1-methylimidazolium (8.2137 g, 100.0 mmol) was transferred. 1-chlorobutane (9.2637 g, 100.1 mmol) was added to the light-yellow solution of 1-methylimidazole. A 200 mm Allihn reflux condenser with Teflon sleeve was attached to the 250 mL Schlenk flask and connected to a recirculating chiller (0 °C) containing a 60:40 ratio of propylene glycol and water, respectively. This apparatus was secured with a ring stand and clamp. The condenser was capped with a rubber septum and the chamber was evacuated quickly to remove air. The chamber was refilled with an N₂ atmosphere. Evacuation and refilling were carried out twice. A syringe

needle was poked through the top of the rubber septum and N₂ flowed through the reaction apparatus with positive pressure. The mixture of 1-methylimidazole and 1-chlorobutane was refluxed (48 h, 100 °C). After reflux, the golden solution of 1-butyl-3-methylimidazolium chloride was transferred to a 40 mL scintillation vial and washed four times with ethyl acetate (10 mL) to remove any unreacted product. Excess solvent was removed via rotary evaporation (2 h, 50 °C). The product was further dried by a vacuum line (~0.5 Torr, 3 h, 60 °C) and stored under vacuum in a desiccator. Yield: golden-yellow liquid, 13.3688 g, 76%.

2.2.2. Synthesis of [HMIm][Cl]

The synthesis of [HMIm][Cl] was carried out using a process similar to [BMIm][Cl] using 1-chlorohexane (12.0950 g, 100.3 mmol) and 1-methylimidazole (8.2104 g, 100.0 mmol). Yield: golden-orange liquid, 18.2287 g, 90%.

2.2.3. Synthesis of [OMIm][Cl]

The synthesis of [OMIm][Cl] was carried out using a process similar to [BMIm][Cl] using 1-chlorooctane (14.8763 g, 100.1 mmol) and 1-methylimidazole (8.2212 g, 100.1 mmol). Yield: golden-orange liquid, 21.6045 g, 94%.

2.3. Synthesis of [R_nC₁Im][Br]

2.3.1. Synthesis of [BMIm][Br]

The synthesis of [BMIm][Br] was carried out using a process similar to [BMIm][Cl] using 1-bromobutane (13.7211 g, 100.1 mmol) and 1-methylimidazole (8.2227 g, 100.1 mmol) with the exception of refluxing temperature. This reaction was refluxed at 80 °C. Yield: golden-orange liquid, 20.3392 g, 93%.

2.3.2. Synthesis of [HMIm][Br]

The synthesis of [HMIm][Br] was carried out using a process similar to [BMIm][Br] using 1-bromohexane (16.5135 g, 100.0 mmol) and 1-methylimidazole (8.2343 g, 100.3 mmol). Yield: golden-orange liquid, 24.0178 g, 97%.

2.3.3. Synthesis of [OMIm][Br]

The synthesis of [OMIm][Br] was carried out using a process similar to [BMIm][Cl] using 1-bromooctane (19.3212 g, 100.0 mmol) and 1-methylimidazole (8.2211 g, 100.1 mmol). Yield: golden-orange liquid, 26.5513 g, 96%.

2.4. Synthesis of [R_nC₁Im][MXCl₃]

2.4.1. Synthesis of [BMIm][FeBrCl₃]

To a 250 mL Schlenk flask with a magnetic stir bar in a heating mantle (30 °C), [BMIm][Br] (6.5988 g, 30.12 mmol) and anhyd. methanol (35 mL) was added. Iron(iii) chloride hexahydrate (8.1183 g, 30.03 mmol) and anhyd. toluene (20 mL) was added to the solution. Immediately, a dark-red solution formed. A 10 mL dean-stark distillation flask fitted with a Teflon sleeve and pre-loaded with anhyd. toluene was attached to the 250 mL Schlenk flask. To this, a 200 mm Allihn reflux condenser fitted with a Teflon sleeve and capped with a rubber septum was attached. Hosing from the recirculating chiller (0 °C) was attached to the reflux condenser. The air was evacuated from the apparatus and refilled with N₂ using the Schlenk line. Evacuation and refilling were carried out twice more. A syringe needle was poked through the top of the rubber septum and positive pressure of N₂ was applied throughout the reaction apparatus. The mixture was refluxed (24 h, 86 °C). After refluxing, the excess solvent was removed via rotary evaporation (2 h, 50 °C) and on

a vacuum line (4 h, 100 °C, ~0.5 Torr). The product was transferred to a 40 mL scintillation vial and stored under vacuum in a desiccator. EA Calcd. (%) for [BMIm][FeBrCl₃]: C, 24.80; H, 4.08; N, 7.23; Cl, 27.45; Br, 20.62. Found: C, 25.14; H, 4.01; N, 7.11; Cl, 28.17; Br, 20.88. Yield: Blood-red liquid, 9.2772 g, 63%.

2.4.2. Synthesis of [HMIm][FeBrCl₃]

Synthesis of [HMIm][FeBrCl₃] was carried out using a similar procedure to [BMIm][FeBrCl₃] using 1-hexyl-3-methylimidazolium bromide (7.4199 g, 30.02 mmol) and iron(iii) chloride hexahydrate (8.1100 g, 30.00 mmol). EA Calcd. (%) for [HMIm][FeBrCl₃]: C, 28.54; H, 4.85; N, 6.66; Cl, 25.28; Br, 18.99. Found: C, 28.86; H, 4.78; N, 6.56; Cl, 26.05; Br, 19.04. Yield: blood-red liquid, 10.9977 g, 70%.

2.4.3. Synthesis of [OMIm][FeBrCl₃]

Synthesis of [OMIm][FeBrCl₃] was carried out using a similar procedure to [BMIm][FeBrCl₃] using 1-octyl-3-methylimidazolium bromide (8.2608 g, 30.01mmol) and iron(iii) chloride hexahydrate (8.1099 g, 30.00 mmol). EA Calcd. (%) for [OMIm][FeBrCl₃]: C, 32.52; H, 5.38; N, 6.32; Cl, 24.00; Br, 18.03. Found: C, 32.63; H, 5.41; N, 6.36; Cl, 24.39; Br, 17.75. Yield: blood-red liquid, 12.1188 g, 74%.

2.4.4. Synthesis of [BMIm][DyBrCl₃]

Synthesis of [BMIm][DyBrCl₃] was carried out using a similar procedure to [BMIm][FeBrCl₃] using 1-butyl-3-methylimidazolium bromide (6.6135 g, 30.18 mmol) and dysprosium(iii) chloride hexahydrate (11.3835 g, 30.20 mmol). EA Calcd. (%) for [BMIm][DyBrCl₃]: C, 17.40; H, 4.04; N, 5.07; Cl, 19.26; Br, 14.47. Found: C, 17.71; H, 3.96; N, 4.98; Cl, 19.25; Br, 14.40. Yield: golden-colored liquid, 8.7815 g, 49%.

2.4.5. Synthesis of [HMIm][DyBrCl₃]

Synthesis of [HMIm][DyBrCl₃] was carried out using a similar procedure to [BMIm][FeBrCl₃] using 1-hexyl-3-methylimidazolium bromide (7.4272 g, 30.05 mmol) and dysprosium(iii) chloride hexahydrate (11.4216 g, 30.30 mmol). EA Calcd. (%) for [HMIm][DyBrCl₃]: C, 19.69; H, 4.86; N, 4.59; Cl, 17.44; Br, 13.10. Found: C, 18.96; H, 4.77; N, 4.51; Cl, 17.54; Br, 12.49. Yield: golden-colored liquid, 14.8309 g, 79%.

2.4.6. Synthesis of [OMIm][DyBrCl₃]

Synthesis of [OMIm][DyBrCl₃] was carried out using a similar procedure to [BMIm][FeBrCl₃] using 1-octyl-3-methylimidazolium bromide (8.2565g, 30.00 mmol) and dysprosium(iii) chloride hexahydrate (11.3311 g, 30.06 mmol). EA Calcd. (%) for [OMIm][DyBrCl₃]: unknown. Yield: golden-colored liquid, 21.1952 g, 47%.

2.4.7. Synthesis of [BMIm][GdBrCl₃]

Synthesis of [BMIm][GdBrCl₃] was carried out using a similar procedure to [BMIm][FeBrCl₃] using 1-butyl-3-methylimidazolium bromide (6.5714 g, 29.99 mmol) and gadolinium(iii) chloride hexahydrate (11.2241 g, 30.20 mmol). EA Calcd. (%) for [BMIm][GdBrCl₃]: C, 18.62; H, 3.65; N, 5.43; Cl, 20.61; Br, 15.48. Found: C, 18.66; H, 3.59; N, 5.33; Cl, 20.19; Br, 15.16. Yield: cream-colored liquid, 14.8309 g, 68%.

2.4.8. Synthesis of [HMIm][GdBrCl₃]

Synthesis of [HMIm][GdBrCl₃] was carried out using a similar procedure to [BMIm][FeBrCl₃] using 1-hexyl-3-methylimidazolium bromide (7.4009 g, 29.94 mmol) and gadolinium(iii) chloride hexahydrate (11.6137 g, 31.24 mmol). EA Calcd. (%) for [HMIm][GdBrCl₃]: unknown. Yield: cream-colored liquid, 7.4206 g, 39%.

2.4.9. Synthesis of [OMIm][GdBrCl₃]

Synthesis of [OMIm][GdBrCl₃] was carried out using a similar procedure to [BMIm][FeBrCl₃] using 1-octyl-3-methylimidazolium bromide (8.2638g, 30.03 mmol) and gadolinium(iii) chloride hexahydrate (11.4155 g, 30.71 mmol). EA Calcd. (%) for [OMIm][GdBrCl₃]: C, 22.74; H, 5.33; N, 4.42; Cl, 16.78; Br, 12.61. Found: C, 22.84; H, 5.17; N, 4.29; Cl, 17.56; Br, 11.29. Yield: cream-colored liquid, 3.8958 g, 20%.

2.4.10. Synthesis of [BMIm][HoBrCl₃]

Synthesis of [BMIm][HoBrCl₃] was carried out using a similar procedure to [BMIm][FeBrCl₃] using 1-butyl-3-methylimidazolium bromide (6.5488 g, 29.89 mmol) and holmium(iii) chloride hexahydrate (11.5474 g, 30.44 mmol). EA Calcd. (%) for [BMIm][HoBrCl₃]: C, 17.18; H, 4.08; N, 5.01; Cl, 19.02; Br, 14.29. Found: C, 17.13; H, 3.96; N, 4.86; Cl, 18.94; Br, 13.94. Yield: light-pink liquid, 7.0626 g, 39%.

2.4.11. Synthesis of [HMIm][HoBrCl₃]

Synthesis of [HMIm][HoBrCl₃] was carried out using a similar procedure to [BMIm][FeBrCl₃] using 1-hexyl-3-methylimidazolium bromide (7.3707 g, 29.82 mmol) and holmium(iii) chloride hexahydrate (11.5945 g, 30.56 mmol). EA Calcd. (%) for [HMIm][HoBrCl₃]: unknown. Yield: light-pink liquid, 9.4415 g, 50%.

2.4.12. Synthesis of [OMIm][HoBrCl₃]

Synthesis of [OMIm][HoBrCl₃] was carried out using a similar procedure to [BMIm][FeBrCl₃] using 1-octyl-3-methylimidazolium bromide (8.3044 g, 30.17 mmol) and holmium(iii) chloride hexahydrate (11.6289 g, 30.65 mmol). EA Calcd. (%) for

[OMIm][HoBrCl₃]: C, 22.89; H, 5.16; N, 4.45; Cl, 16.89; Br, 12.69. Found: C, 22.39; H, 4.90; N, 4.23; Cl, 17.74; Br, 10.58. Yield: light-pink liquid, 8.3172 g, 42%.

2.5. Synthesis of [R_nC₁Im][MCl₄]

2.5.1. Synthesis of [BMIm][FeCl₄]

To a 250 mL Schlenk flask with a magnetic stir bar in a heating mantle (30 °C), [BMIm][Cl] (4.9216 g, 28.18 mmol) and anhyd. methanol (35 mL) was added. Iron(iii) chloride hexahydrate (8.1142 g, 30.02 mmol) and anhyd. toluene (20 mL) was added to the solution. Immediately, a dark-brown solution formed. A 10 mL dean-stark distillation flask fitted with a Teflon sleeve and pre-loaded with anhyd. toluene was attached to the 250 mL Schlenk flask. To this, a 200 mm Allihn reflux condenser fitted with a Teflon sleeve and capped with a rubber septum was attached. Hosing from the recirculating chiller (0 °C) was attached to the reflux condenser. The air was evacuated from the apparatus and refilled with N₂ using the Schlenk line. Evacuation and refilling were carried out twice more. A syringe needle was poked through the top of the rubber septum and positive pressure of N₂ was applied throughout the reaction apparatus. The mixture was refluxed (24 h, 86 °C). After refluxing, the excess solvent was removed via rotary evaporation (2 h, 50 °C) and on a vacuum line (4 h, 100 °C, ~0.5 Torr). The product was transferred to a 40 mL scintillation vial and stored under vacuum in a desiccator. EA Calcd. (%) for [BMIm][FeCl₄]: C, 27.80; H, 4.66; N, 8.10; Cl, 41.03. Found: C, 27.46; H, 4.63; N, 8.06; Cl, 40.77. Yield: Dark brown liquid, 9.3034 g, 71%.

2.5.2. Synthesis of [HMIm][FeCl₄]

Synthesis of [HMIm][FeCl₄] was carried out using a similar procedure to [BMIm][FeCl₄] using 1-hexyl-3-methylimidazolium chloride (6.0862 g, 30.02 mmol) and iron(iii) chloride hexahydrate (8.1118 g, 30.01 mmol). EA Calcd. (%) for [HMIm][FeCl₄]: C, 31.69; H, 5.47; N, 7.39; Cl, 37.42. Found: C, 32.05; H, 5.37; N, 7.26; Cl, 38.20. Yield: dark brown liquid, 10.0049 g, 70%.

2.5.3. Synthesis of [OMIm][FeCl₄]

Synthesis of [OMIm][FeCl₄] was carried out using a similar procedure to [BMIm][FeCl₄] using 1-octyl-3-methylimidazolium chloride (6.9351 g, 30.05 mmol) and iron(iii) chloride hexahydrate (8.1121 g, 30.01 mmol). EA Calcd. (%) for [OMIm][FeCl₄]: C, 35.76; H, 6.03; N, 6.95; Cl, 35.19. Found: C, 35.94; H, 6.03; N, 6.95; Cl, 35.87. Yield: dark brown liquid, 10.3471 g, 69%.

2.5.4. Synthesis of [BMIm][DyCl₄]

Synthesis of [BMIm][DyCl₄] was carried out using a similar procedure to [BMIm][FeCl₄] using 1-butyl-3-methylimidazolium chloride (5.2252 g, 29.91 mmol) and dysprosium(iii) chloride hexahydrate (11.3155 g, 30.02 mmol). EA Calcd. (%) for [BMIm][DyCl₄]: C, 19.28; H, 4.26; N, 5.62; Cl, 28.46. Found: C, 20.24; H, 4.23; N, 5.57; Cl, 27.73. Yield: golden-colored liquid, 9.7395 g, 59%.

2.5.5. Synthesis of [HMIm][DyCl₄]

Synthesis of [HMIm][DyCl₄] was carried out using a similar procedure to [BMIm][FeCl₄] using 1-hexyl-3-methylimidazolium chloride (6.1059 g, 30.12 mmol) and dysprosium(iii) chloride hexahydrate (11.3173 g, 30.02 mmol). EA Calcd. (%) for

[HMIm][DyCl₄]: C, 23.77; H, 4.54; N, 5.54; Cl, 28.06. Found: C, 23.66; H, 4.47; N, 5.46; Cl, 27.73. Yield: golden-colored liquid, 5.6108 g, 32%.

2.5.6. Synthesis of [OMIm][DyCl₄]

Synthesis of [OMIm][DyCl₄] was carried out using a similar procedure to [BMIm][FeCl₄] using 1-octyl-3-methylimidazolium chloride (6.9823 g, 30.26 mmol) and dysprosium(iii) chloride hexahydrate (11.3625 g, 30.14 mmol). EA Calcd. (%) for [OMIm][DyCl₄]: C, 27.44; H, 4.96; N, 5.33; Cl, 27.00. Found: C, 27.66; H, 4.95; N, 5.32; Cl, 25.64. Yield: golden-colored liquid, 8.6472 g, 47%.

2.5.7. Synthesis of [BMIm][GdCl₄]

Synthesis of [BMIm][GdCl₄] was carried out using a similar procedure to [BMIm][FeCl₄] using 1-butyl-3-methylimidazolium chloride (4.9734 g, 28.47 mmol) and gadolinium(iii) chloride hexahydrate (11.2582 g, 30.29 mmol). EA Calcd. (%) for [BMIm][GdCl₄]: unknown. Yield: cream-colored liquid, 9.7229 g, 60%.

2.5.8. Synthesis of [HMIm][GdCl₄]

Synthesis of [HMIm][GdCl₄] was carried out using a similar procedure to [BMIm][FeCl₄] using 1-hexyl-3-methylimidazolium chloride (6.0247 g, 29.72 mmol) and gadolinium(iii) chloride hexahydrate (11.4661 g, 30.85 mmol). EA Calcd. (%) for [HMIm][GdCl₄]: C, 21.17; H, 5.37; N, 4.94; Cl, 24.99. Found: C, 21.21; H, 5.23; N, 4.80; Cl, 24.65. Yield: cream-colored liquid, 10.0393 g, 57%.

2.5.9. Synthesis of [OMIm][GdCl₄]

Synthesis of [OMIm][GdCl₄] was carried out using a similar procedure to [BMIm][FeCl₄] using 1-octyl-3-methylimidazolium chloride (6.9268 g, 30.01 mmol) and gadolinium(iii) chloride hexahydrate (11.5473 g, 31.07 mmol). EA Calcd. (%) for [OMIm][GdCl₄]: C, 24.57; H, 5.71; N, 4.78; Cl, 24.18. Found: C, 24.33; H, 5.36; N, 4.63; Cl, 23.83. Yield: cream-colored liquid, g, %.

2.5.10. Synthesis of [BMIm][HoCl₄]

Synthesis of [BMIm][HoCl₄] was carried out using a similar procedure to [BMIm][FeCl₄] using 1-butyl-3-methylimidazolium chloride (5.2466 g, 30.04 mmol) and holmium(iii) chloride hexahydrate (11.8605 g, 31.26 mmol). EA Calcd. (%) for [BMIm][HoCl₄]: unknown. Yield: light-pink liquid, 10.3752 g, 61%.

2.5.11. Synthesis of [HMIm][HoCl₄]

Synthesis of [HMIm][HoCl₄] was carried out using a similar procedure to [BMIm][FeCl₄] using 1-hexyl-3-methylimidazolium chloride (6.0603 g, 29.89 mmol) and holmium(iii) chloride hexahydrate (11.9309 g, 31.45 mmol). EA Calcd. (%) for [HMIm][HoCl₄]: unknown. Yield: light-pink liquid, 10.3752 g, 65%.

2.5.12. Synthesis of [OMIm][HoCl₄]

Synthesis of [OMIm][HoCl₄] was carried out using a similar procedure to [BMIm][FeCl₄] using 1-octyl-3-methylimidazolium chloride (6.9065 g, 29.93 mmol) and holmium(iii) chloride hexahydrate (11.5728 g, 30.50 mmol). EA Calcd. (%) for [OMIm][HoCl₄]: C, 27.06; H, 4.99; N, 5.26; Cl, 26.62. Found: C, 26.65; H, 4.90; N, 5.16; Cl, 26.01. Yield: light-pink liquid, 10.3752 g, 63%.

CHAPTER III
DATA AND RESULTS

3.1. FTIR Data

All data were obtained using an Agilent 670 FTIR-ATR spectrometer. A sensitivity of 1 was used for all experiments. A resolution of 8 cm^{-1} was used for all liquid sample experiments. A 32-scan background spectrum was taken before each sample spectra was taken. Each sample spectra were obtained using 32 scans, respectively.

3.1.1. 1-Alkyl-3-Methylimidazolium Halides

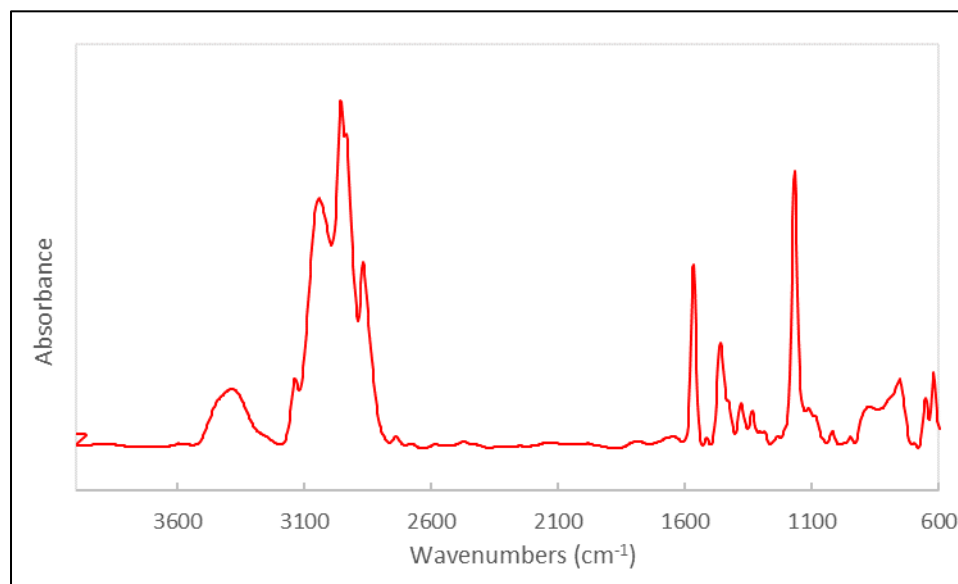


Figure 4. FTIR Spectra of [BMIm][Cl].

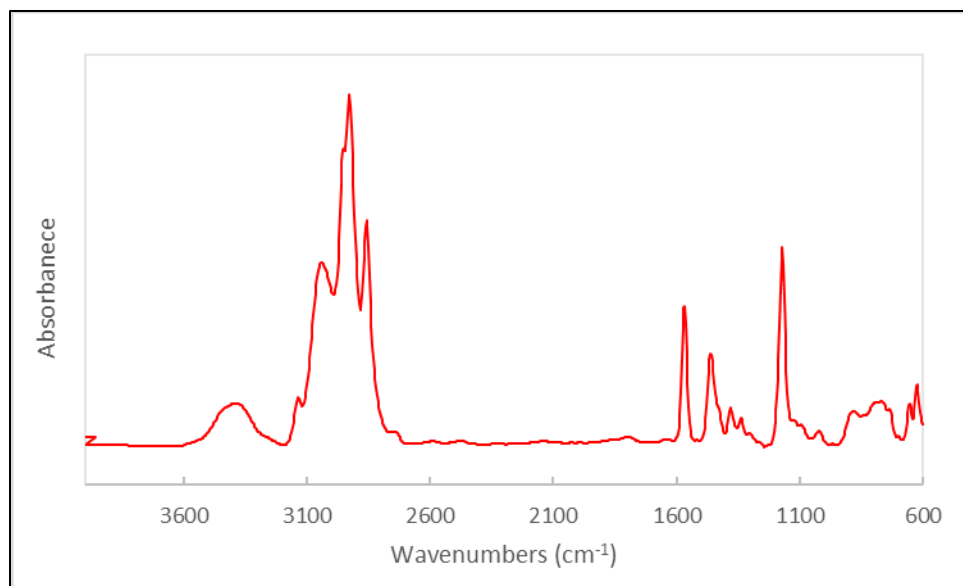


Figure 5. FTIR Spectra of [HMIm][Cl].

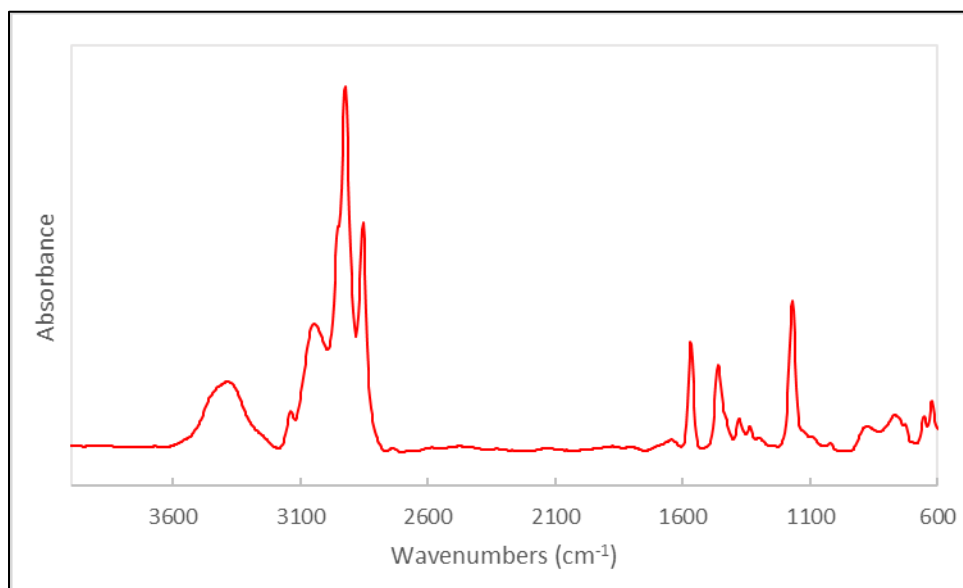


Figure 6. FTIR Spectra of [OMIm][Cl].

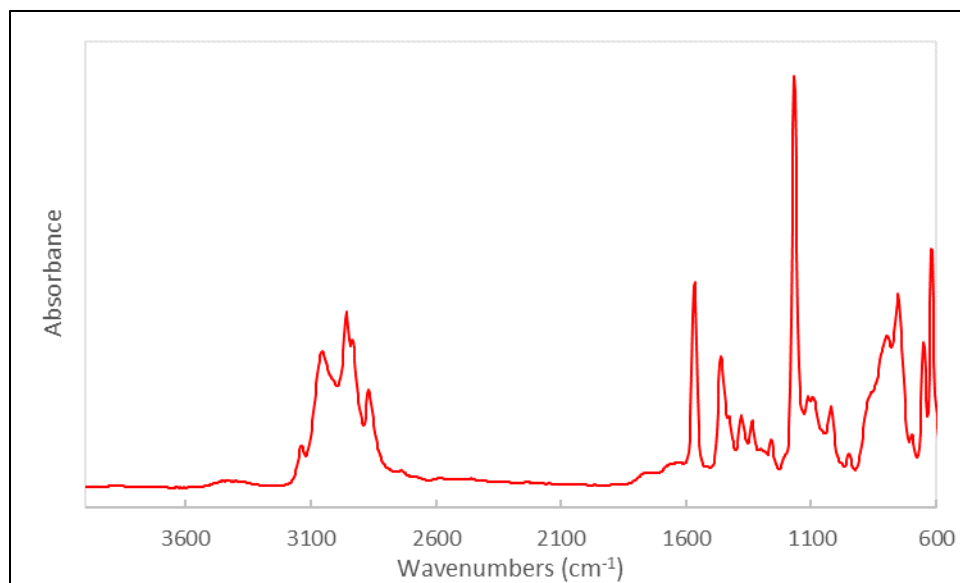


Figure 7. FTIR Spectra of [BMIm][Br].

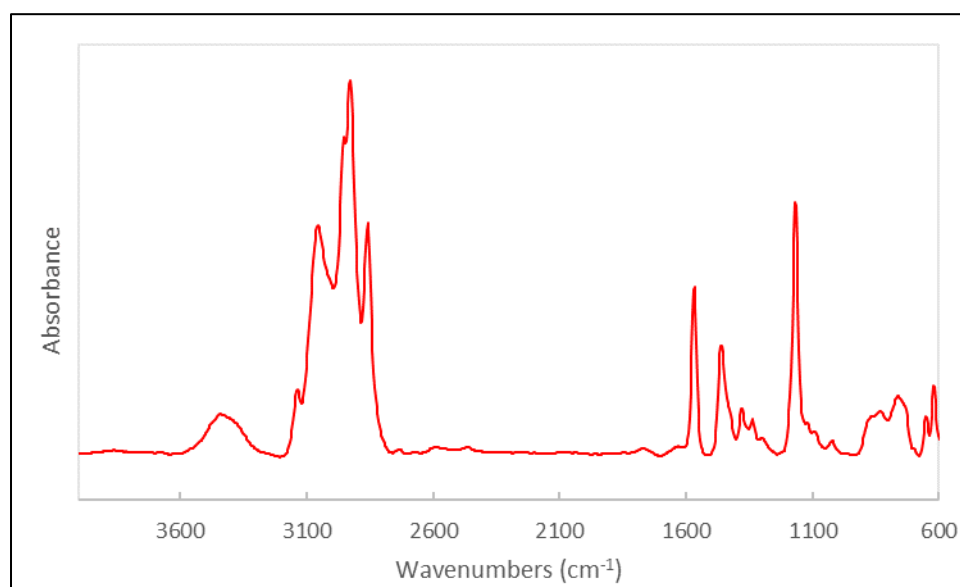


Figure 8. FTIR Spectra of [HMIm][Br].

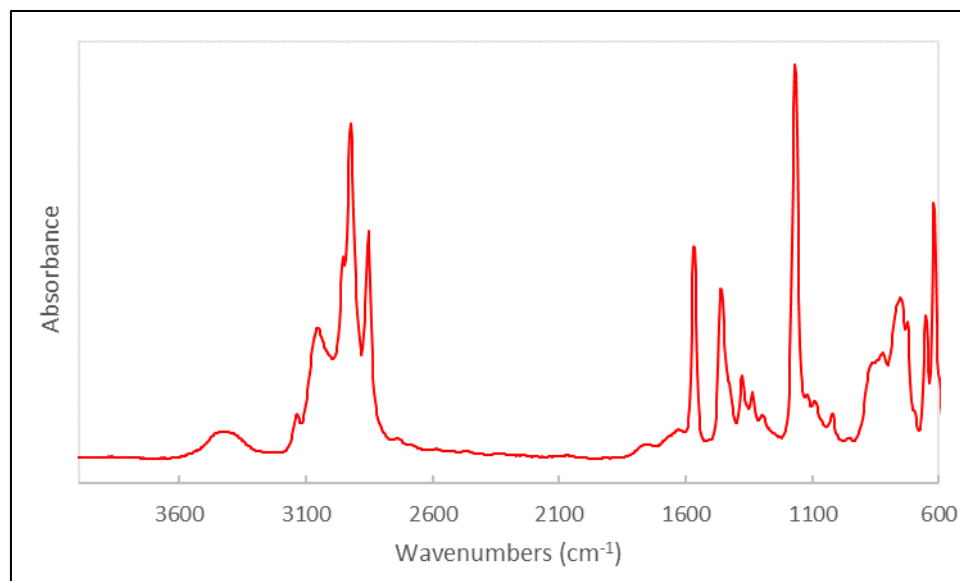


Figure 9. FTIR Spectra of [OMIm][Br].

3.1.2. Paramagnetic Ionic Liquids

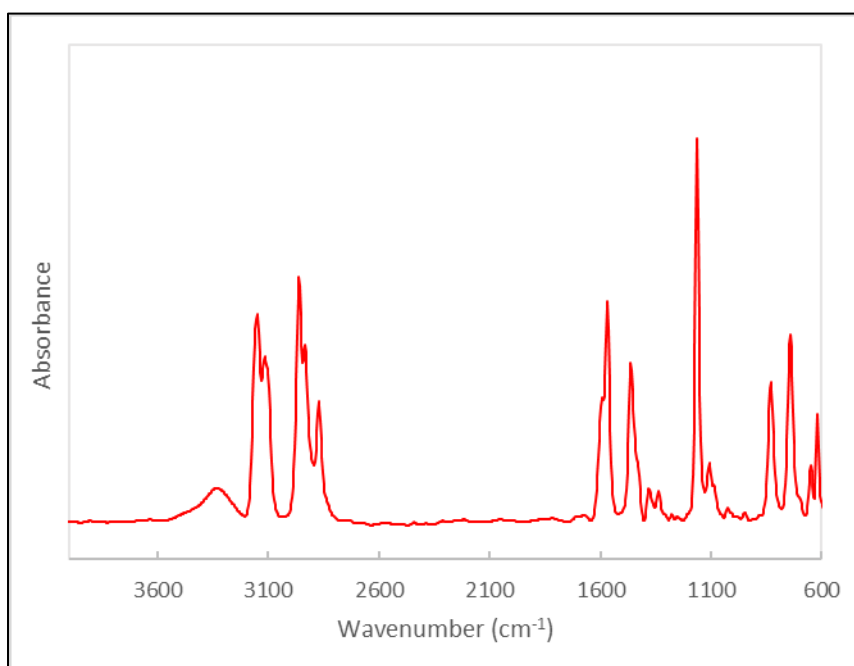


Figure 10. FTIR Spectra of [BMIm][FeCl₄].

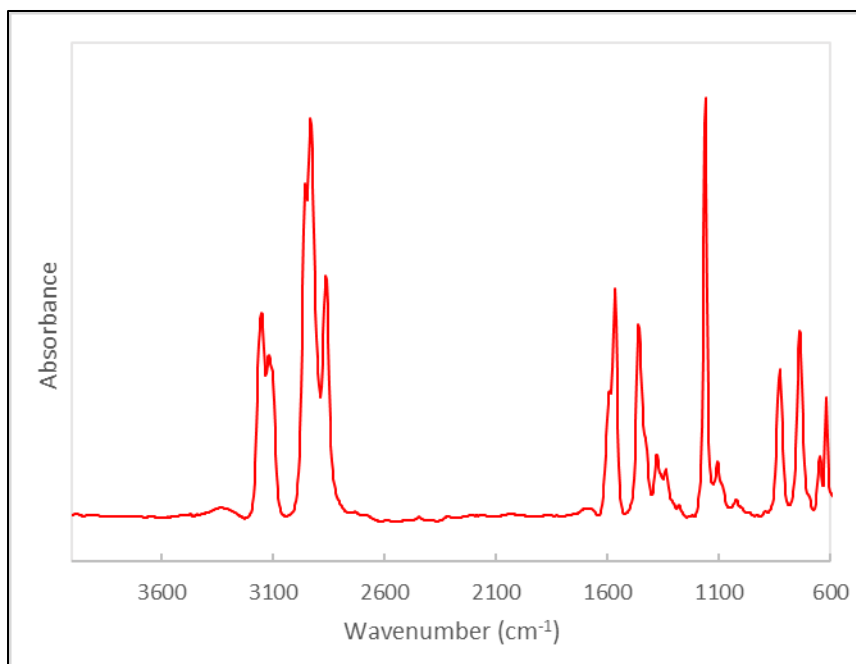


Figure 11. FTIR Spectra of [HMIm][FeCl₄].

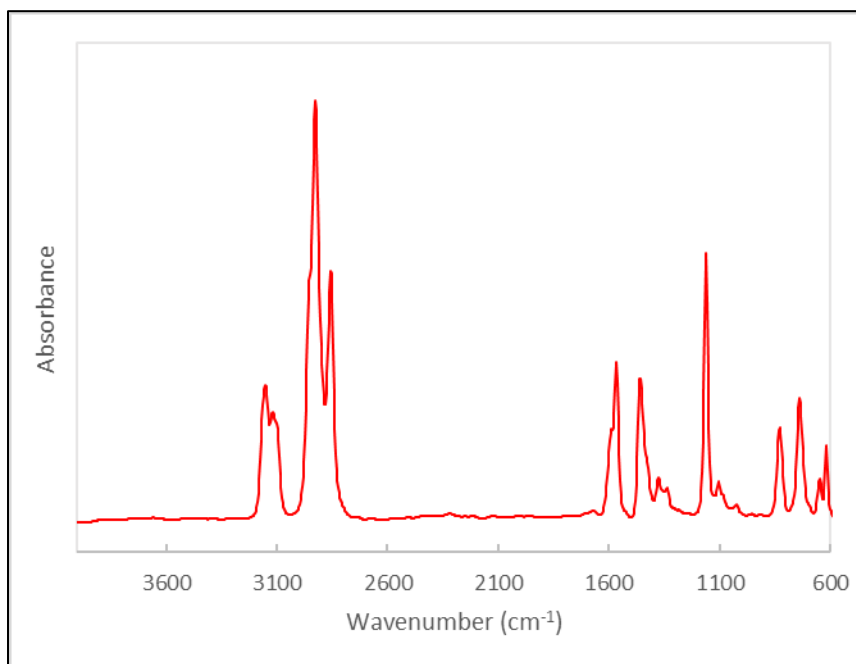


Figure 12. FTIR Spectra of [OMIm][FeCl₄].

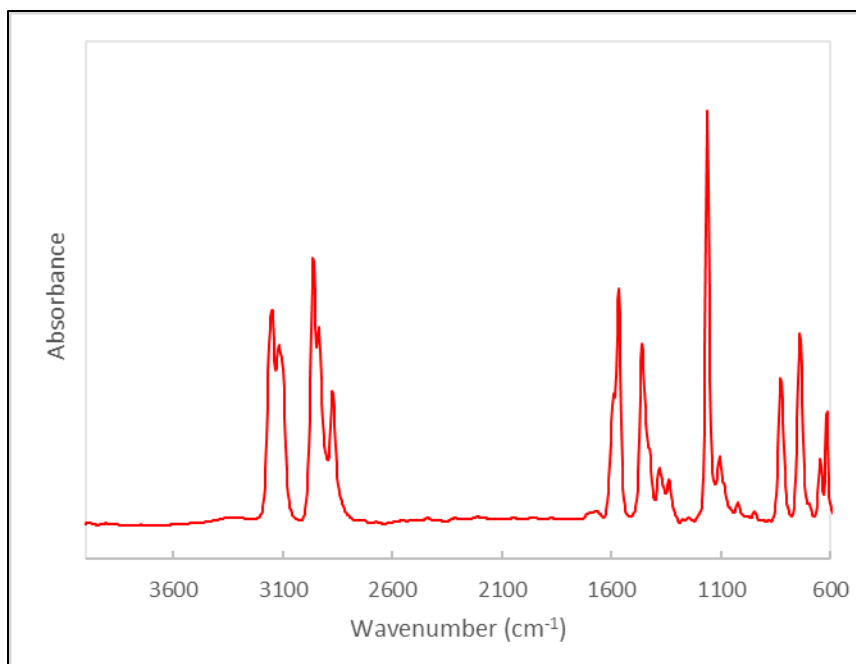


Figure 13. FTIR Spectra of [BMIm][FeBrCl₃].

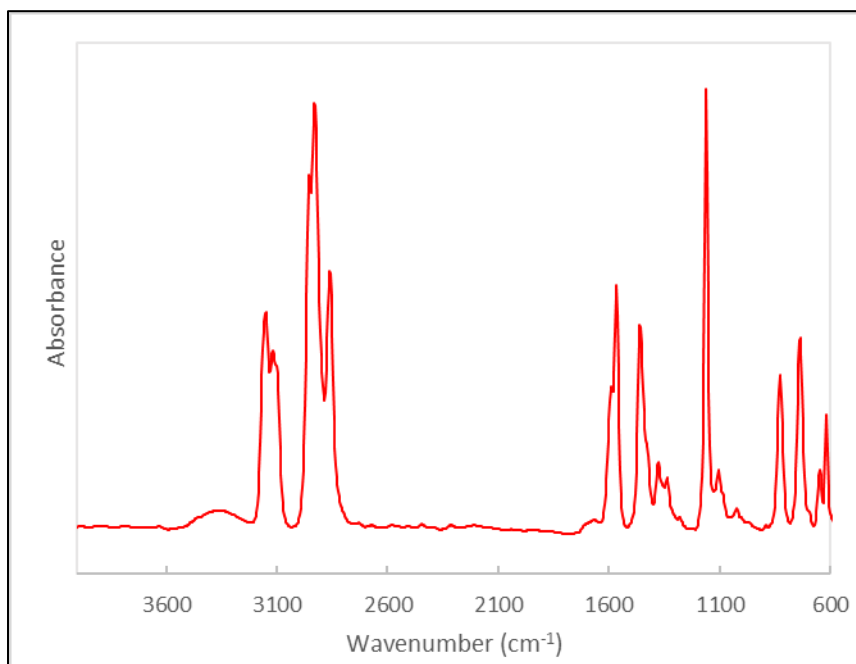


Figure 14. FTIR Spectra of [HMIm][FeBrCl₃].

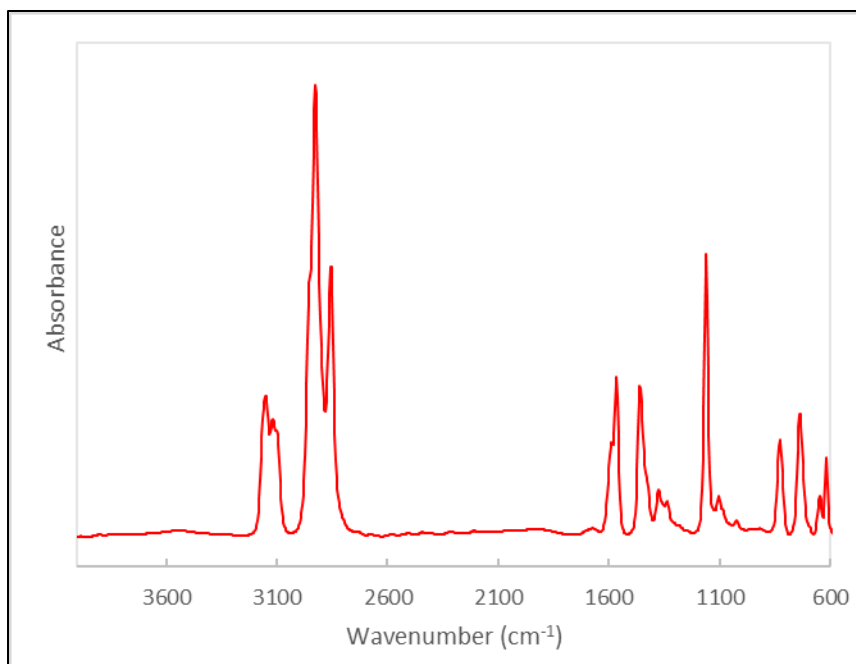


Figure 15. FTIR Spectra of [OMIm][FeBrCl₃].

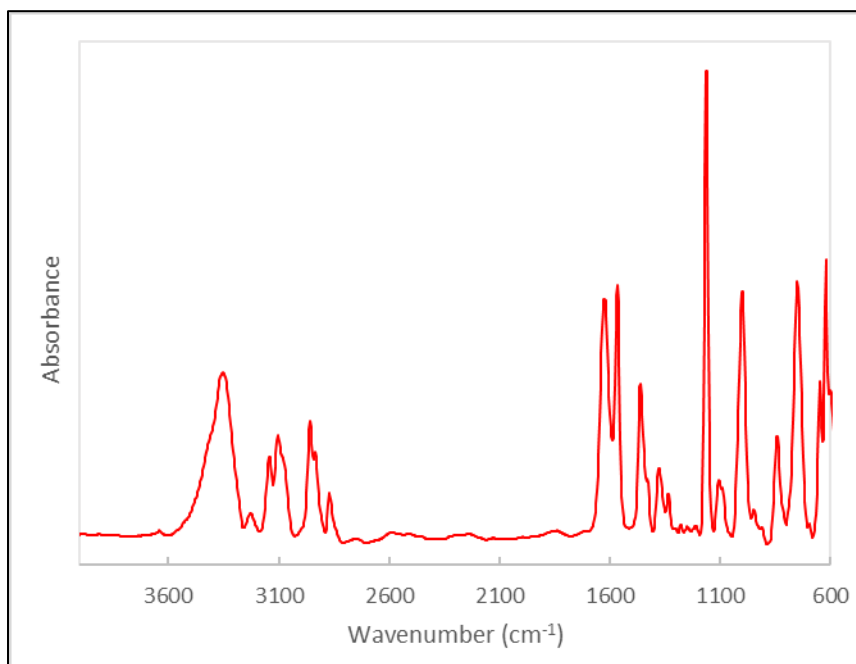


Figure 16. FTIR Spectra of [BMIm][DyCl₄].

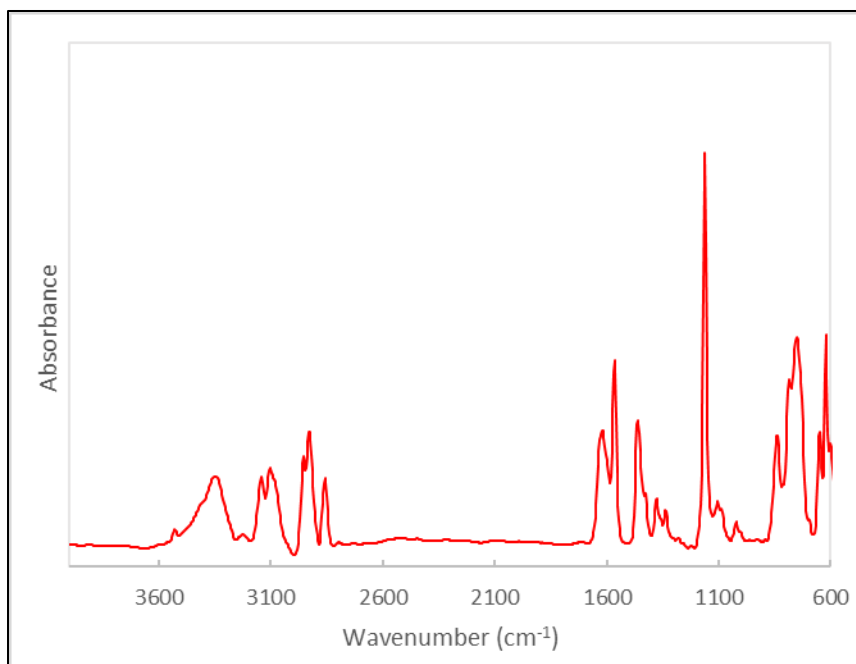


Figure 17. FTIR Spectra of [HMIm][DyCl₄].

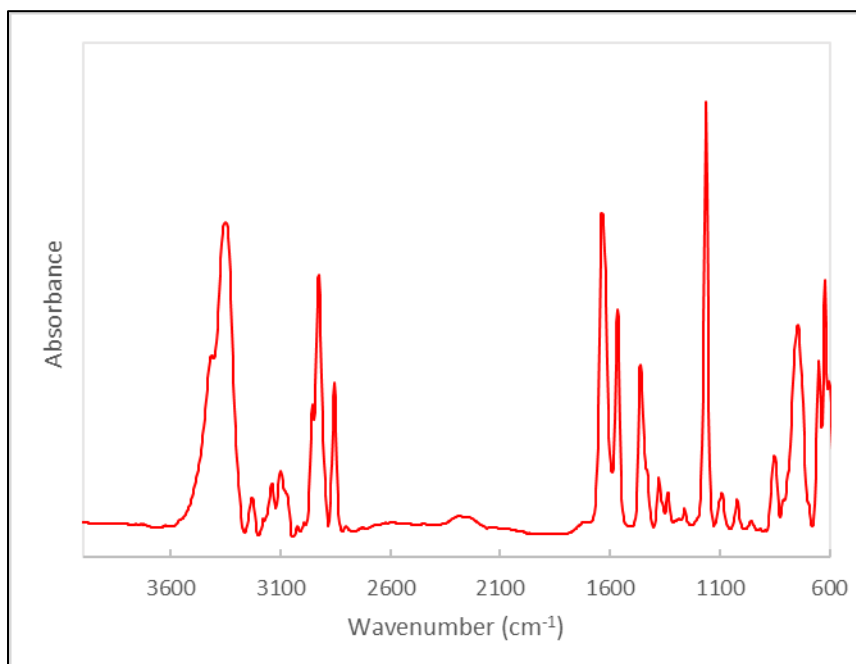


Figure 18. FTIR Spectra of [OMIm][DyCl₄].

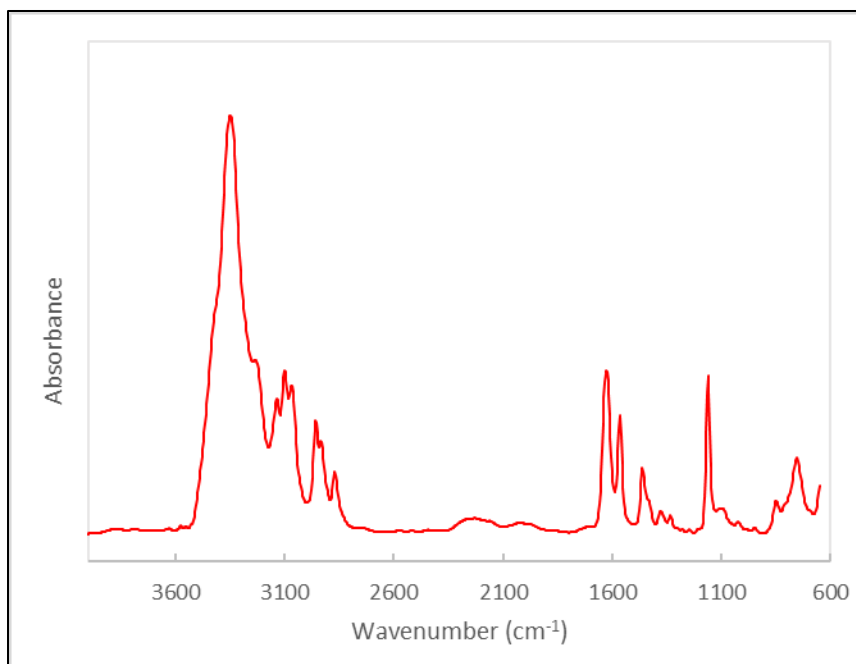


Figure 19. FTIR Spectra of [BMIm][DyBrCl₃].

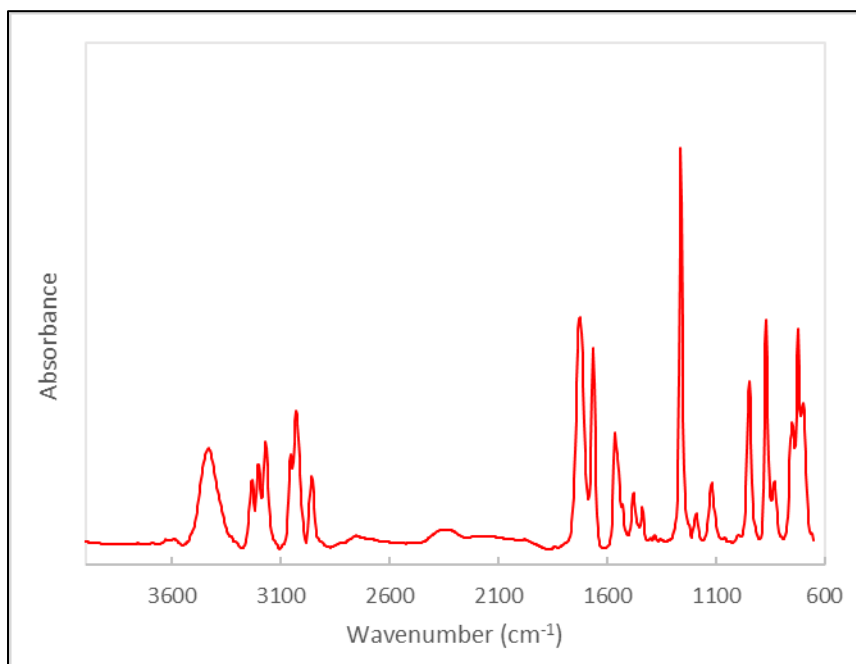


Figure 20. FTIR Spectra of [HMIm][DyBrCl₃].

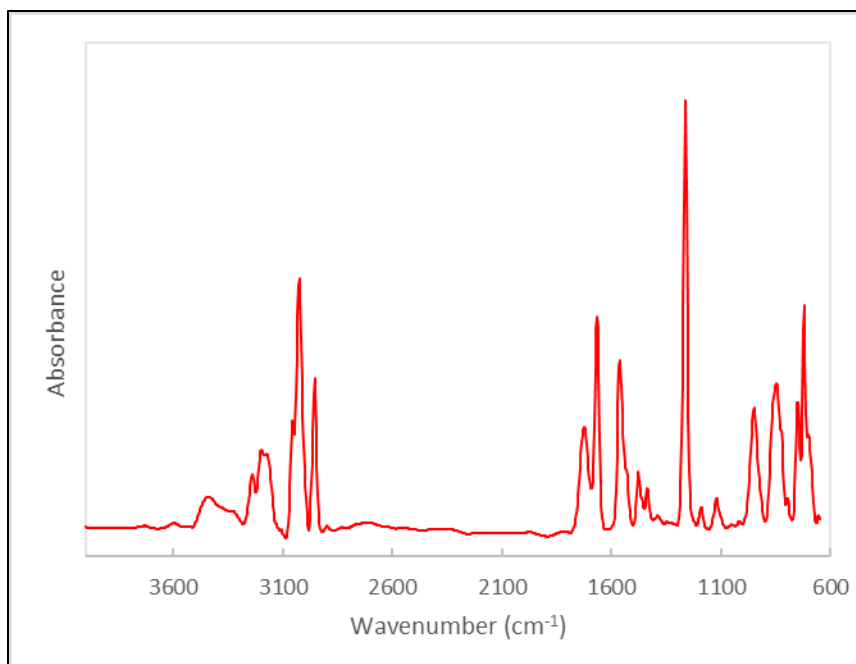


Figure 21. FTIR Spectra of [OMIm][DyBrCl₃].

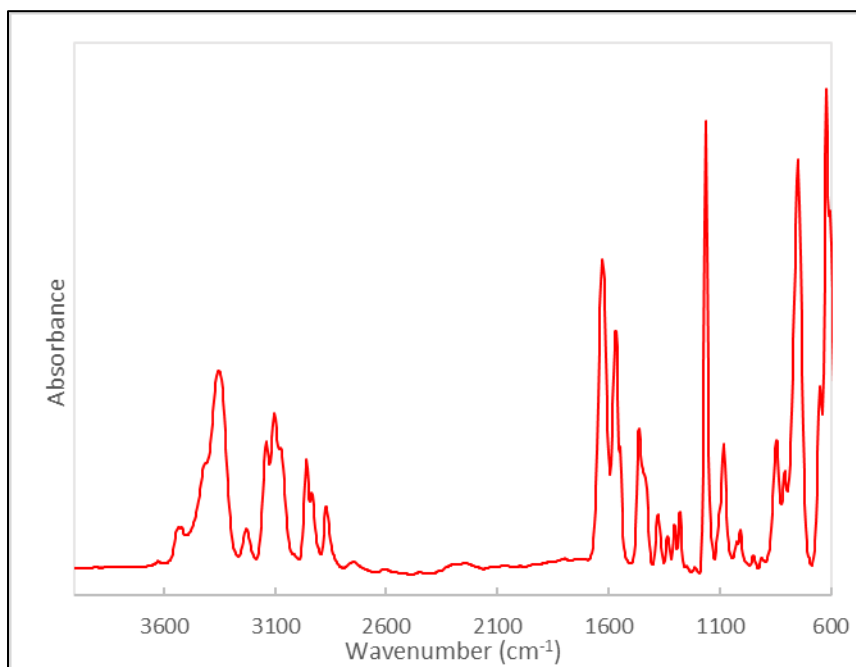


Figure 22. FTIR Spectra of [BMIm][HoCl₄].

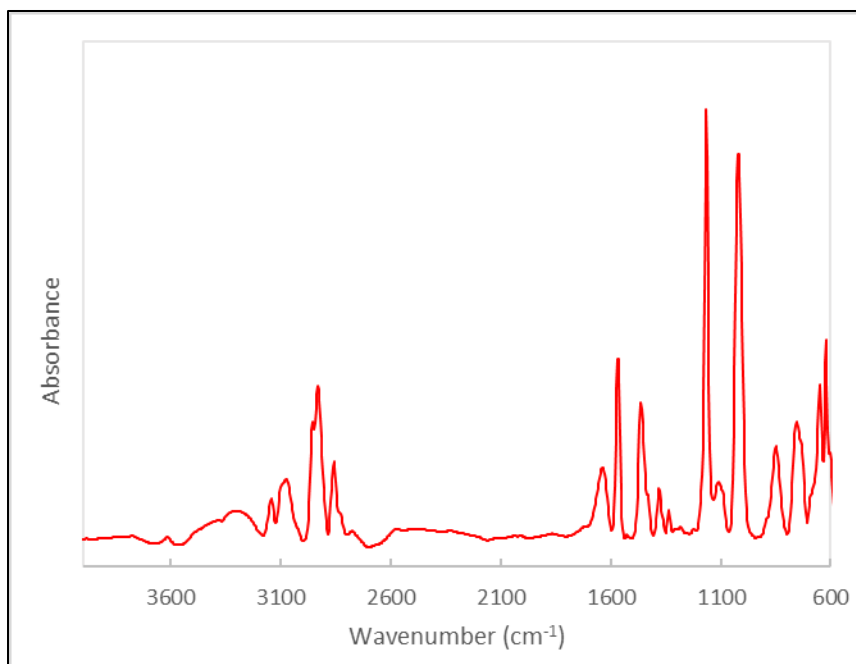


Figure 23. FTIR Spectra of [HMIm][HoCl₄].

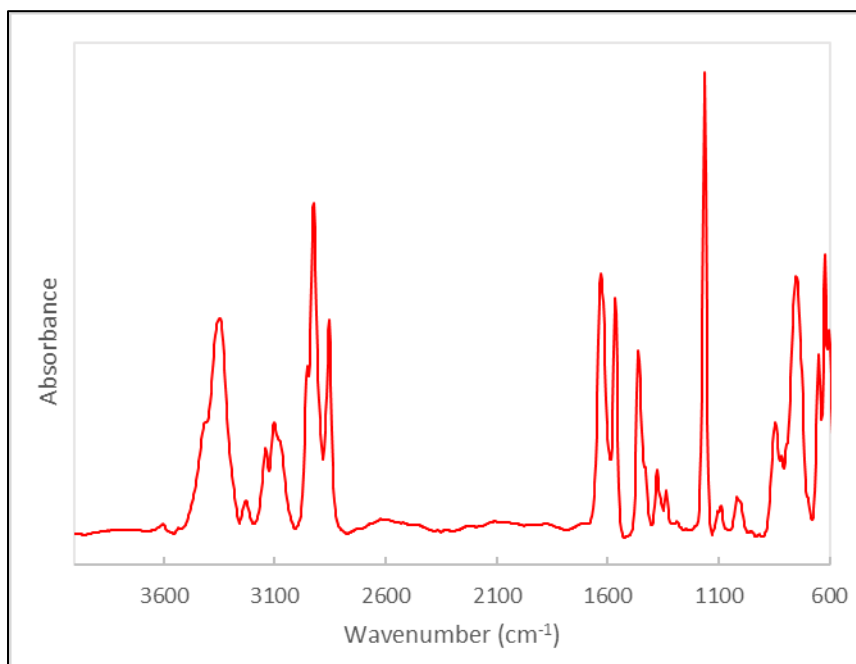


Figure 24. FTIR Spectra of [OMIm][HoCl₄].

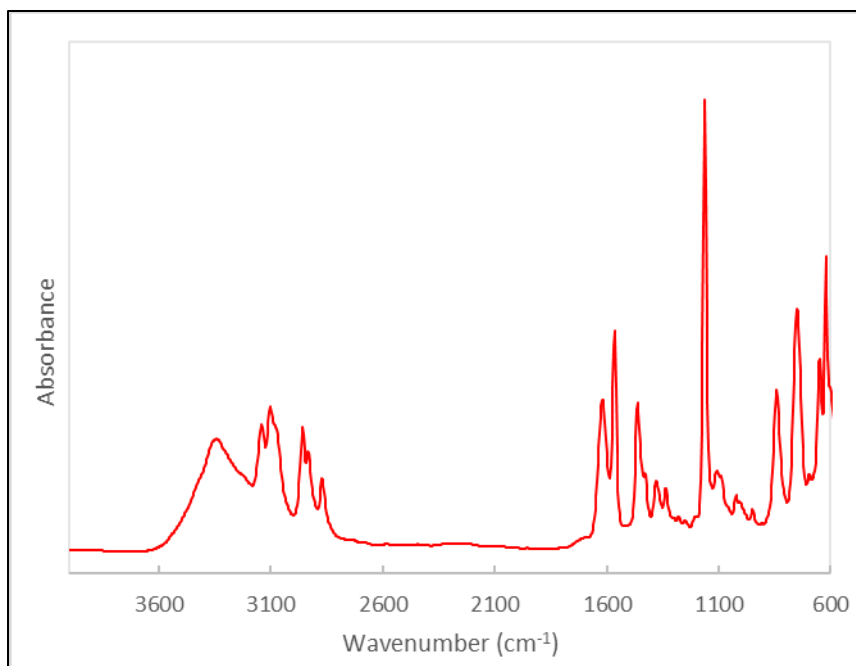


Figure 25. FTIR Spectra of [BMIm][HoBrCl₃].

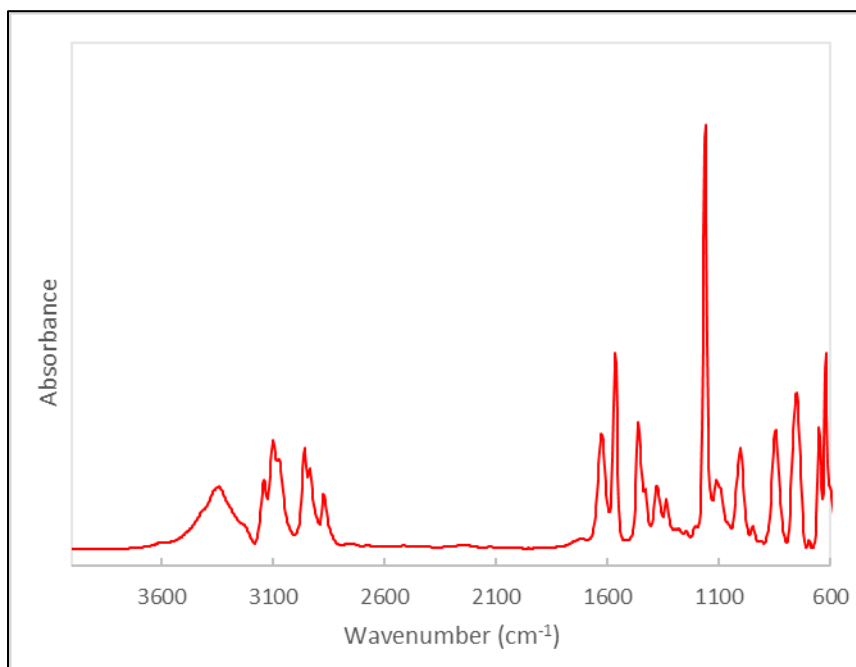


Figure 26. FTIR Spectra of [HMIm][HoBrCl₃].

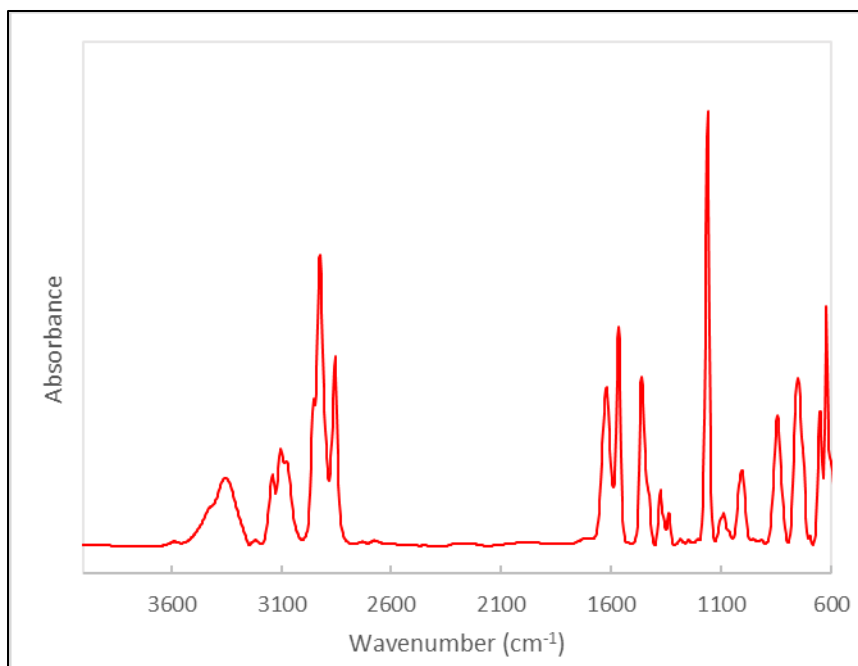


Figure 27. FTIR Spectra of [OMIm][HoBrCl₃].

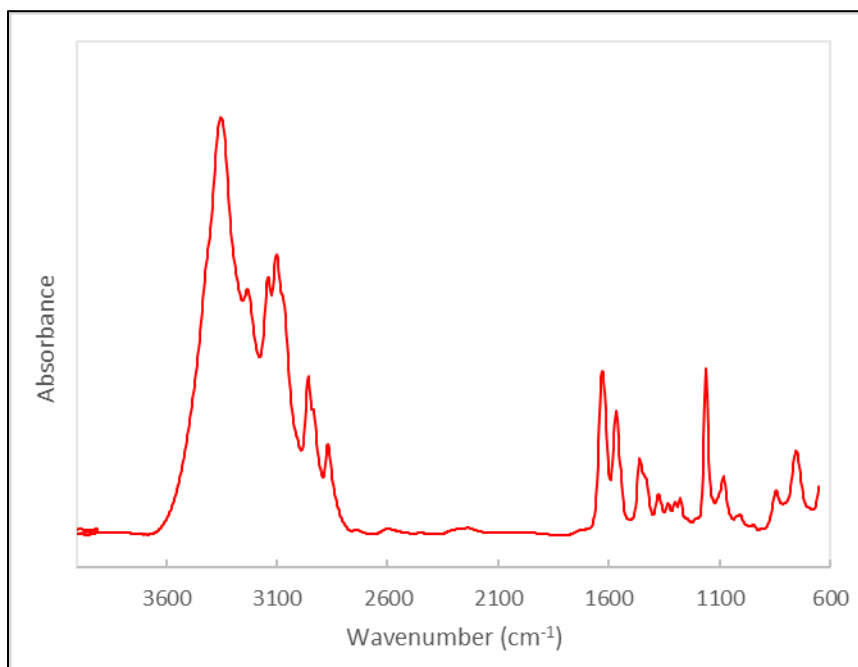


Figure 28. FTIR Spectra of [BMIm][GdCl₄].

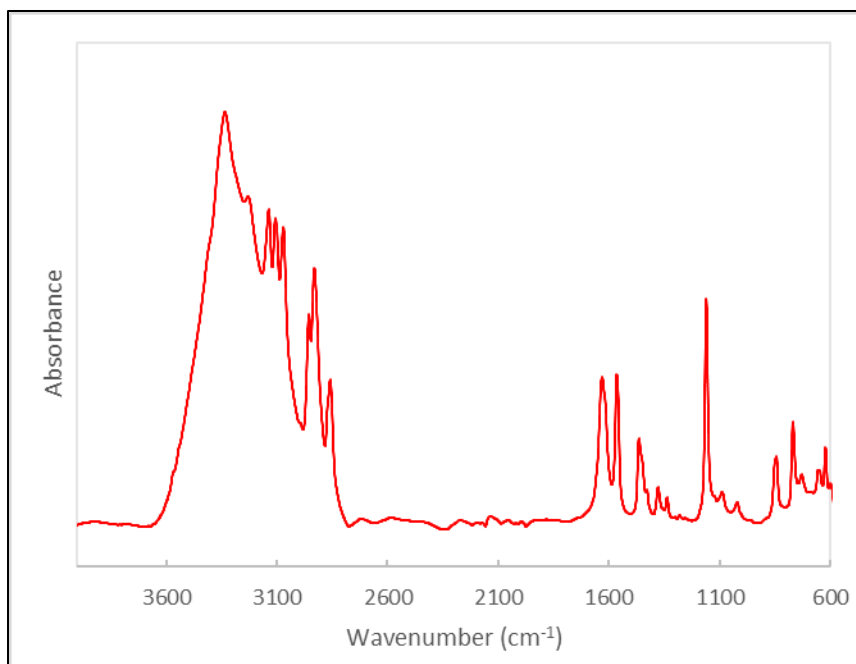


Figure 29. FTIR Spectra of [HMIIm][GdCl₄].

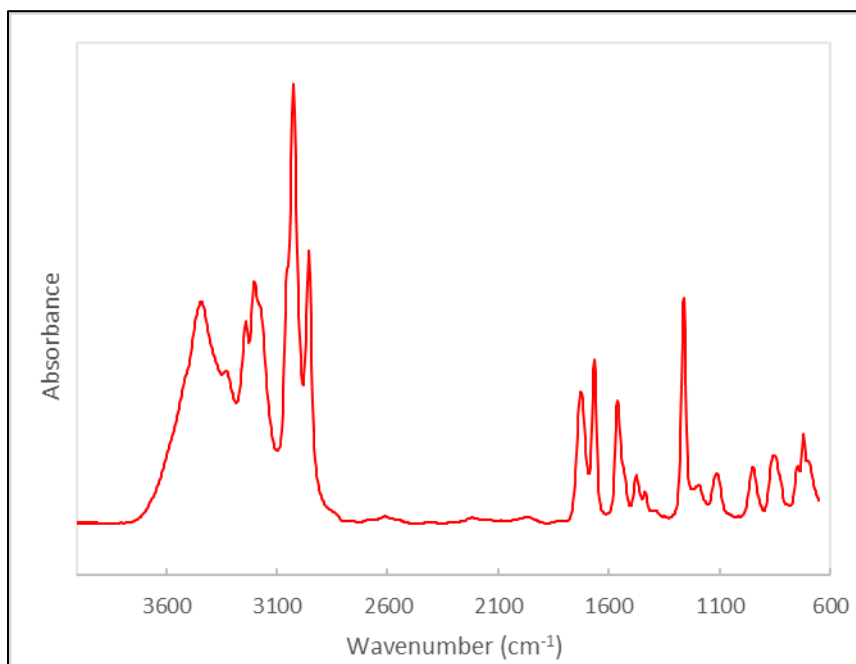


Figure 30. FTIR Spectra of [OMIm][GdCl₄].

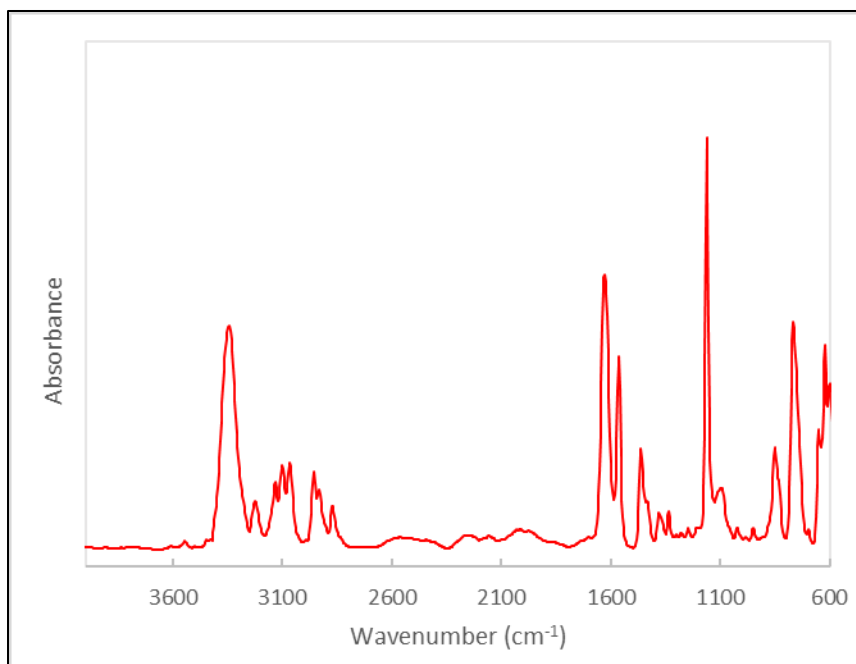


Figure 31. FTIR Spectra of [BMIm][GdBrCl₃].

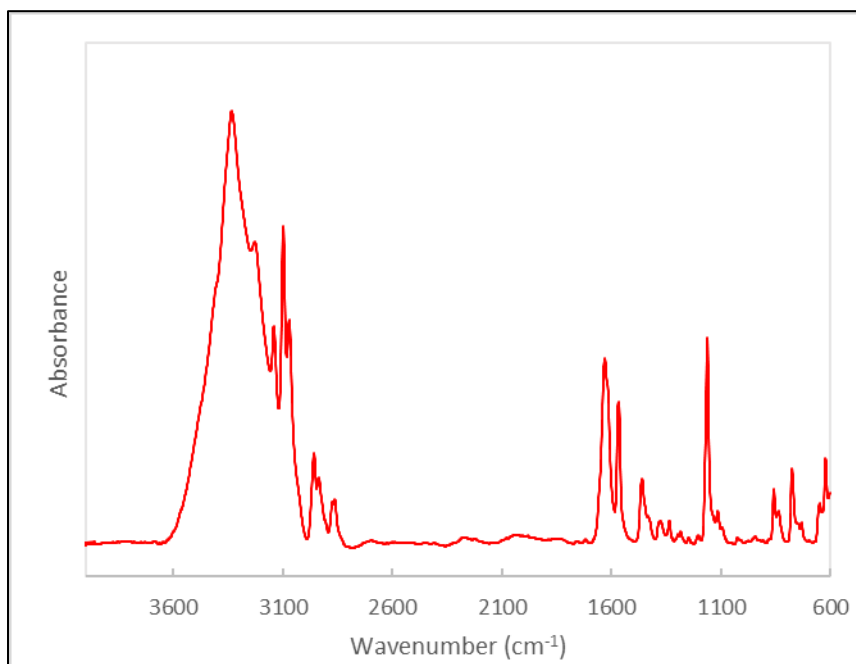


Figure 32. FTIR Spectra of [HMIm][GdBrCl₃].

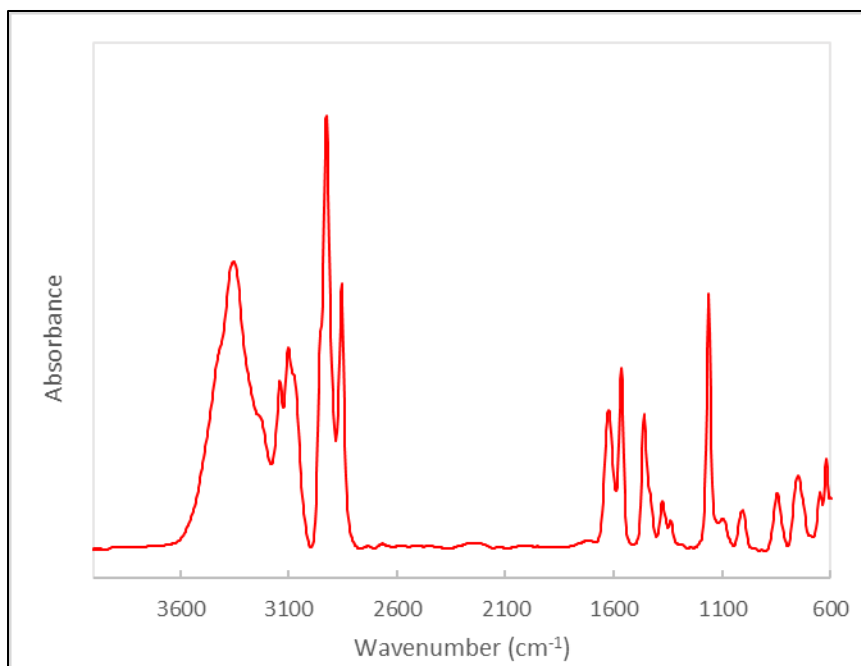


Figure 33. FTIR Spectra of [OMIm][GdBrCl₃].

3.2. TGA Data

All experiments were performed using a TA Q500 Thermogravimetric Analyzer. A ramp rate of 10 °C was used for all experiments and temperature ramped until 500 °C. Nitrogen gas was used for all experiments with a flow rate of 60 mL min⁻¹.

3.2.1. 1-Alkyl-3-Methylimidazolium Halides

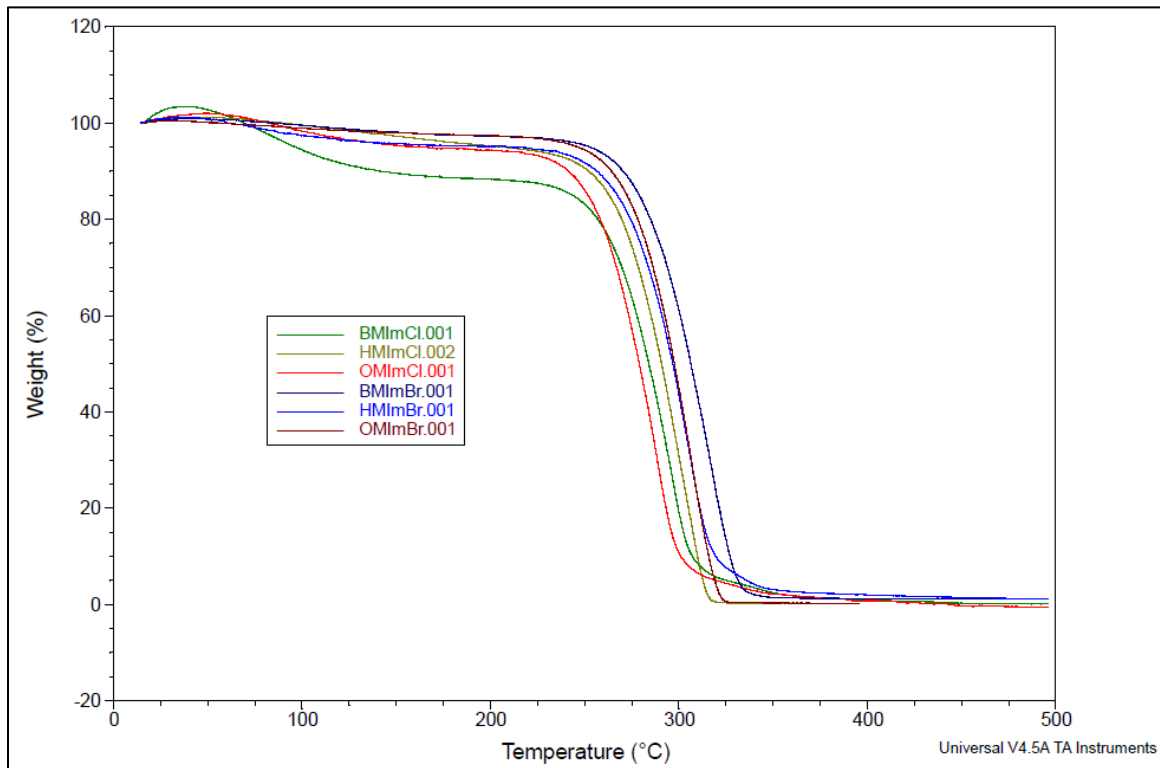


Figure 34. Thermal Curves of 1-Alkyl-3-Methylimidazolium Halide ILs.

Table 1. 1-Alkyl-3-Methylimidazolium Halide 5 wt% Thermal Degradation Temperatures.

Compound	5 wt% Thermal Degradation Temperature (°C)
[BMIm][Cl]	202
[HMIm][Cl]	215
[OMIm][Cl]	230
[BMIm][Br]	255
[HMIm][Br]	251
[OMIm][Br]	253

3.2.2. Paramagnetic Ionic Liquids

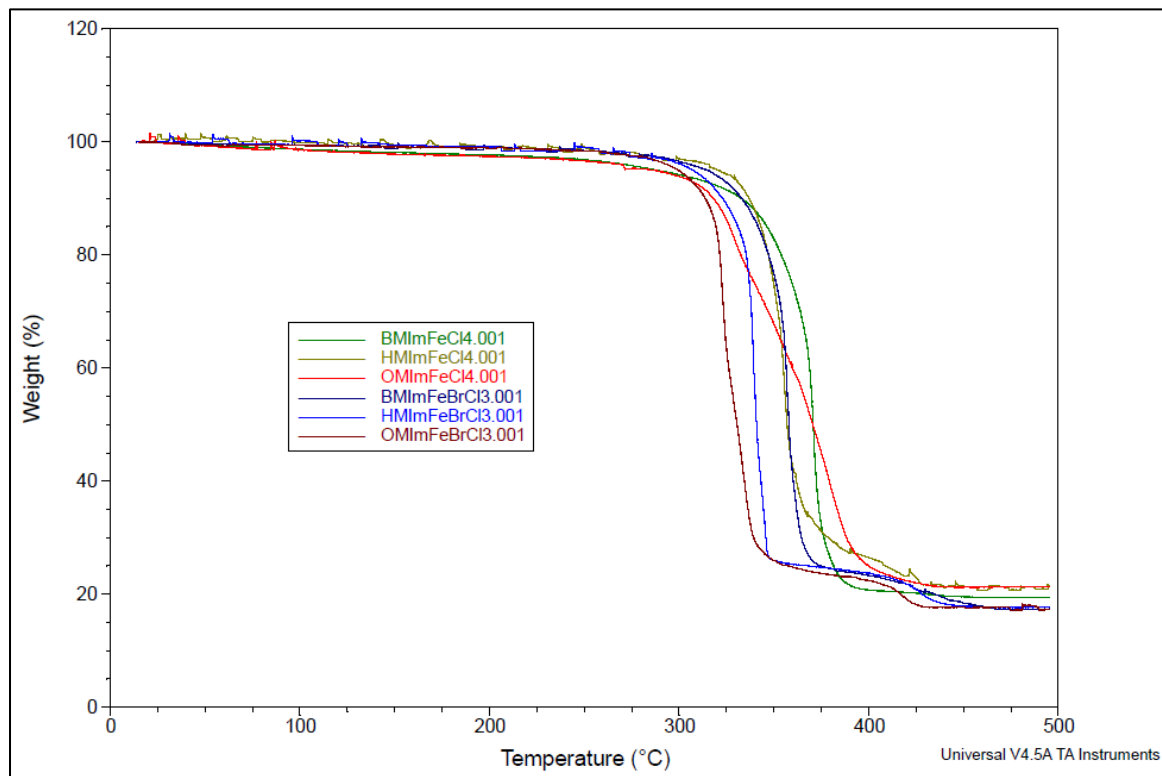


Figure 35. Thermal Curves of Iron-Based PILs.

Table 2. Iron-Based PILs 5 wt% Thermal Degradation Temperatures.

Compound	5 wt% Thermal Degradation Temperature (°C)
[BMIm][FeCl ₄]	289
[HMIm][FeCl ₄]	320
[OMIm][FeCl ₄]	288
[BMIm][FeBrCl ₃]	315
[HMIm][FeBrCl ₃]	307
[OMIm][FeBrCl ₃]	300

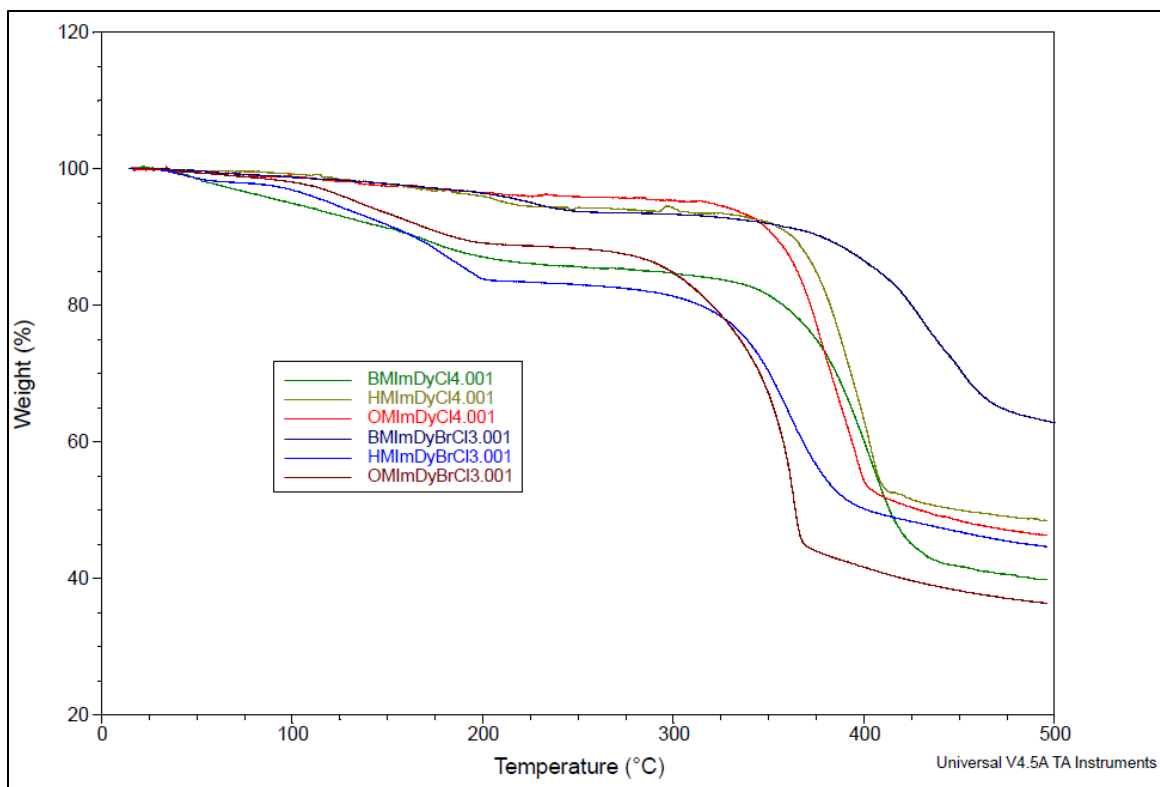


Figure 36. Thermal Curves of Dysprosium-Based PILs.

Table 3. Dysprosium-Based PILs 5 wt% Thermal Degradation Temperatures.

Compound	5 wt% Thermal Degradation Temperature (°C)
[BMIm][DyCl ₄]	349
[HMIm][DyCl ₄]	363
[OMIm][DyCl ₄]	322
[BMIm][DyBrCl ₃]	389
[HMIm][DyBrCl ₃]	321
[OMIm][DyBrCl ₃]	303

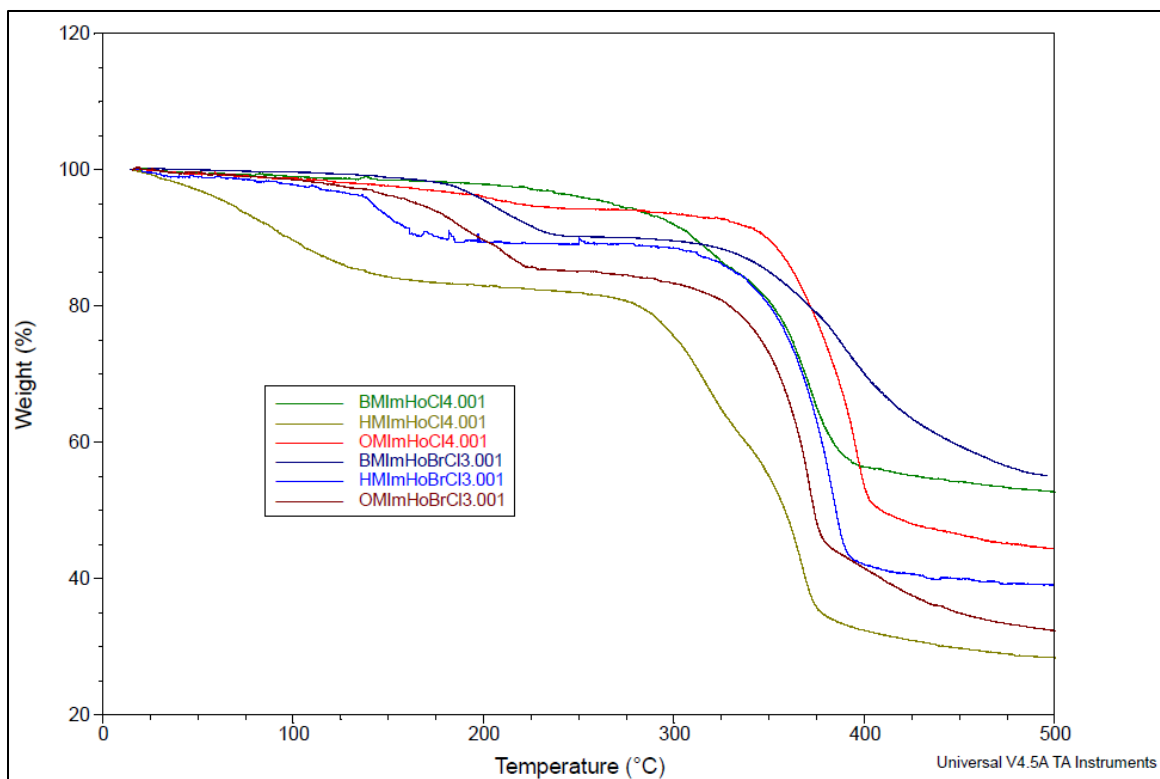


Figure 37. Thermal Curves of Holmium-Based PILs.

Table 4. Holmium-Based PILs 5 wt% Thermal Degradation Temperatures.

Compound	5 wt% Thermal Degradation Temperature (°C)
[BMIm][HoCl ₄]	285
[HMIIm][HoCl ₄]	278
[OMIm][HoCl ₄]	349
[BMIm][HoBrCl ₃]	346
[HMIIm][HoBrCl ₃]	333
[OMIm][HoBrCl ₃]	326

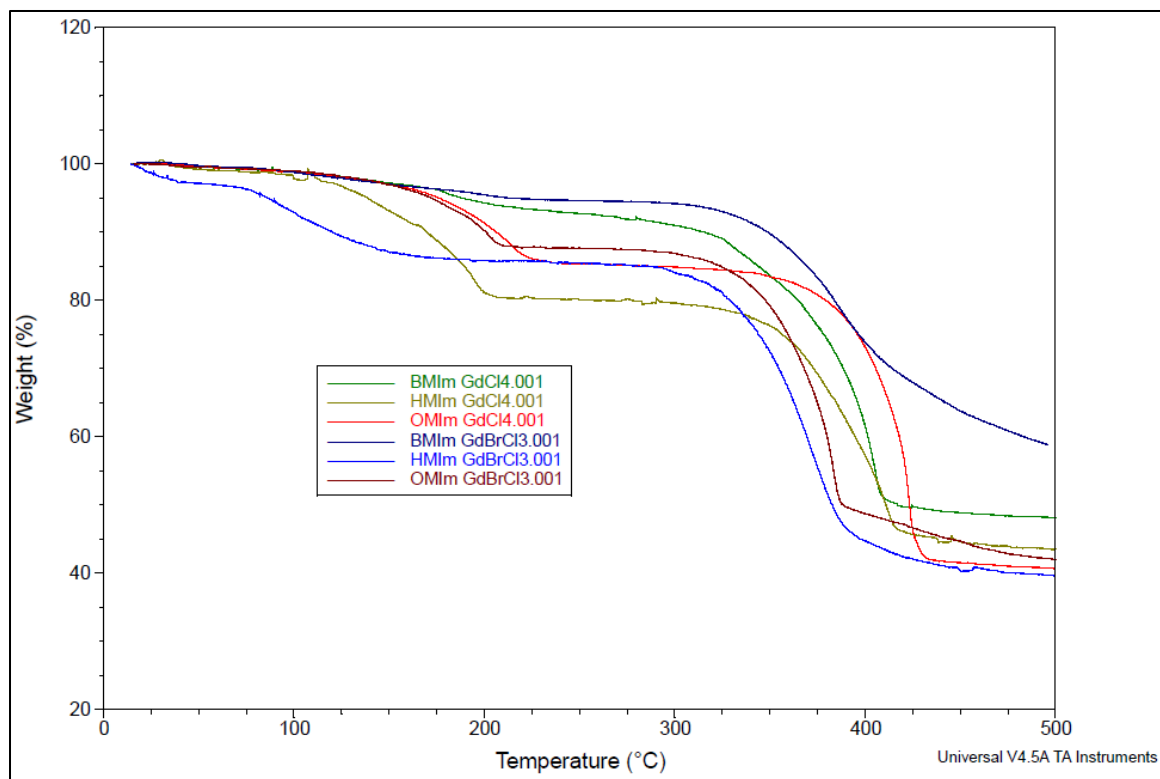


Figure 38. Thermal Curves of Gadolinium-Based PILs.

Table 5. Gadolinium-Based PILs 5 wt% Thermal Degradation Temperatures.

Compound	5 wt% Thermal Degradation Temperature (°C)
[BMIm][GdCl ₄]	326
[HMIm][GdCl ₄]	351
[OMIm][GdCl ₄]	373
[BMIm][GdBrCl ₃]	349
[HMIm][GdBrCl ₃]	321
[OMIm][GdBrCl ₃]	335

3.3. NMR Data

Proton and carbon NMR spectra of 1-alkyl-3-methylimidazolium halides are listed below. For all spectra, CDCl₃ was used unless otherwise stated. Spectra were obtained using a JEOL 500 MHz NMR spectrometer.

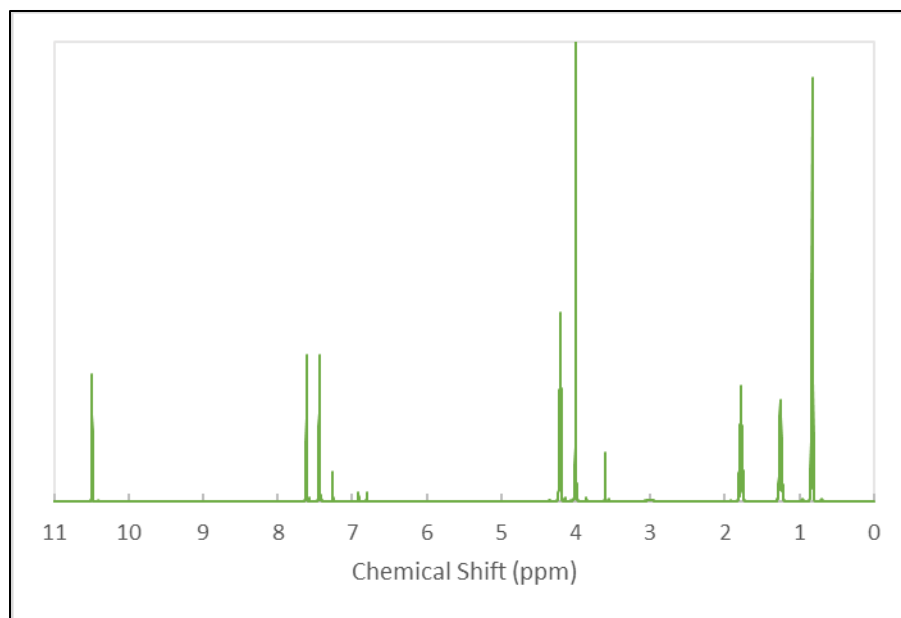


Figure 39. ^1H NMR Spectra of [BMIm][Cl]. ^1H NMR (CDCl_3) (δ): 0.8278 (3H, t, CH_3); 1.2499 (2H, sext, CH_2); 1.7791 (2H, p CH_2); 4.0040 (3H, s, CH_3); 4.2127 (2H, t, CH_2); 7.4430 (1H, t, CH); 7.6142 (1H, t, CH); 10.4929 (1H, s, CH).

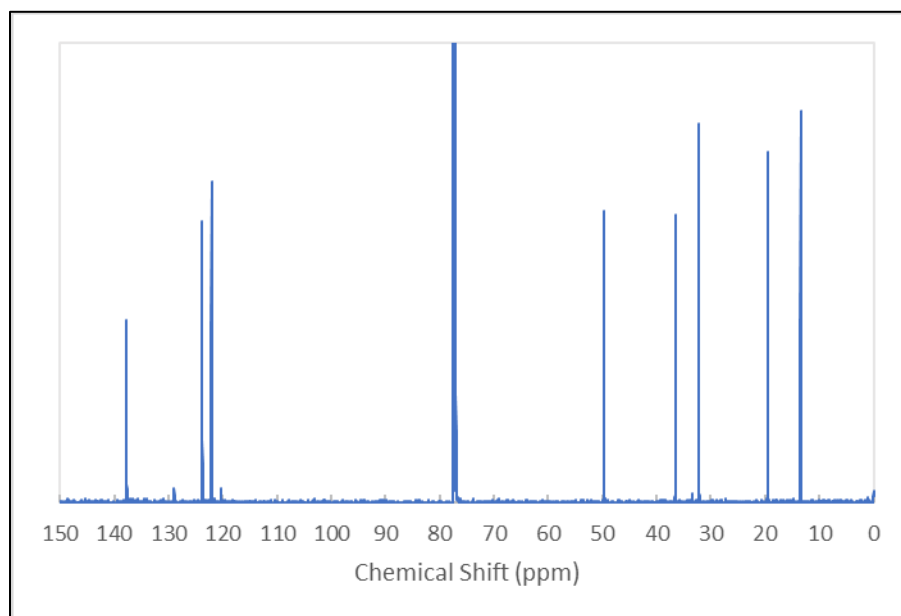


Figure 40. ^{13}C NMR Spectra of [BMIm][Cl]. ^{13}C NMR (CDCl_3) (δ): 13.4588 (CH_3); 19.4584 (CH_2); 32.1826 (CH_2); 36.5225 (CH_3); 49.7331 (CH_2); 122.0908 (CH); 123.7886 (CH); 137.7909 (CH).

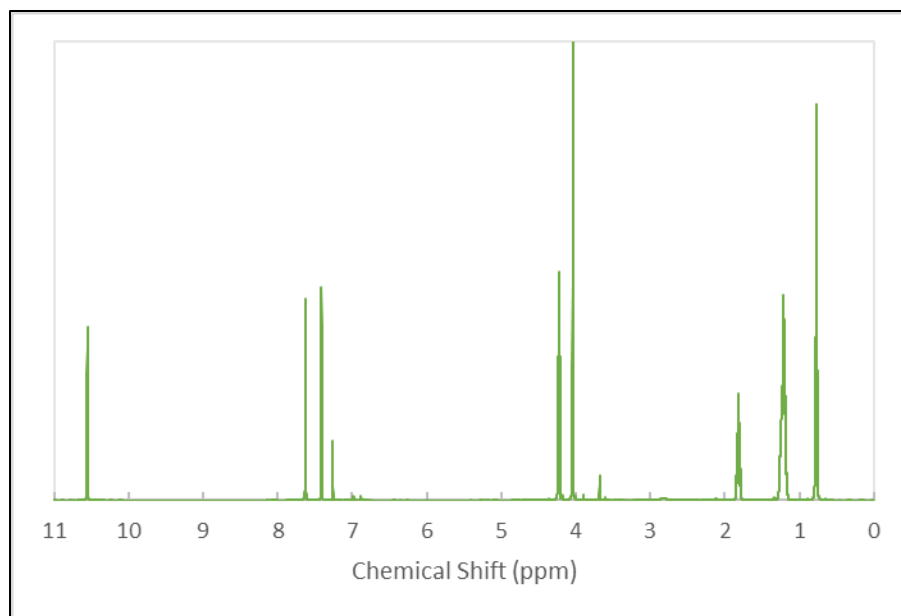


Figure 41. ^1H NMR Spectra of [HMIm][Cl]. ^1H NMR (CDCl_3) (δ): 0.7720 (3H, t, CH_3); 1.2179 (6H, m, CH_2); 1.8176 (2H, p, CH_2); 4.0398 (3H, s, CH_3); 4.2256 (2H, t, CH_2); 7.4129 (1H, t, CH); 7.6271 (1H, t, CH); 10.5561 (1H, s, CH).

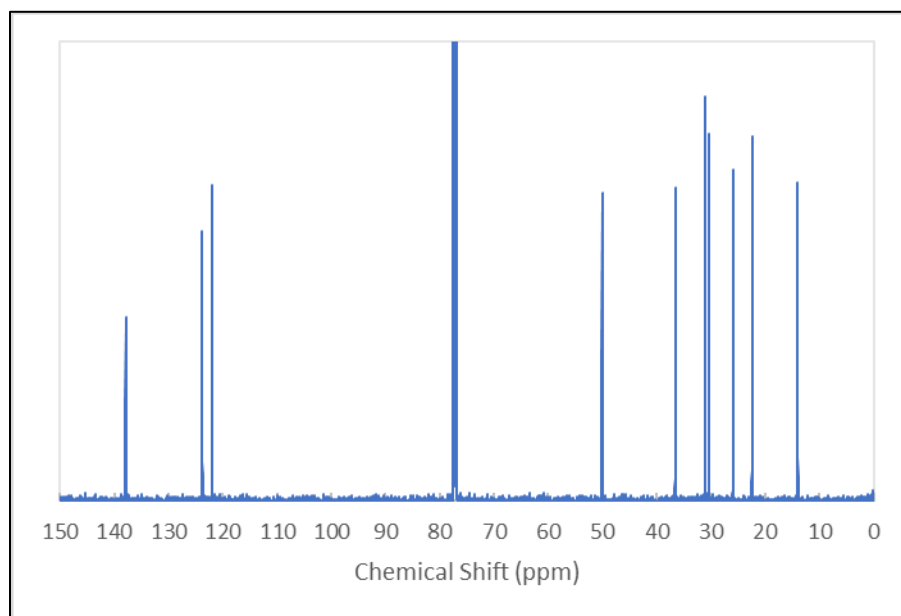


Figure 42. ^{13}C NMR Spectra of [HMIm][Cl]. ^{13}C NMR (CDCl_3) (δ): 13.9739 (CH_3); 22.3962 (CH_2); 25.9063 (CH_2); 30.3035 (CH_2); 31.1047 (CH_2); 36.5702 (CH_3); 50.0669 (CH_2); 121.9573 (CH); 123.7982 (CH); 137.9053 (CH).

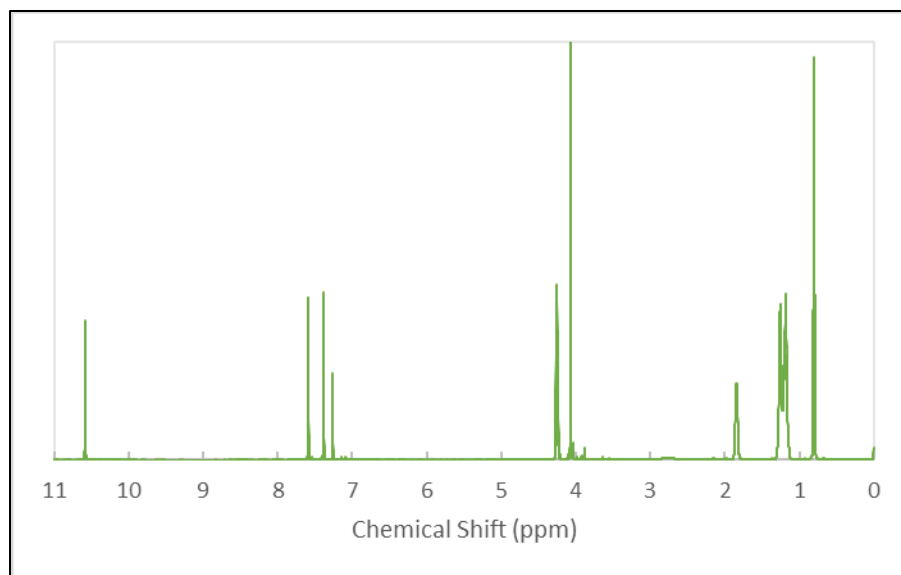


Figure 43. ^1H NMR Spectra of [OMIm][Cl]. ^1H NMR (CDCl_3) (δ): 0.8005 (3H, t, CH_3); 1.2152 (10H, m, CH_2); 1.8433 (2H, p, CH_2); 4.0683 (3H, s, CH_3); 4.2505 (2H, t, CH_2); 7.3846 (1H, t, CH); 7.5906 (1H, t, CH); 10.5846 (1H, s, CH).

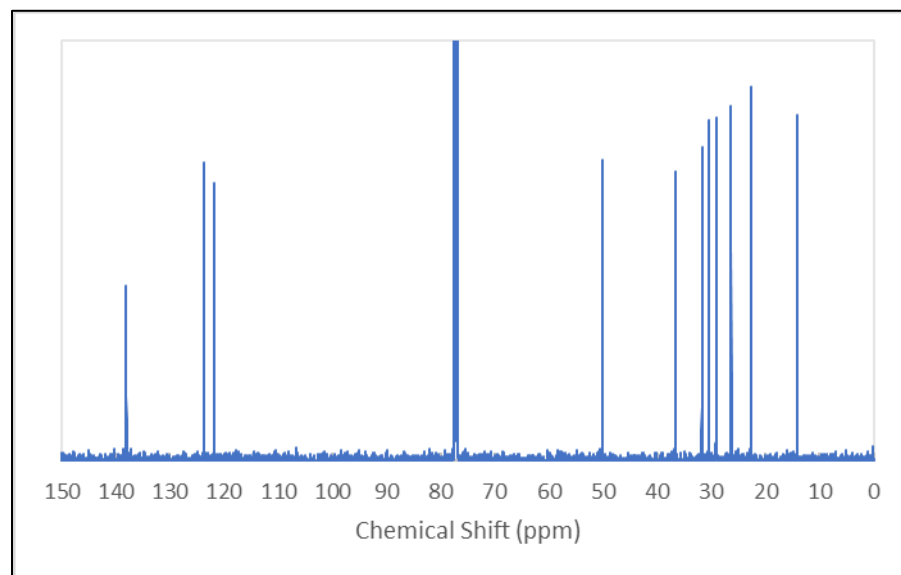


Figure 44. ^{13}C NMR Spectra of [OMIm][Cl]. ^{13}C NMR (CDCl_3) (δ): 14.1170 (CH_3); 22.6156 (CH_2); 26.22974 (CH_2); 28.9872 (CH_2); 29.0635 (CH_2); 30.3894 (CH_2); 31.66961 (CH_2); 36.6274 (CH_3); 50.1337 (CH_2); 121.8619 (CH); 123.7028 (CH); 138.0484 (CH).

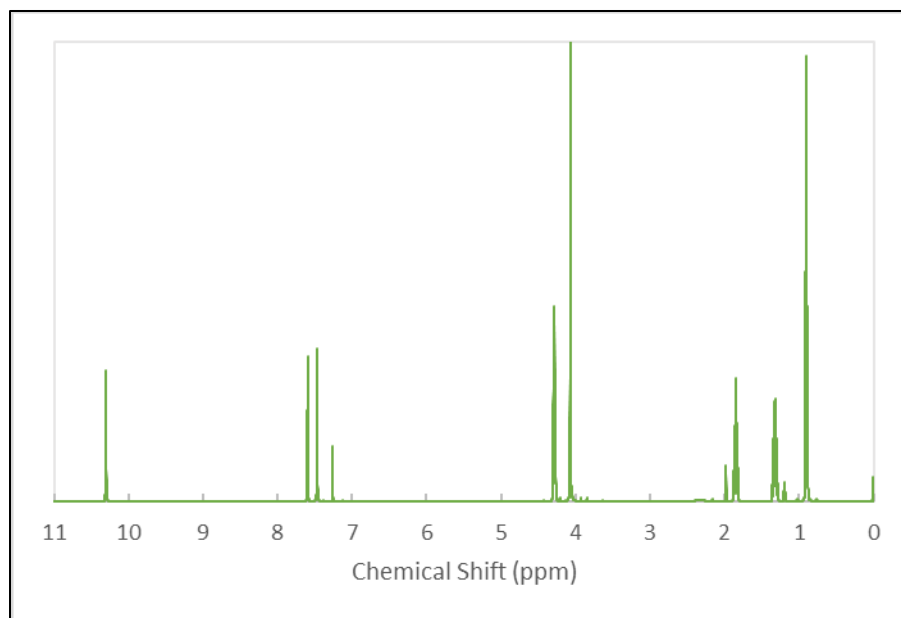


Figure 45. ^1H NMR Spectra of [BMIm][Br]. ^1H NMR (CDCl_3) (δ): 0.8994 (3H, t, CH_3); 1.3242 (2H, sext, CH_2); 1.8489 (2H, p, CH_2); 4.0719 (3H, s, CH_3); 4.2843 (2H, t, CH_2); 7.4697 (1H, t, CH); 7.5970 (1H, t, CH); 10.3053 (1H, s, CH).

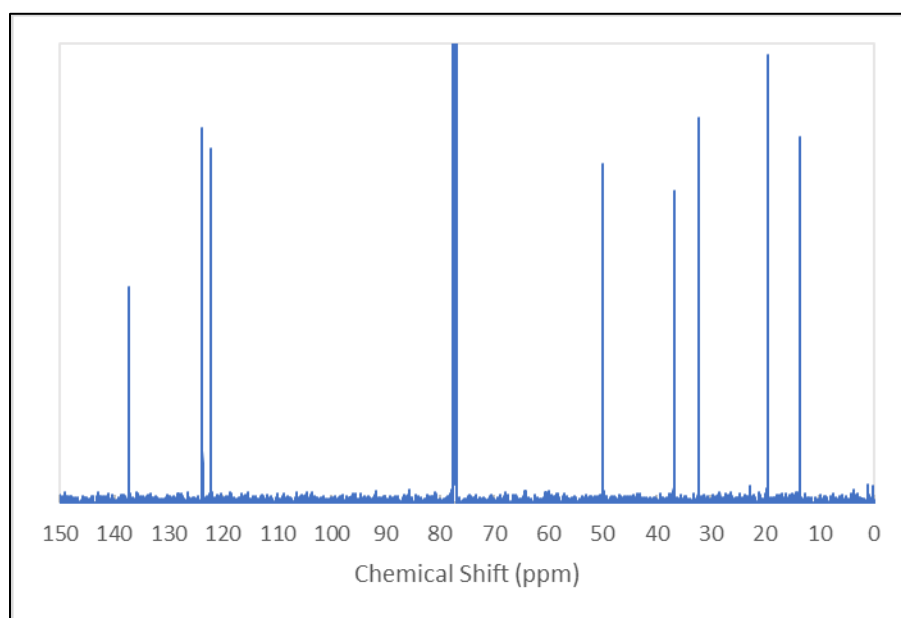


Figure 46. ^{13}C NMR Spectra of [BMIm][Br]. ^{13}C NMR (CDCl_3) (δ): 13.5351 (CH_3); 19.5157 (CH_2); 32.2302 (CH_2); 36.7800 (CH_3); 49.8952 (CH_2); 122.1862 (CH); 123.7886 (CH); 137.3712 (CH).

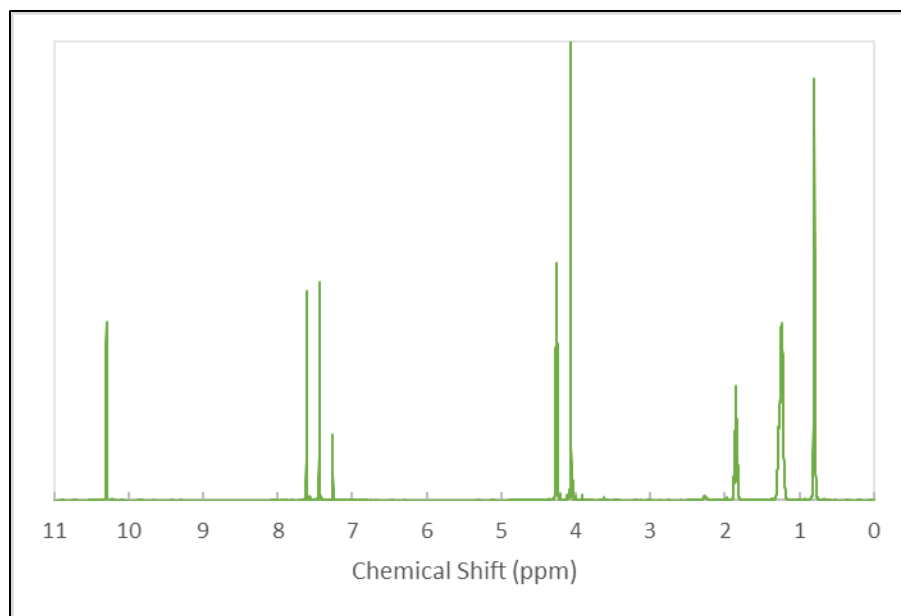


Figure 47. ^1H NMR Spectra of [HMIm][Br]. ^1H NMR (CDCl_3) (δ): 0.7958 (3H, t, CH_3); 1.2445 (6H, m, CH_2); 1.8478 (2H, p, CH_2); 4.0654 (3H, s, CH_3); 4.2577 (2H, t, CH_2); 7.4412 (1H, t, CH); 7.6125 (1H, t, CH); 10.2997 (1H, s, CH).

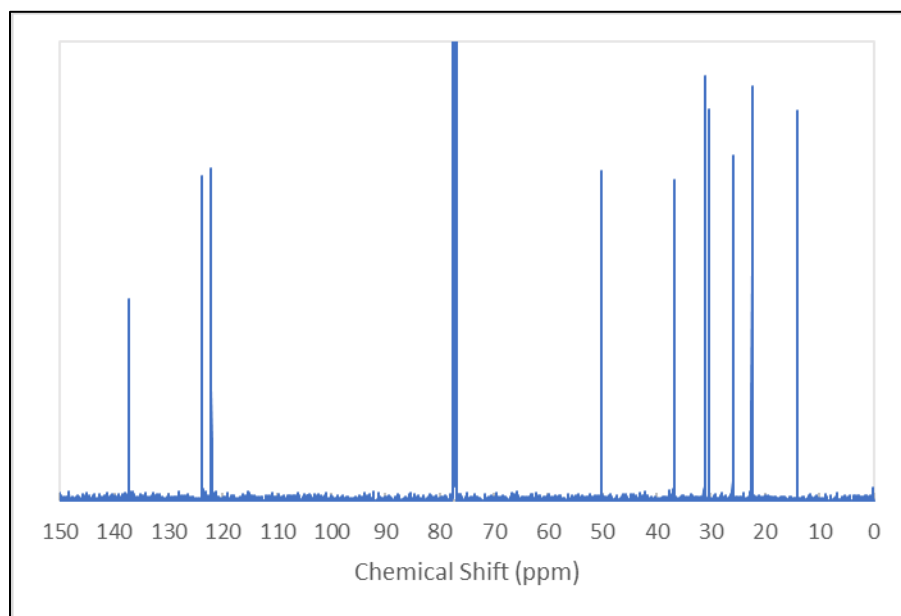


Figure 48. ^{13}C NMR Spectra of [HMIm][Br]. ^{13}C NMR (CDCl_3) (δ): 14.0025 (CH_3); 22.4248 (CH_2); 25.9254 (CH_2); 30.32226 (CH_2); 31.1143 (CH_2); 36.7705 (CH_3); 50.1528 (CH_2); 122.1194 (CH); 123.8459 (CH); 137.3426 (CH).

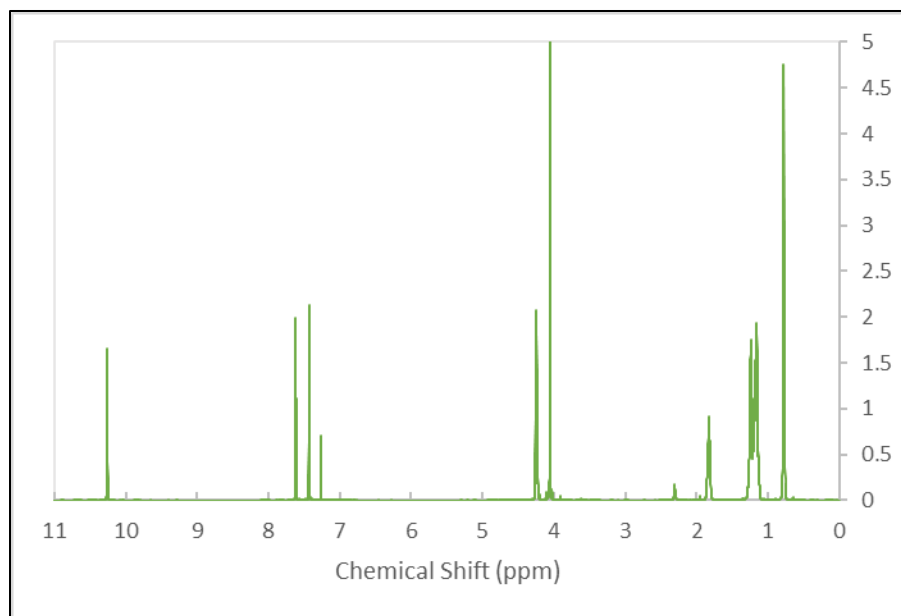


Figure 49. ^1H NMR Spectra of [OMIm][Br]. ^1H NMR (CDCl_3) (δ): 0.7758 (3H, t, CH_3); 1.2043 (10H, m, CH_2); 1.8306 (2H, p, CH_2); 4.0518 (3H, s, CH_3); 4.2404 (2H, t, CH_2); 7.4285 (1H, t, CH); 7.6162 (1H, t, CH); 10.2577 (1H, s, CH).

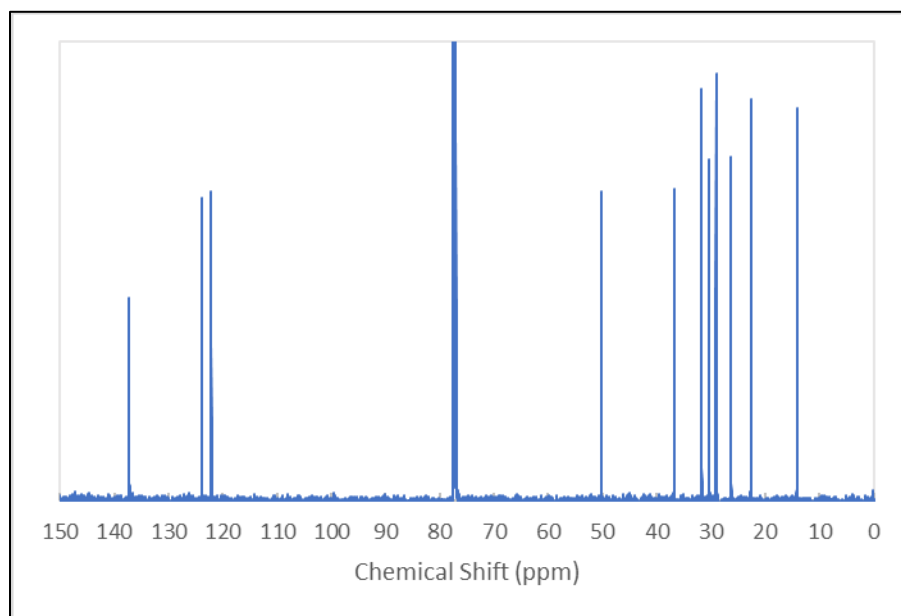


Figure 50. ^{13}C NMR Spectra of [OMIm][Br]. ^{13}C NMR (CDCl_3) (δ): 14.1074 (CH_3); 22.5965 (CH_2); 26.2592 (CH_2); 28.9681 (CH_2); 29.0444 (CH_2); 30.3702 (CH_2); 31.6865 (CH_2); 36.7609 (CH_3); 50.1527 (CH_2); 122.1098 (CH); 123.8744 (CH); 137.2758 (CH).

3.4. Magnetic Susceptibility Data

Magnetic Susceptibility data were obtained using Evan's NMR method. For all spectra, CD₃OD was used unless otherwise stated. Spectra were collected using an Agilent 700 MHz NMR spectrometer.

The following equation was used to calculate the molar magnetic susceptibility of all PILS: $\chi_m = (3\Delta f)(4\pi Fc)^{-1}$, where χ_m is molar magnetic susceptibility, Δf is the difference in chemical shift in Hz between the paramagnetic sample dissolved in deuterated solvent and the pure deuterated solvent, F is the frequency of the NMR in Hz, and c is the concentration of the dissolved PIL in mol mL⁻¹.

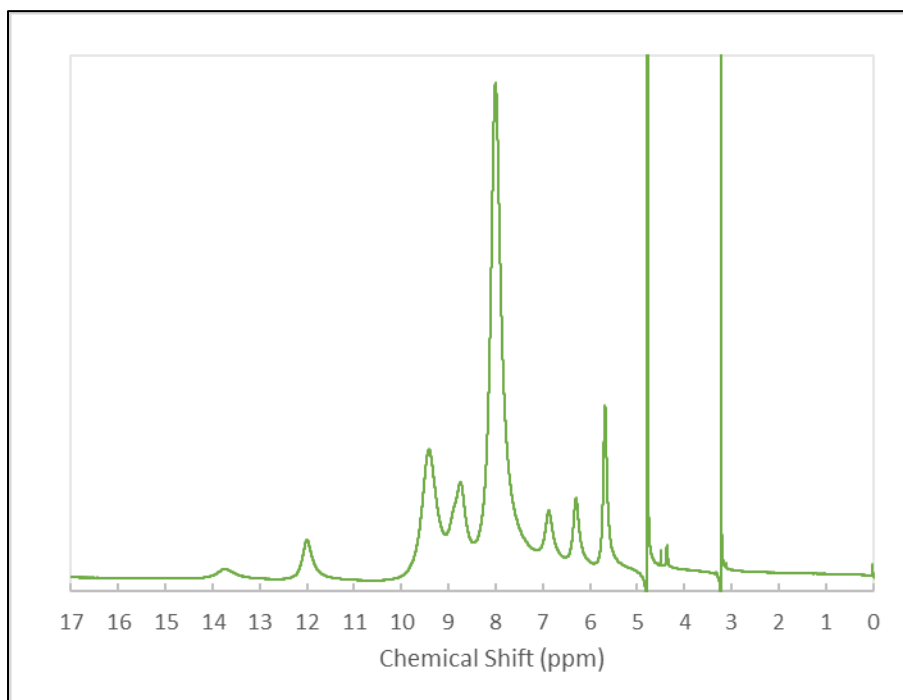


Figure 51. ¹H NMR Spectra of [BMIm][FeCl₄] Standard.

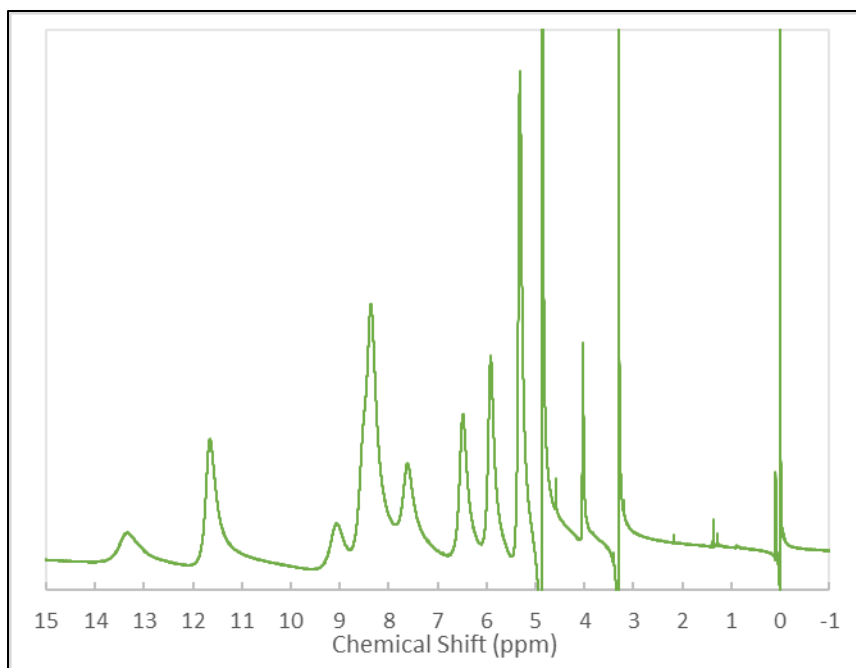


Figure 52. ^1H NMR Spectra of [BMIm][FeCl₄].

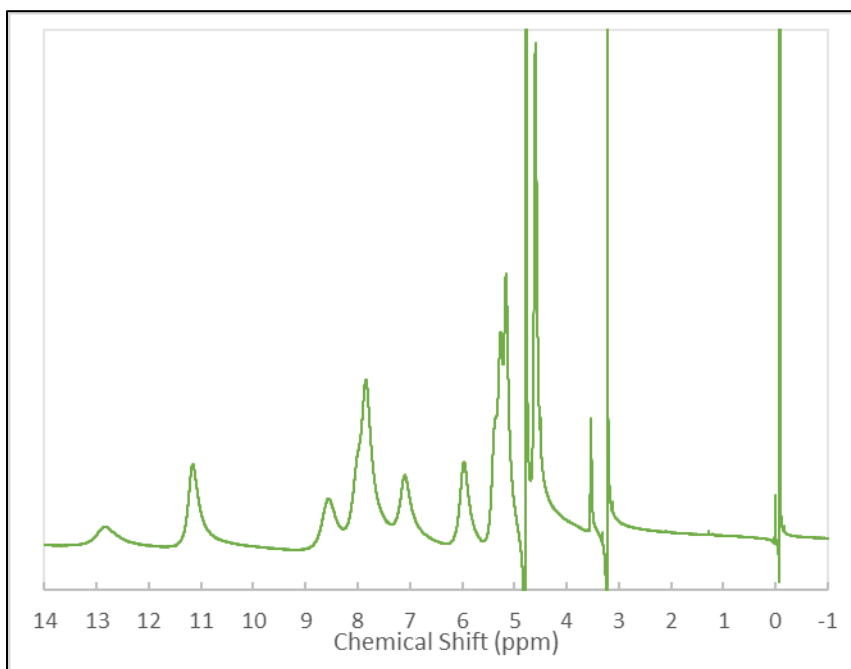


Figure 53. ^1H NMR Spectra of [HMIm][FeCl₄].

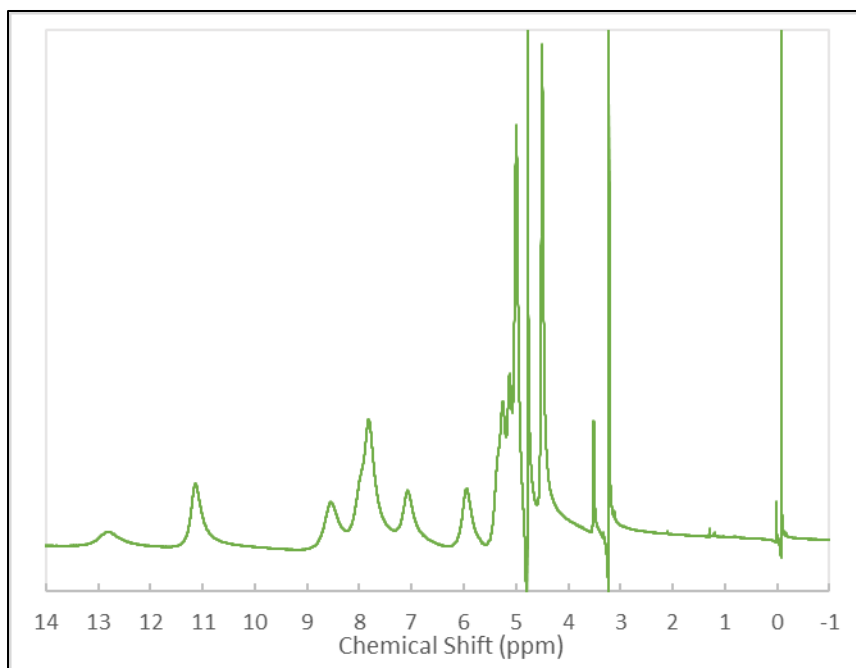


Figure 54. ¹H NMR Spectra of [OMIm][FeCl₄].

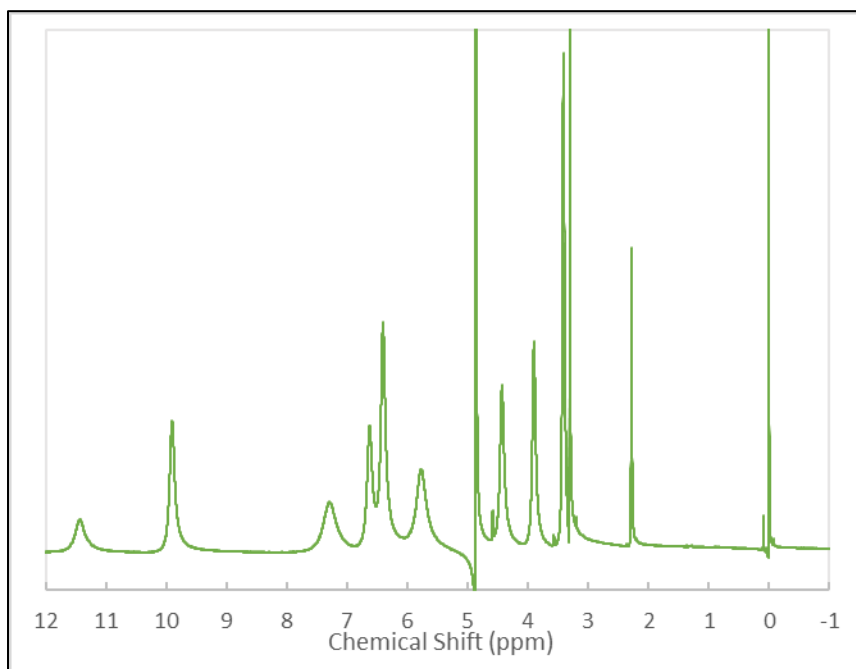


Figure 55. ¹H NMR Spectra of [BMIm][FeBrCl₃].

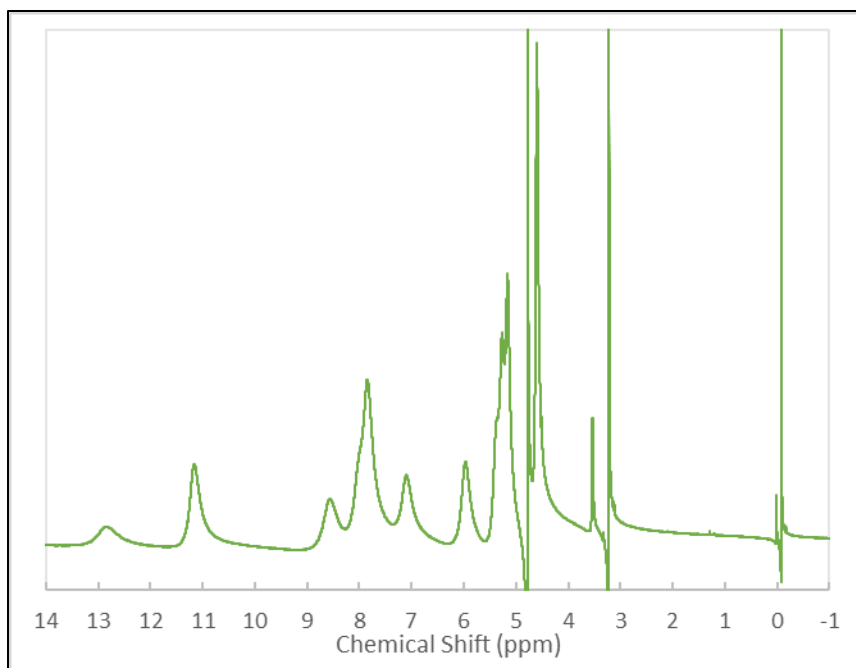


Figure 56. ¹H NMR Spectra of [HMIm][FeBrCl₃].

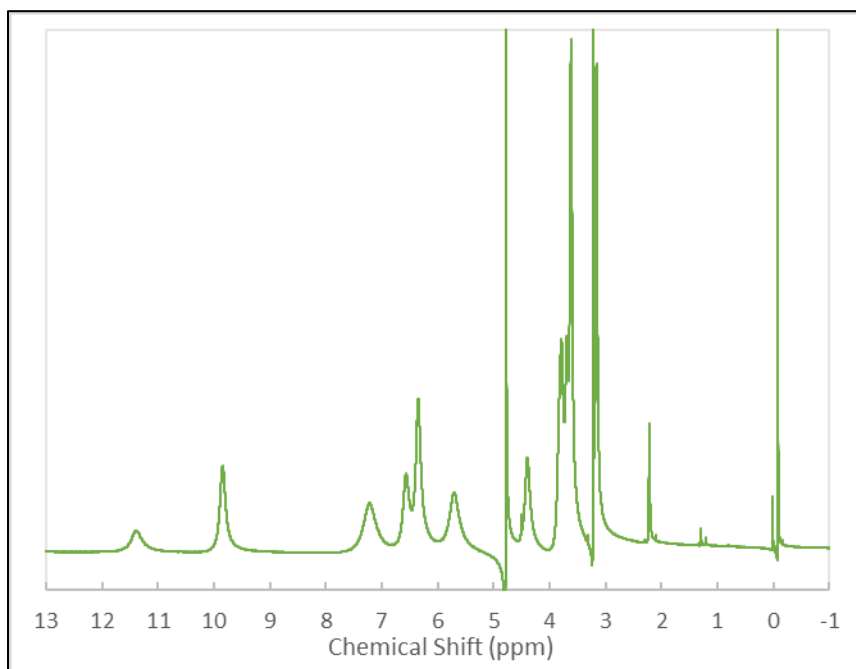


Figure 57. ¹H NMR Spectra of [OMIm][FeBrCl₃].

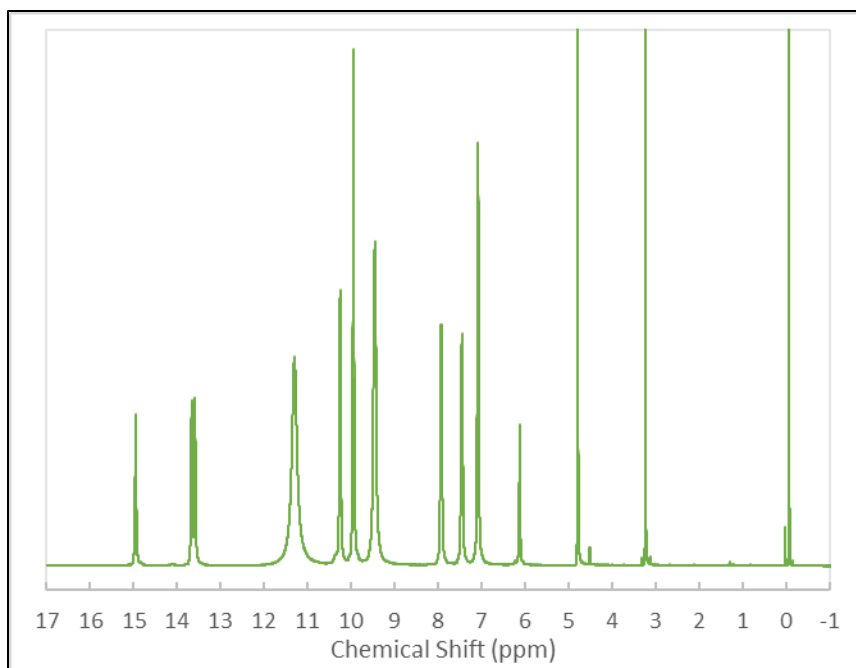


Figure 58. ¹H NMR Spectra of [BMIm][DyCl₄].

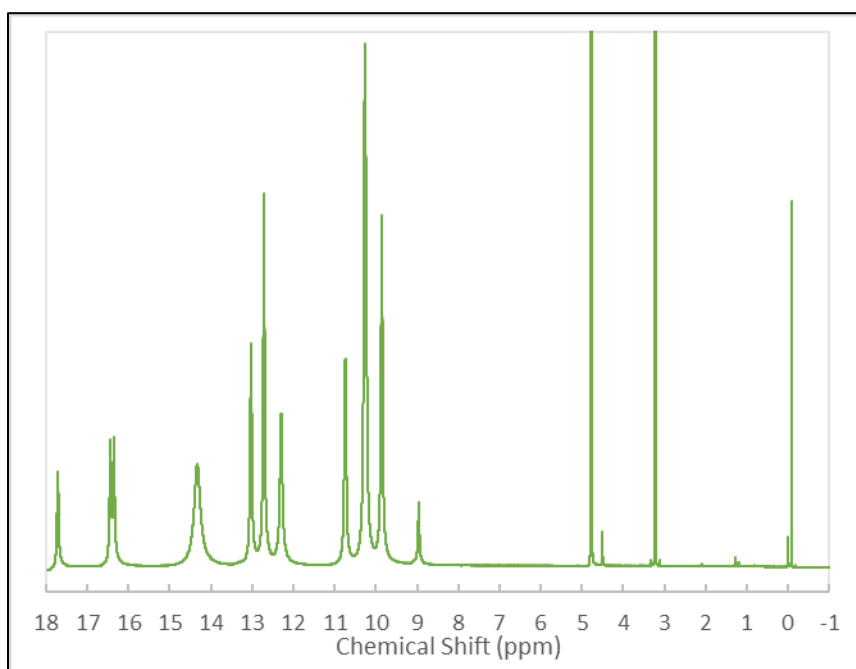


Figure 59. ¹H NMR Spectra of [HMIm][DyCl₄].

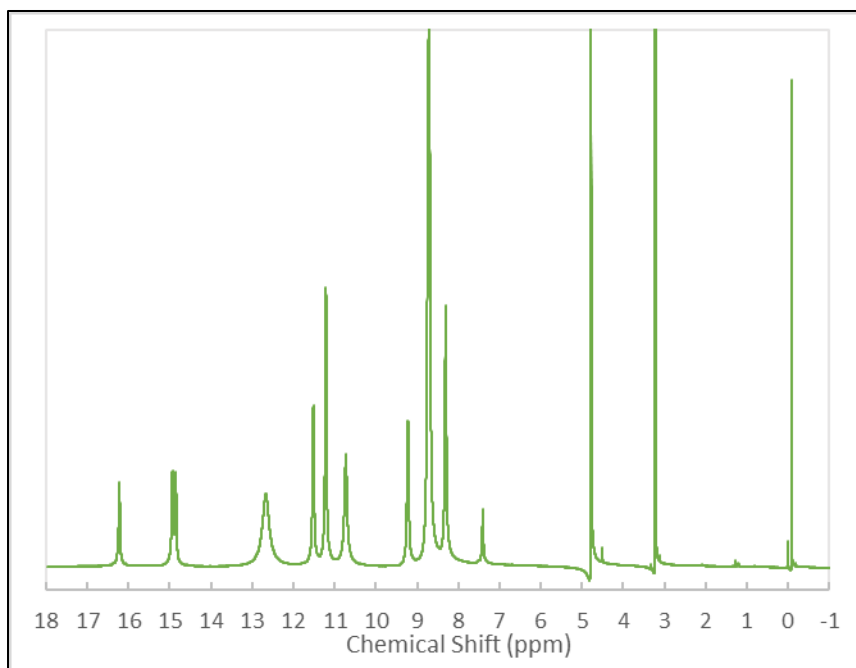


Figure 60. ¹H NMR Spectra of [OMIm][DyCl₄].

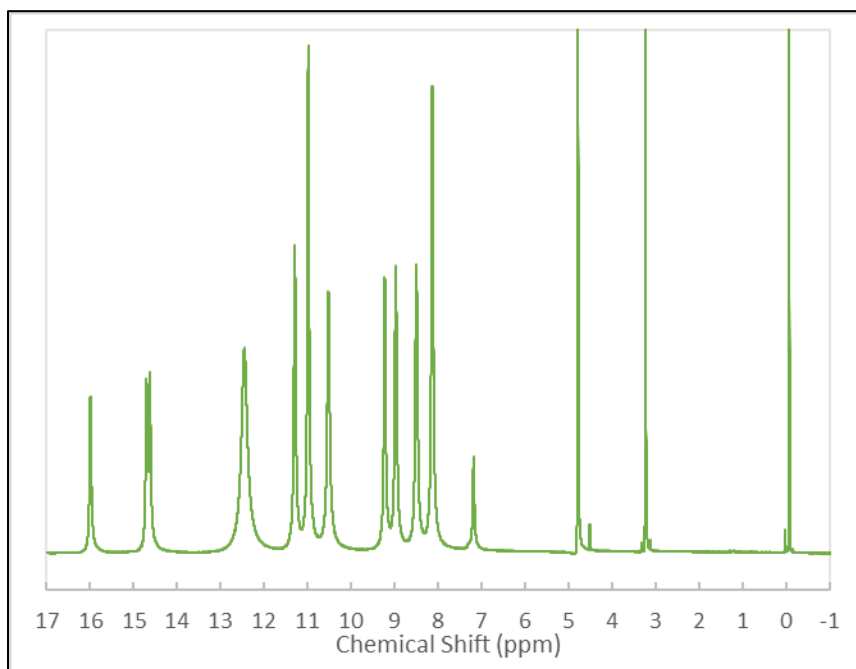


Figure 61. ¹H NMR Spectra of [BMIm][DyBrCl₃].

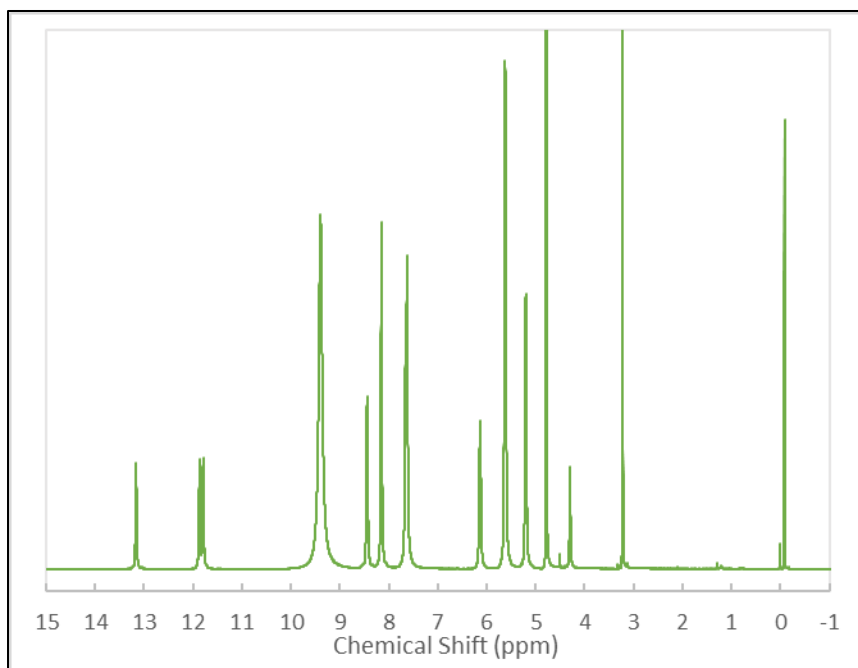


Figure 62. ^1H NMR Spectra of [HMIm][DyBrCl₃].

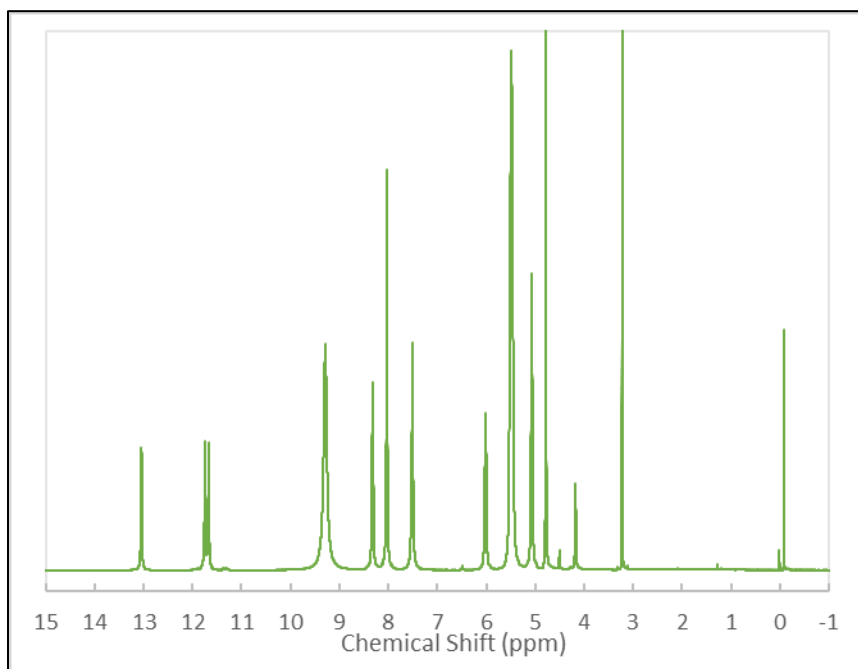


Figure 63. ^1H NMR Spectra of [OMIm][DyBrCl₃].

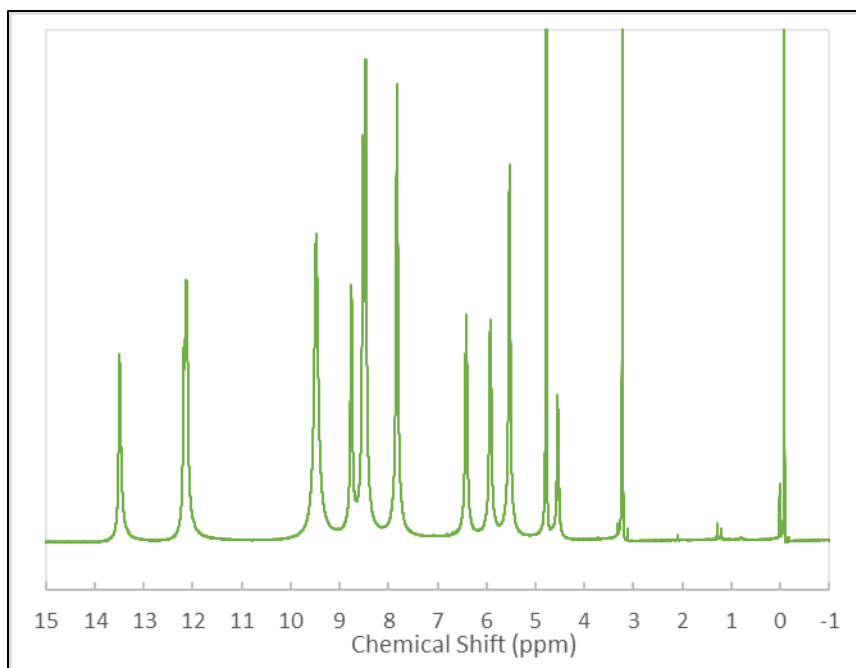


Figure 64. ^1H NMR Spectra of [BMIm][HoCl₄].

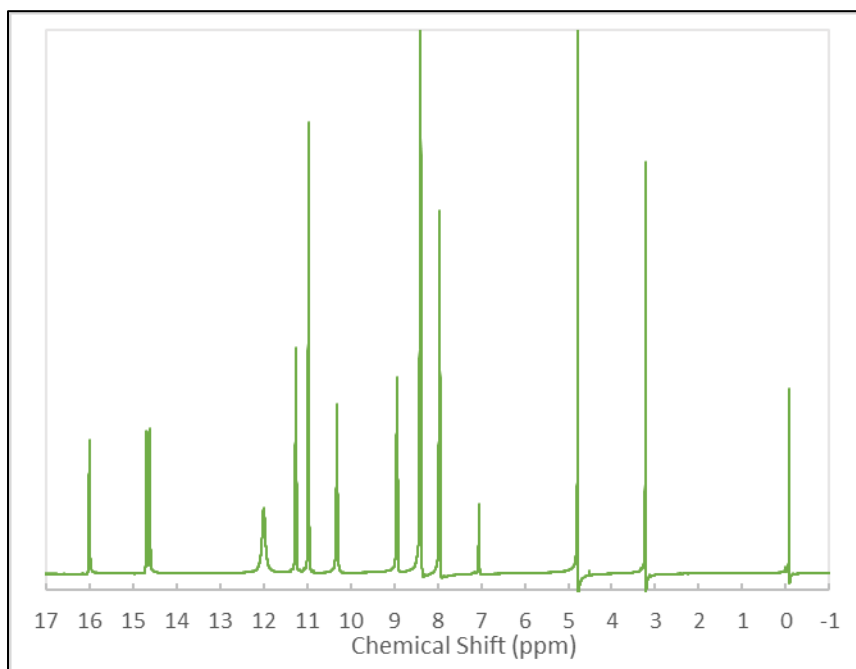


Figure 65. ^1H NMR Spectra of [HMIm][HoCl₄].

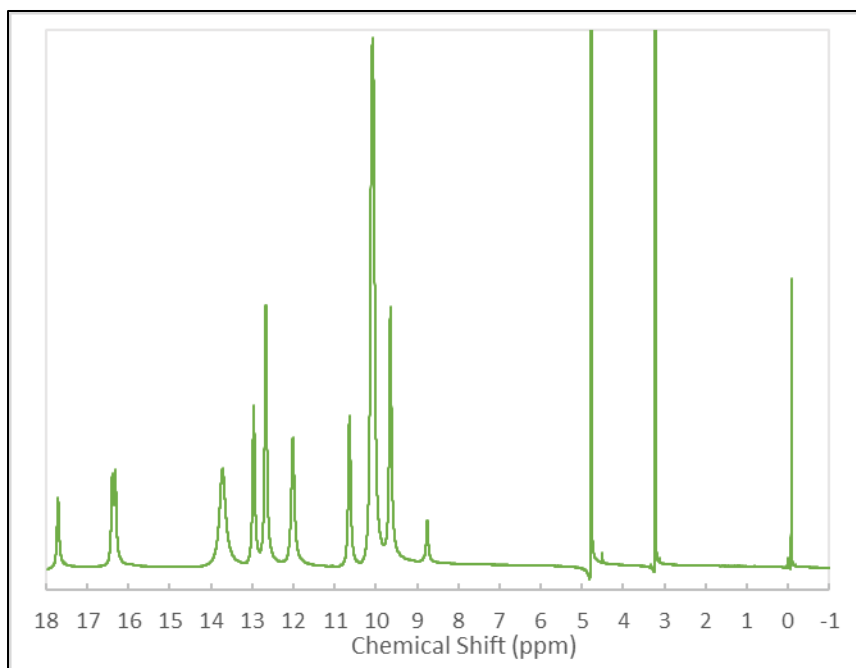


Figure 66. ¹H NMR Spectra of [OMIm][HoCl₄].

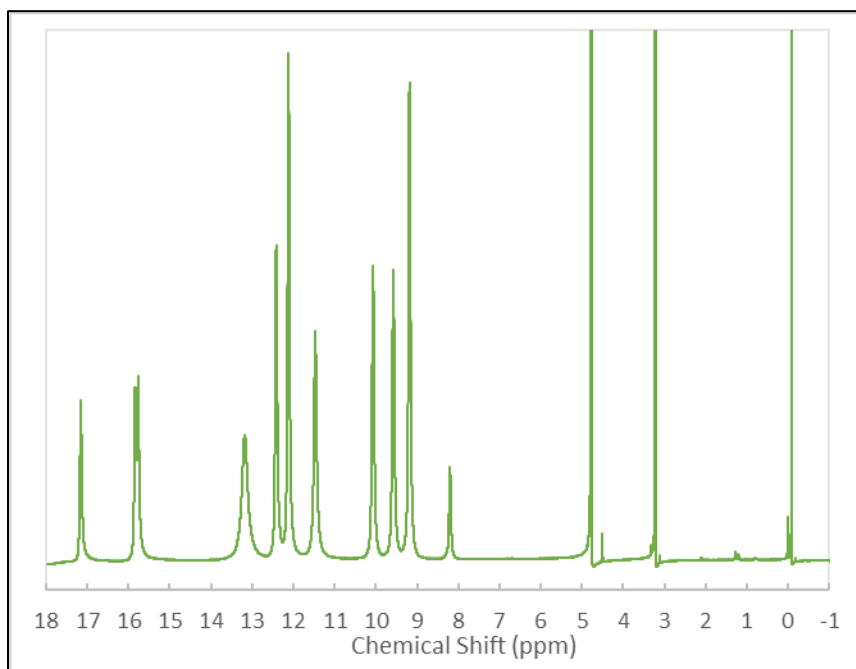


Figure 67. ¹H NMR Spectra of [BMIm][HoBrCl₃].

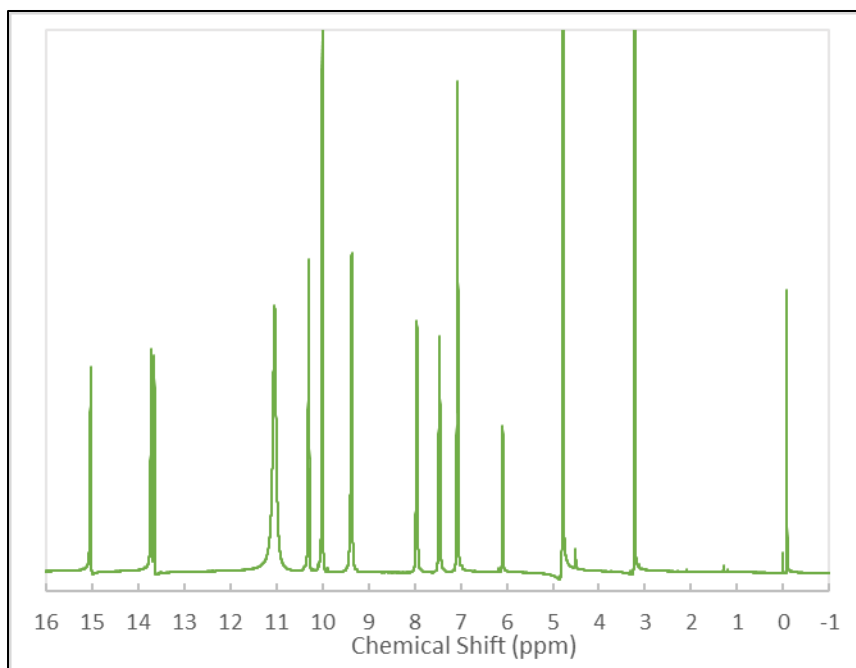


Figure 68. ¹H NMR Spectra of [HMIm][HoBrCl₃].

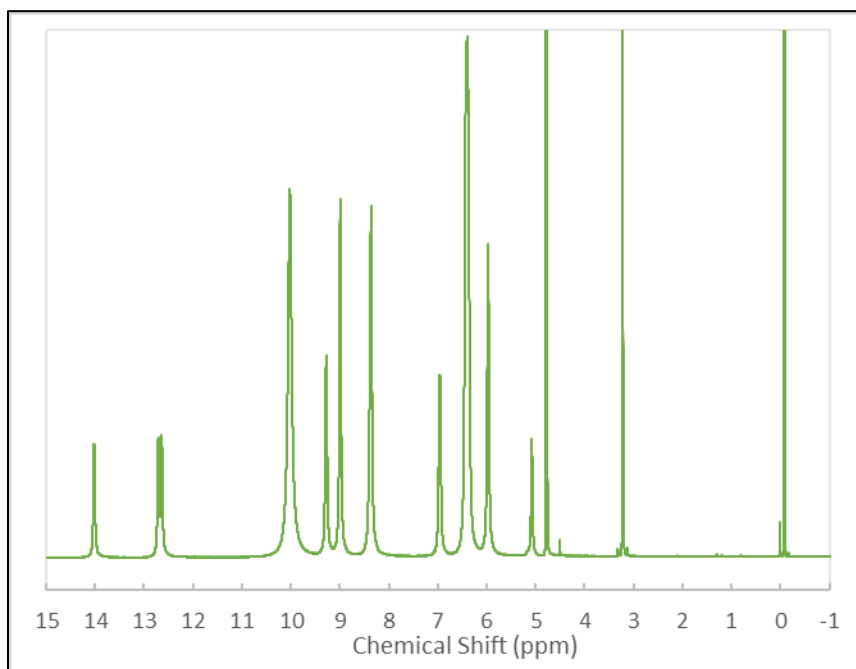


Figure 69. ¹H NMR Spectra of [OMIm][HoBrCl₃].

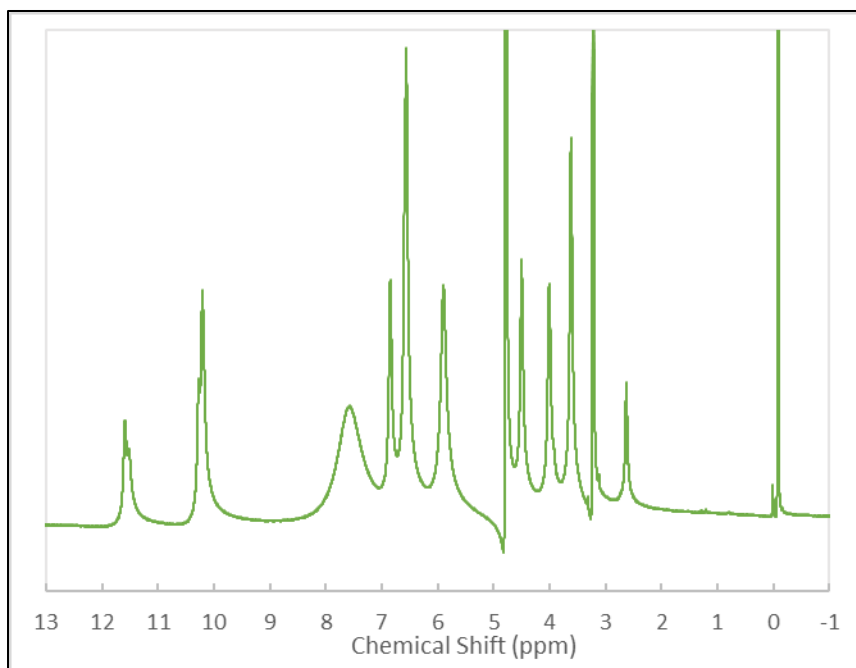


Figure 70. ¹H NMR Spectra of [BMIm][GdCl₄].

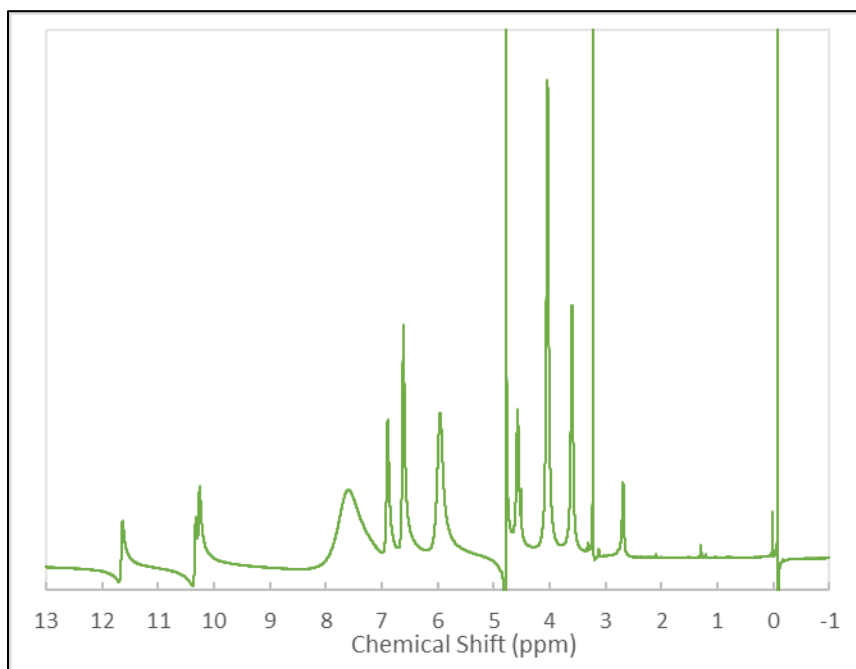


Figure 71. ¹H NMR Spectra of [HMIm][GdCl₄].

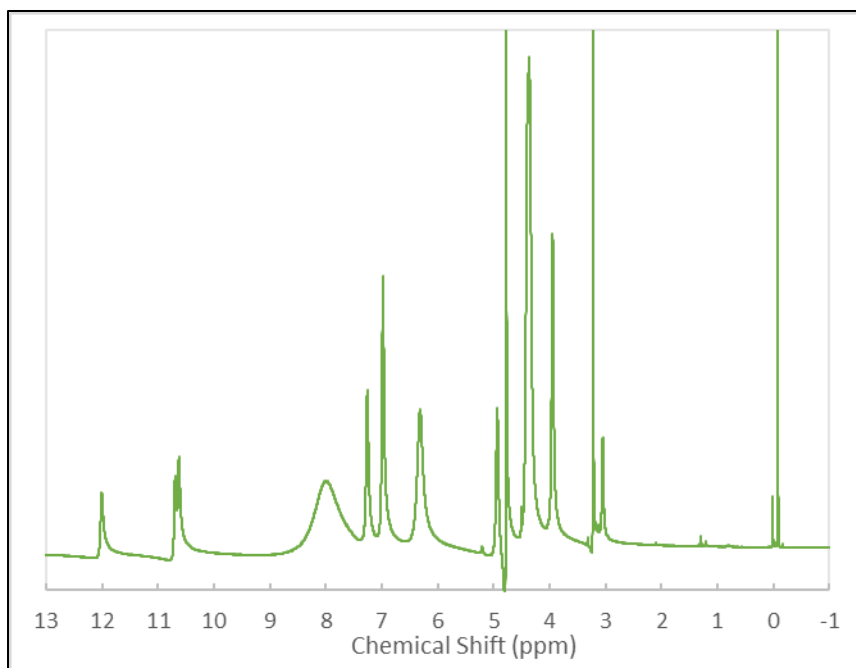


Figure 72. ^1H NMR Spectra of [OMIm][GdCl₄].

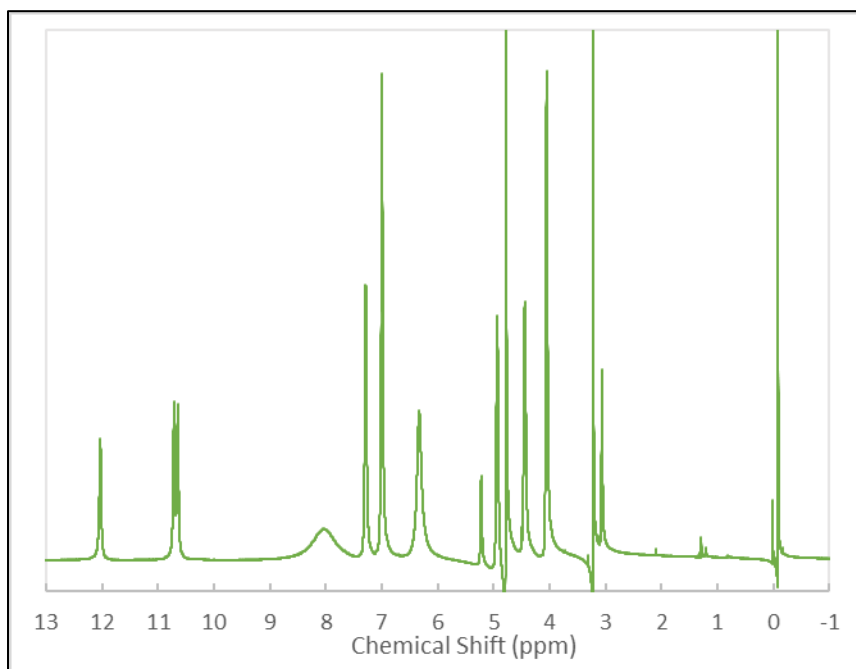


Figure 73. ^1H NMR Spectra of [BMIm][GdBrCl₃].

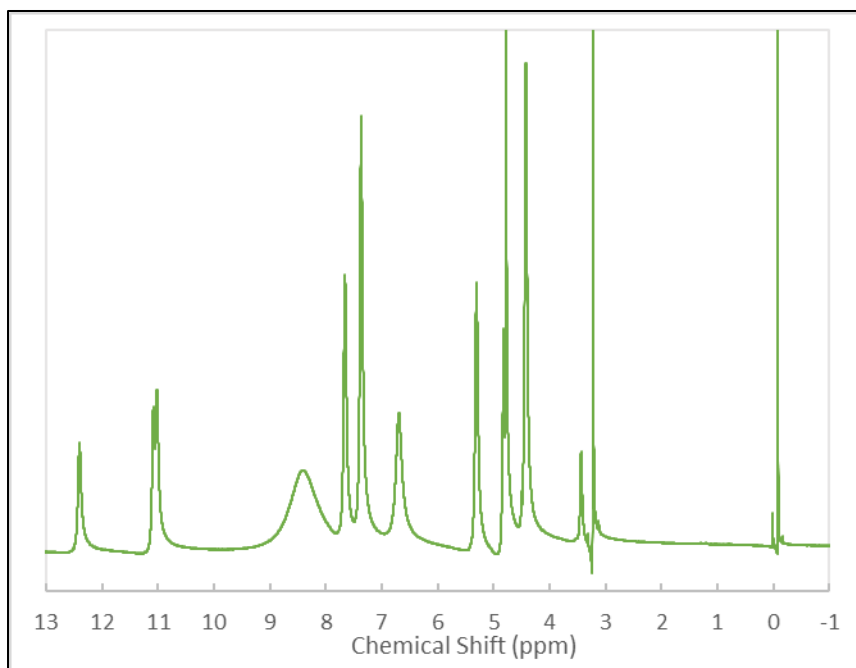


Figure 74. ¹H NMR Spectra of [HMIm][GdBrCl₃].

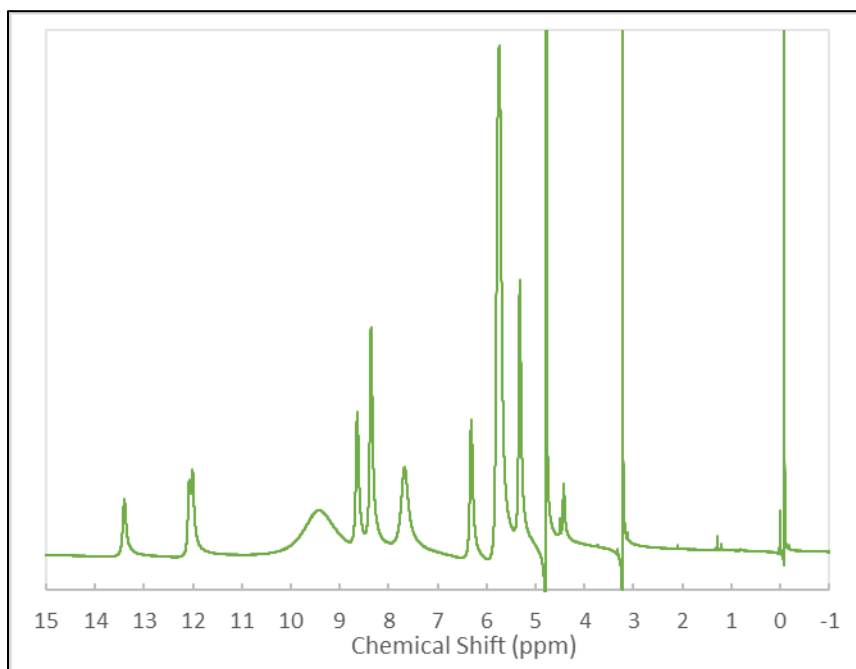


Figure 75. ¹H NMR Spectra of [OMIm][GdBrCl₃].

Table 6. Magnetic Susceptibility Data of all PILs.

Compound	χ_m (cm ³ mol ⁻¹)	Std. Dev. (cm ³ mol ⁻¹)
[BMIm][FeCl ₄] Standard	0.0141	0.0003
[BMIm][FeCl ₄]	0.0146	0.0002
[HMIm][FeCl ₄]	0.0159	0.0003
[OMIm][FeCl ₄]	0.0161	0.0003
[BMIm][FeBrCl ₃]	0.0146	0.0002
[HMIm][FeBrCl ₃]	0.0152	0.0003
[OMIm][FeBrCl ₃]	0.0162	0.0003
[BMIm][DyCl ₄]	0.0210	0.001
[HMIm][DyCl ₄]	0.0244	0.0007
[OMIm][DyCl ₄]	0.0214	0.0007
[BMIm][DyBrCl ₃]	0.0278	0.0007
[HMIm][DyBrCl ₃]	0.0261	0.0007
[OMIm][DyBrCl ₃]	0.0277	0.0007
[BMIm][HoCl ₄]	0.0301	0.0003
[HMIm][HoCl ₄]	0.0427	0.0003
[OMIm][HoCl ₄]	0.0433	0.0003
[BMIm][HoBrCl ₃]	0.0445	0.0004
[HMIm][HoBrCl ₃]	0.0466	0.0004
[OMIm][HoBrCl ₃]	0.0460	0.0003
[BMIm][GdCl ₄]	0.0200	0.0005
[HMIm][GdCl ₄]	0.0274	0.0007
[OMIm][GdCl ₄]	0.0265	0.0008
[BMIm][GdBrCl ₃]	0.0272	0.0006
[HMIm][GdBrCl ₃]	0.0252	0.0006
[OMIm][GdBrCl ₃]	0.0249	0.0007

CHAPTER IV
DISCUSSION AND CONCLUSION

4.1. Discussion

4.1.1. FTIR

Examining the 1-alkyl-3-methylimidazolium halide FTIR spectrums, there are many representative peaks of the imidazolium ring structure and aliphatic carbon chains. Short, broad peaks at 3300-3400 cm^{-1} are representative of O-H bond stretching in water. Large, sharp peaks at 3100 cm^{-1} are representative of alkene C-H sigma bond stretching in the imidazolium ring. The medium, sharp peaks at 2840-3000 cm^{-1} are representative of the aliphatic C-H sigma bond stretches of the alkyl chain attached to the imidazolium heterocyclic ring. Notably, these peaks increase in size as the alkyl chain increases from butyl to octyl functional groups. Moreover, the peaks around 2840-2871 cm^{-1} represent the C-H bond stretching on the methyl group attached to the tertiary amine of the imidazolium heterocyclic ring. The sharp, medium peaks at 1610-1637 cm^{-1} are representative of the C=C double bond stretches of the imidazolium heterocyclic ring. Next, to this peak, there is a discernable sharp, medium peak at 1565-1566 cm^{-1} which is representative of in-plane ring vibrations as a result of the sigma and pi bond stretches. Sharp, small peaks at 1462 cm^{-1} represent C-H bond bending of the methyl group attached to the imidazolium heterocyclic ring. The large, sharp peaks at 1162 cm^{-1} are representative of the C-N sigma bond stretching of the imidazolium ring.

4.1.2. TGA

Examining the thermal curves from the 1-alkyl-3-methylimidazolium halide ILs, high thermal stability is observed in the range of 202-255 °C. Notably, there is an observable trend in increasing thermal stability for the 1-alkyl-3-methylimidazolium chloride ILs as alkyl chain length increases from butyl to octyl functional groups. There was no significant trend observed for increasing alkyl chain length for the 1-alkyl-3-methylimidazolium bromide ILs. However, the ILs with bromine anions demonstrated higher thermal stability between 251-255 °C compared to chloride anions which had thermal stabilities between 202-230 °C.

The iron-based, dysprosium-based, holmium-based, and gadolinium-based PILs all demonstrated high thermal stability in the range of 278-389 °C. This was exciting to discover that the PILs demonstrated higher thermal stability compared to the alkylimidazolium halide ILs. There was no significant trend of thermal stability between the PILs containing a different metal in the anion. However, a trend of alkyl chain length is easily observed. The highest thermal stabilities were associated with PILs that contained a butyl alkyl chain attached to the imidazolium ring with the exception of the 1-alkyl-3-methylimidazolium tetrachlorogadolate(iii) PILs. Like the 1-alkyl-3-methylimidazolium bromide ILs, there is an observable trend of increasing thermal stability with increasing alkyl chain length associated with the 1-alkyl-3-methylimidazolium tetrachlorogadolate(iii) PILs.

Notably, we believe the lanthanide PILs to be hydrated. Examining the thermal curves of dysprosium, holmium, and gadolinium, respectively, we see water tightly bound

to the PILs until 150-200 °C. Upon heating above 200 °C, we see nice plateaus which indicate the dehydrated PILs before thermal degradation. The 5 wt.% degradation was calculated based upon the plateaus in the thermal curves after the PILs were dehydrated. Using the water mass loss, the moles of hydrate content was calculated and furthered verified by EA.

Table 7. Moles of Hydrate in Lanthanide PILs.

Compound	Hydrate (mol)
[BMIm][DyCl ₄]	3
[HMIm][DyCl ₄]	2
[OMIm][DyCl ₄]	2
[BMIm][DyBrCl ₃]	4
[HMIm][DyBrCl ₃]	5
[OMIm][DyBrCl ₃]	4
[BMIm][HoCl ₄]	0
[HMIm][HoCl ₄]	4
[OMIm][HoCl ₄]	2
[BMIm][HoBrCl ₃]	4
[HMIm][HoBrCl ₃]	3
[OMIm][HoBrCl ₃]	5
[BMIm][GdCl ₄]	2
[HMIm][GdCl ₄]	6
[OMIm][GdCl ₄]	5
[BMIm][GdBrCl ₃]	2
[HMIm][GdBrCl ₃]	6
[OMIm][GdBrCl ₃]	5

4.1.3. NMR

Examining the ¹H NMR spectrums of the 1-alkyl-3-methylimidazolium halide ILs we observe spectrums which are confirmed by literature. A characteristic triplet is observed at 0.7720-0.8894 ppm and represents a methyl group. The integration gives three protons as expected. Characteristic sextets are observed for the ILs containing butyl-chains and

characteristic multiplets are observed for the ILs containing hexyl- and octyl-chains, respectively, at chemical shifts of 1.2043-1.3242 ppm.

These represent the methylene groups closest to the methyl functional group in the aliphatic alkyl chain attached to the imidazolium heterocyclic ring. Integration of the sextet results in two protons for the two ILs with butyl chains. Integration of the multiplets results in six protons for the two ILs with hexyl chains and 10 protons for the two ILs with octyl chains, respectively. A characteristic quintet is observed at 1.7791-1.8489 ppm is observed for the methylene group closer to the imidazolium ring. Integration of these peaks results in two protons for all 1-alkyl-3-methylimidazolium halide ILs. A characteristic singlet is observed at 4.0040-4.0719 ppm for the methyl group that is attached to the tertiary amine of the imidazolium heterocyclic ring. Integration of this peak results in three protons for all 1-alkyl-3-methylimidazolium halide ILs.

A characteristic triplet is observed at 4.2127-4.2843 ppm representing the methylene group which is directly attached to the tertiary amine of the imidazolium heterocyclic ring. Integration of this peak results in two protons. A virtual triplet is observed at 7.3846-7.4697 and 7.5906-7.6271 ppm, respectively. These virtual triplets represent the two methine groups that make up the C=C alkene bond in the imidazolium heterocyclic ring. The virtual triplet arises from delocalized coupling with the methine group that is bonded to both tertiary amines in the imidazolium heterocyclic ring. Without this coupling effect, a doublet would have been observed. Integration of both these peaks results in one proton, respectively. The characteristic singlet at 10.2577-10.5846 ppm

represents the methine group which is bonded to both tertiary amines in the imidazolium heterocyclic ring. The integration for this peak results in one proton.

The ^{13}C NMR spectra of the 1-alkyl-3-methylimidazolium halides further verify the structures of these PILs. From the spectra, we observe 8, 10, and 12 carbon peaks for the 1-butyl-, 1-hexyl-, and 1-octyl-3-methylimidazolium halides, respectively. The three carbons on the imidazolium heterocyclic rings are found at 137-138, 122-123, and 121-122 ppm, respectively. The peak at 137-138 ppm represents the N-C-N carbon in the imidazolium ring. The peaks at 122-123 and 121-122 ppm for each spectrum, respectively, represent the C=C alkene carbons. The peak shifted more downfield at 122-123 ppm is representative of the carbon which is closest to the methyl group on the imidazolium ring while the peak at 121-122 ppm is representative of the carbon closest to the alkyl chain attached to the imidazolium ring. The carbon peak at 49-50 ppm for each spectrum, respectively, is representative of the methylene carbon on the alkyl chain that is attached to the nitrogen of the imidazolium ring. The carbon peak at 36 ppm for each spectrum, respectively, is representative of the methyl group attached to the imidazolium ring. For the 1-butyl-3-methylimidazolium halides, we see the alkyl chain methylene carbon peaks at 32 and 19 ppm, respectively, and the alkyl chain methyl carbon peak at 13 ppm. For the 1-hexyl-3-methylimidazolium halides, we see the alkyl chain methylene carbon peaks at 31, 30, 25, and 22 ppm, respectively, and the alkyl chain methyl carbon peak at 14 ppm. For the 1-octyl-3-methylimidazolium halides, we see the alkyl chain methylene carbon peaks at 31, 30, 29, 28, 26, and 22 ppm, respectively, and the alkyl chain methyl carbon peak at 14 ppm.

4.1.4. Evan's Method

The Evan's method is a simple, quick, and cheap method to measure the molar magnetic susceptibility of paramagnetic compounds.⁶⁵⁻⁶⁸ After the determination of the molar magnetic susceptibility, the number of unpaired electrons of the metal complex may be determined. This is useful to establish structure-property relationships of the metal complex. Moreover, the oxidation state of the metal species and the electron population of the metals molecular orbital may also be determined. Evan's method is performed using an auxiliary capillary insert and an NMR tube. The auxiliary insert, containing pure deuterated solvent, is inserted into the NMR tube and acts as an internal reference. The NMR tube contains the paramagnetic compound dissolved in the same deuterated solvent. After running a ¹H NMR experiment, the difference in chemical shift between the pure and non-pure solvent may be used to determine the molar magnetic susceptibility using the equation: $\chi_m = (3\Delta f)(4\pi Fc)^{-1}$.

When performing Evan's method, one should be careful not to overfill the NMR tube so that the solution spills out when the auxiliary tube is inserted. Furthermore, to calculate the molar magnetic susceptibility accurately, the concentration of the paramagnetic species should be calculated quantitatively. This may be done practically by weighing the mass of the paramagnetic sample, by weighing the mass of deuterated solvent drawn into a syringe, and by using a temperature-dependent density calculation to determine the volume of solvent drawn into the syringe. Typically, ~15 mg of the paramagnetic sample is sufficient for accurate determination.

In general, for NMR experiments on paramagnetic species, the coordination of elements to a paramagnetic metal causes peak broadening. Normally, this would not influence the integration value of a chemical shift, but the paramagnetic metal also causes nearby protons to relax faster than normal, compared to protons further away from the metal center. This distortion of proton relaxation near the metal results in major peak broadening and skews the integration value of ^1H NMR on paramagnetic species compared to ^1H NMR on non-paramagnetic species. Integration is not useful for NMR on paramagnetic species and the spectrums of ^1H experiments should be considered as qualitative results instead of quantitative results. However, as discussed previously, useful data may still be obtained from proton NMR of paramagnetic samples.

After performing Evan's method, the difference in chemical shift between the pure and non-pure solvent peaks may be hard to identify upon examining the proton spectra. To overcome this challenge, a small amount of protonated solvent (roughly 30 μL) may be added to the paramagnetic deuterated solution. Following this step, a clear increase in the peak height of the shifted solvent peak from the paramagnetic solution is elucidated. This allows for accurate determination of the molar magnetic susceptibility. Another solution to overcome this challenge is to increase the concentration of the paramagnetic solution. This causes an increase in the chemical shift between the pure and non-pure solvent and makes the determination of the solvent peak from the paramagnetic solution discernable.

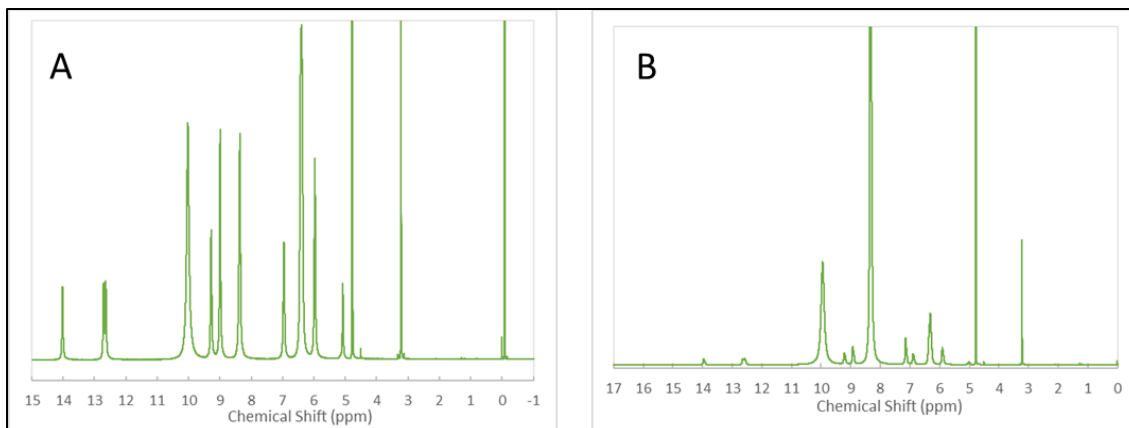


Figure 76. Elucidation of Solvent Chemical Shift: a) [OMIm][HoBrCl₃] and b) [OMIm][HoBrCl₃] with 30 μ L anhyd. MeOH addition.

Examining the NMR spectra taken for the iron PILs, peak broadening and peak overlap are observed. Mainly, sharp and broad peaks of medium height are observed. Clearly, large and sharp methanol and TMS reference peaks are observed at 4.78, 3.22, and 0 ppm, respectively. Examining the NMR spectra of the dysprosium and holmium PILs, there are mainly tall and sharp singlets. However, one doublet is resolved as the second-farthest peak that is shifted downfield. This doublet is not resolved for the iron species ¹H NMR spectra. Although coupling resonance between peaks is not quantifiable for proton NMR of paramagnetic species, we believe the doublet and singlet shifted furthest downfield are due to the protons of the imidazolium heterocyclic ring. This applies to the farthest downshifted singlets observed from the iron PILs ¹H NMR spectra.

Examining the ¹H NMR spectra of the gadolinium PILs, differences in the proton spectra are observed when compared to the spectra of the dysprosium and holmium PILs. For instance, one noticeably short and broad peak appears, and the resolved doublet observed in the dysprosium and holmium spectra is not as well-resolved in the gadolinium

spectra. This may be due to an increased attractiveness between the gadolinium ion and imidazolium heterocyclic ring.

From the determination of the molar magnetic susceptibility, the holmium-based PILs have the highest molar magnetic susceptibility while the dysprosium- and gadolinium-based PILs have relatively similar molar magnetic susceptibilities. The iron-based PILs exhibit the lowest magnetic susceptibility.

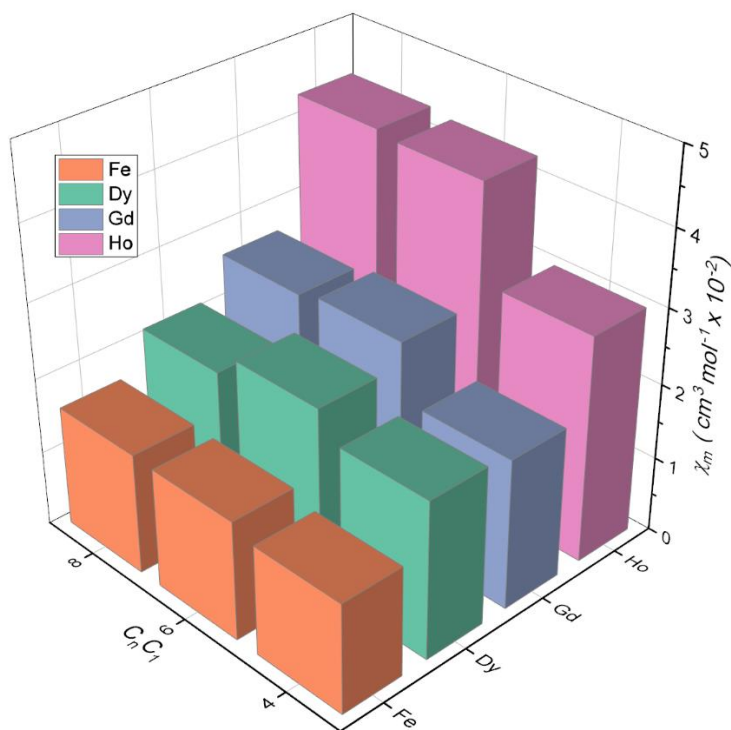


Figure 77. Molar Magnetic Susceptibility of Tetrachloro-Halide PILs.

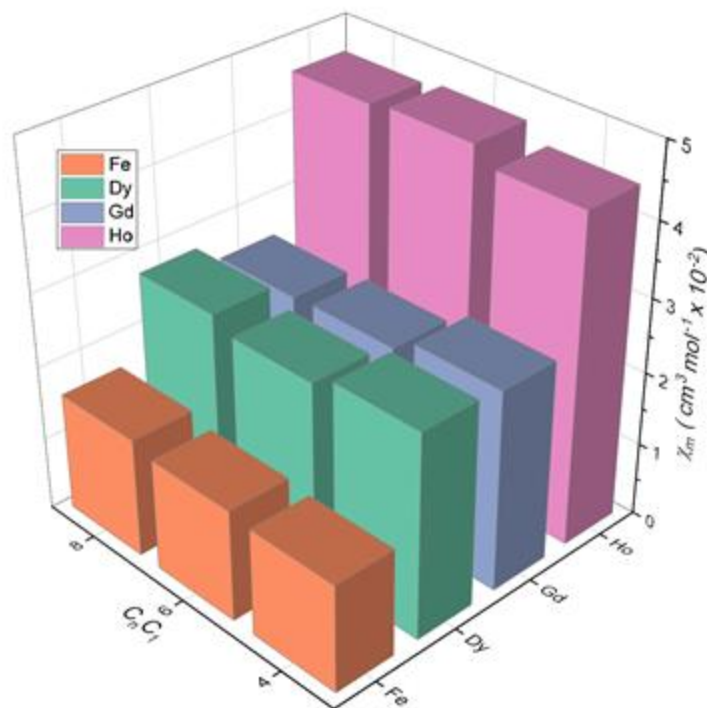


Figure 78. Molar Magnetic Susceptibility of Bromotrichloro-Halide PILs.

4.2. Conclusion

The goal of this project was to synthesize a series of lanthanide paramagnetic ionic liquids and measure their molar magnetic susceptibilities. The PILs with the highest molar magnetic susceptibility would be then investigated for CO₂ adsorption properties in future work. We believe the lanthanide-containing PILs to be hydrated due to TGA thermal curves and evidence from EA. Herein, 18 novel lanthanide-based PILs and six iron-based PILs were synthesized and characterized by EA, FTIR spectroscopy, TGA, NMR spectroscopy, and Evan's method. The molar magnetic susceptibility of 1-butyl-3-methylimidazolium tetrachloroferrate(iii) synthesized in lab and bought from TCI America was determined to be 0.0146 ± 0.0002 and 0.0141 ± 0.0003 , respectively. These values

were in good agreement from those in literature with values near 0.014.^{69, 70} The molar magnetic susceptibilities of the holmium-based PILs were found to be the highest.

Table 8. Summary of PILs Physical Properties.

Compound	χ_m (cm ³ mol ⁻¹)	Hydrates	5 wt.% Thermal Degradation
[BMIm][FeCl ₄] Standard	0.0141 ± 0.0003	-	-
[BMIm][FeCl ₄]	0.0146 ± 0.0002	0	289
[HMIm][FeCl ₄]	0.0159 ± 0.0003	0	320
[OMIm][FeCl ₄]	0.0161 ± 0.0003	0	288
[BMIm][FeBrCl ₃]	0.0146 ± 0.0002	0	315
[HMIm][FeBrCl ₃]	0.0152 ± 0.0003	0	307
[OMIm][FeBrCl ₃]	0.0162 ± 0.0003	0	300
[BMIm][DyCl ₄]	0.021 ± 0.001	3	349
[HMIm][DyCl ₄]	0.0244 ± 0.0007	2	363
[OMIm][DyCl ₄]	0.0214 ± 0.0007	2	322
[BMIm][DyBrCl ₃]	0.0278 ± 0.0007	4	389
[HMIm][DyBrCl ₃]	0.0261 ± 0.0007	5	321
[OMIm][DyBrCl ₃]	0.0277 ± 0.0007	4	303
[BMIm][HoCl ₄]	0.0301 ± 0.0003	0	285
[HMIm][HoCl ₄]	0.0427 ± 0.0003	4	278
[OMIm][HoCl ₄]	0.0433 ± 0.0003	2	349
[BMIm][HoBrCl ₃]	0.0445 ± 0.0004	4	346
[HMIm][HoBrCl ₃]	0.0466 ± 0.0004	3	333
[OMIm][HoBrCl ₃]	0.0460 ± 0.0003	5	326
[BMIm][GdCl ₄]	0.0200 ± 0.0005	2	326
[HMIm][GdCl ₄]	0.0274 ± 0.0007	6	351
[OMIm][GdCl ₄]	0.0265 ± 0.0008	5	373
[BMIm][GdBrCl ₃]	0.0272 ± 0.0006	2	349
[HMIm][GdBrCl ₃]	0.0252 ± 0.0006	6	321
[OMIm][GdBrCl ₃]	0.0249 ± 0.0006	5	335

4.3. Future Work

Future work includes characterization using DSC, obtaining crystal structures, obtaining density values, conducting preliminary CO₂ adsorption measurements, determining viscosities of degassed and gassed PILs. Furthermore, to decrease viscosity and increase CO₂ adsorption capacity, synthesis of imidazolium cations containing fluorinated and perfluorinated alkyl chains will be done. The FPILs will receive the same characterization and their molar magnetic susceptibilities will be compared to the PILs synthesized for this thesis. To compare different methods of measuring magnetic susceptibility, we will use SQUID to measure the molar magnetic susceptibility of all PILs synthesized.

REFERENCES

1. Welton, T., Ionic liquids: a brief history. *Biophys Rev* **2018**, *10* (3), 691-706.
2. Freemantle, M., DESIGNER SOLVENTS - Ionic liquids may boost clean technology development. *Chem. Eng. News* **1998**, *76* (13), 32-37.
3. Carmichael, A. J.; Seddon, K. R., Polarity study of some 1-alkyl-3-methylimidazolium ambient-temperature ionic liquids with the solvatochromic dye, Nile Red. *Journal of Physical Organic Chemistry* **2000**, *13* (10), 591-595.
4. Walden, P., Molecular weights and electrical conductivity of several fused salts. *Bull. Acad. Imp. Sci. St. Petersburg* **1914**, *8*, 405.
5. Graenacher, C. Cellulose Solution. U.S. Patent 1,943,176, Jan. 9th 1934.
6. Hurley, F. H. Electrodeposition of Aluminum. U.S. Patent 2,446,331, Aug. 3rd, 1948.
7. Wier, T. P. H., F. H. Electrodeposition of Aluminum. U.S. Patent 2,446,349, Aug. 3rd, 1948.
8. Robinson, J. O., R. A., An electrochemical and spectroscopic study of some aromatic hydrocarbons in the room temperature molten salt system aluminum chloride-n-butylpyridinium chloride. *J. Am. Chem. Soc.* **1979**, *101* (2), 323-327.
9. Wilkes, J. S. L., J. A.; Wilson, R. A.; Hussey, C. L., Dialkylimidazolium chloroaluminate melts: a new class of room-temperature ionic liquids for electrochemistry, spectroscopy and synthesis. *Inorganic Chemistry* **1982**, *21* (3), 1263-1264.
10. Dieter, K. M.; Dymek, C. J.; Heimer, N. E.; Rovang, J. W.; Wilkes, J. S., Ionic structure and interactions in 1-methyl-3-ethylimidazolium chloride-aluminum chloride molten salts. *J. Am. Chem. Soc.* **1988**, *110* (9), 2722-2726.
11. Tait, S.; Osteryoung, R. A., Infrared study of ambient-temperature chloroaluminates as a function of melt acidity. *Inorganic Chemistry* **1984**, *23* (25), 4352-4360.
12. Lungwitz, R.; Spange, S., Determination of hydrogen-bond-accepting and -donating abilities of ionic liquids with halogeno complex anions by means of ¹H NMR spectroscopy. *Chemphyschem* **2012**, *13* (7), 1910-6.

13. Hunt, P. A., Quantum Chemical Modeling of Hydrogen Bonding in Ionic Liquids. *Top Curr Chem (Cham)* **2017**, *375* (3), 59.
14. Elaiwi, A.; Hitchcock, P. B.; Seddon, K. R.; Srinivasan, N.; Tan, Y.-M.; Welton, T.; Zora, J. A., Hydrogen bonding in imidazolium salts and its implications for ambient-temperature halogenoaluminate(III) ionic liquids. *Journal of the Chemical Society, Dalton Transactions* **1995**, (21), 3467-3472.
15. Pacholec, F.; Butler, H. T.; Poole, C. F., Molten organic salt phase for gas-liquid chromatography. *Anal. Chem.* **2002**, *54* (12), 1938-1941.
16. Harris, T. V. D., M.; Elomari, S.; Timken, H-K. C. Alkylation Process Using An Alkyl Halide Promoted Ionic Liquid Catalyst. US Patent 7,531,707, May 12th, 2009.
17. Kusters, J.; Schonhoff, M.; Stolwijk, N. A., Mass and Charge Transport in the Polymer-Ionic-Liquid System PEO-EMIml: From Ionic-Liquid-in-Polymer to Polymer-in-Ionic-Liquid Electrolytes. *J Phys Chem B* **2015**, *119* (17), 5693-700.
18. Lozano, L. J.; Godínez, C.; de los Ríos, A. P.; Hernández-Fernández, F. J.; Sánchez-Segado, S.; Alguacil, F. J., Recent advances in supported ionic liquid membrane technology. *Journal of Membrane Science* **2011**, *376* (1), 1-14.
19. Uchida, Y.; Oki, S.; Tamura, R.; Sakaguchi, T.; Suzuki, K.; Ishibashi, K.; Yamauchi, J., Electric, electrochemical and magnetic properties of novel ionic liquid nitroxides, and their use as an EPR spin probe. *Journal of Materials Chemistry* **2009**, *19* (37).
20. Cui, G.; Wang, J.; Zhang, S., Active chemisorption sites in functionalized ionic liquids for carbon capture. *Chem Soc Rev* **2016**, *45* (15), 4307-39.
21. Martins, I. C. B.; Gomes, J. R. B.; Duarte, M. T.; Mafra, L., Understanding Polymorphic Control of Pharmaceuticals Using Imidazolium-Based Ionic Liquid Mixtures as Crystallization Directing Agents. *Crystal Growth & Design* **2017**.
22. Sharma, R. K.; Chouryal, Y. N.; Chaudhari, S.; Saravanakumar, J.; Dey, S. R.; Ghosh, P., Adsorption-Driven Catalytic and Photocatalytic Activity of Phase Tuned In₂S₃ Nanocrystals Synthesized via Ionic Liquids. *ACS Applied Materials & Interfaces* **2017**, *9* (13), 11651-11661.
23. Itoh, T., Ionic Liquids as Tool to Improve Enzymatic Organic Synthesis. *Chem Rev* **2017**, *117* (15), 10567-10607.
24. Zhang, J.; Wu, J.; Yu, J.; Zhang, X.; He, J.; Zhang, J., Application of ionic liquids for dissolving cellulose and fabricating cellulose-based materials: state of the art and future trends. *Materials Chemistry Frontiers* **2017**, *1* (7), 1273-1290.

25. Amiril, S. A. S.; Rahim, E. A.; Syahrullail, S., A review on ionic liquids as sustainable lubricants in manufacturing and engineering: Recent research, performance, and applications. *Journal of Cleaner Production* **2017**, *168*, 1571-1589.
26. Brandt, A.; Gräsvik, J.; Hallett, J. P.; Welton, T., Deconstruction of lignocellulosic biomass with ionic liquids. *Green Chemistry* **2013**, *15* (3).
27. Hayes, R.; Warr, G. G.; Atkin, R., Structure and nanostructure in ionic liquids. *Chem Rev* **2015**, *115* (13), 6357-426.
28. Blanchard, L. A.; Hancu, D.; Beckman, E. J.; Brennecke, J. F., Green processing using ionic liquids and CO₂. *Nature* **1999**, *399* (6731), 28-29.
29. Wang, L.-y.; Xu, Y.-l.; Li, Z.-d.; Wei, Y.-n.; Wei, J.-p., CO₂/CH₄ and H₂S/CO₂ Selectivity by Ionic Liquids in Natural Gas Sweetening. *Energy & Fuels* **2018**, *32* (1), 10-23.
30. Kim, H.; Lee, K. S., Energy analysis of an absorption-based CO₂ capture process. *International Journal of Greenhouse Gas Control* **2017**, *56*, 250-260.
31. Liu, X.; Huang, Y.; Zhao, Y.; Gani, R.; Zhang, X.; Zhang, S., Ionic Liquid Design and Process Simulation for Decarbonization of Shale Gas. *Industrial & Engineering Chemistry Research* **2016**, *55* (20), 5931-5944.
32. Gimeno, M. P.; Mayoral, M. C.; Andrés, J. M., Influence of Temperature on CO₂ Absorption Rate and Capacity in Ionic Liquids. *Energy & Fuels* **2013**, *27* (7), 3928-3935.
33. Shannon, M. S.; Bara, J. E., Reactive and Reversible Ionic Liquids for CO₂ Capture and Acid Gas Removal. *Separation Science and Technology* **2012**, *47* (2), 178-188.
34. Albo, J.; Santos, E.; Neves, L. A.; Simeonov, S. P.; Afonso, C. A. M.; Crespo, J. G.; Irabien, A., Separation performance of CO₂ through Supported Magnetic Ionic Liquid Membranes (SMILMs). *Separation and Purification Technology* **2012**, *97*, 26-33.
35. Moganty, S. S.; Baltus, R. E., Diffusivity of Carbon Dioxide in Room-Temperature Ionic Liquids. *Industrial & Engineering Chemistry Research* **2010**, *49* (19), 9370-9376.
36. Bara, J. E.; Camper, D. E.; Gin, D. L.; Noble, R. D., Room-Temperature Ionic Liquids and Composite Materials: Platform Technologies for CO₂ Capture. *Accounts of Chemical Research* **2010**, *43* (1), 152-159.
37. Bara, J. E.; Carlisle, T. K.; Gabriel, C. J.; Camper, D.; Finotello, A.; Gin, D. L.; Noble, R. D., Guide to CO₂ Separations in Imidazolium-Based Room-Temperature Ionic Liquids. *Industrial & Engineering Chemistry Research* **2009**, *48* (6), 2739-2751.

38. Scovazzo, P.; Havard, D.; McShea, M.; Mixon, S.; Morgan, D., Long-term, continuous mixed-gas dry fed CO₂/CH₄ and CO₂/N₂ separation performance and selectivities for room temperature ionic liquid membranes. *Journal of Membrane Science* **2009**, *327* (1), 41-48.
39. Muldoon, M. J.; Aki, S. N. V. K.; Anderson, J. L.; Dixon, J. K.; Brennecke, J. F., Improving Carbon Dioxide Solubility in Ionic Liquids. *The Journal of Physical Chemistry B* **2007**, *111* (30), 9001-9009.
40. Hou, Y.; Baltus, R. E., Experimental Measurement of the Solubility and Diffusivity of CO₂ in Room-Temperature Ionic Liquids Using a Transient Thin-Liquid-Film Method. *Industrial & Engineering Chemistry Research* **2007**, *46* (24), 8166-8175.
41. Almantariotis, D.; Gefflaut, T.; Pádua, A. A. H.; Coxam, J. Y.; Costa Gomes, M. F., Effect of Fluorination and Size of the Alkyl Side-Chain on the Solubility of Carbon Dioxide in 1-Alkyl-3-methylimidazolium Bis(trifluoromethylsulfonyl)amide Ionic Liquids. *The Journal of Physical Chemistry B* **2010**, *114* (10), 3608-3617.
42. Almantariotis, D.; Pensado, A. S.; Gunaratne, H. Q.; Hardacre, C.; Padua, A. A.; Coxam, J. Y.; Costa Gomes, M. F., Influence of Fluorination on the Solubilities of Carbon Dioxide, Ethane, and Nitrogen in 1-n-Fluoro-alkyl-3-methylimidazolium Bis(n-fluoroalkylsulfonyl)amide Ionic Liquids. *J Phys Chem B* **2017**, *121* (2), 426-436.
43. Lv, B.; Guo, B.; Zhou, Z.; Jing, G., Mechanisms of CO₂ Capture into Monoethanolamine Solution with Different CO₂ Loading during the Absorption/Desorption Processes. *Environ Sci Technol* **2015**, *49* (17), 10728-35.
44. Ramdin, M.; de Loos, T. W.; Vlugt, T. J. H., State-of-the-Art of CO₂ Capture with Ionic Liquids. *Industrial & Engineering Chemistry Research* **2012**, *51* (24), 8149-8177.
45. Bishnoi, S.; Rochelle, G. T., Absorption of carbon dioxide in aqueous piperazine/methyldiethanolamine. *AIChE Journal* **2002**, *48* (12), 2788-2799.
46. Hayashi, S.; Hamaguchi, H.-o., Discovery of a Magnetic Ionic Liquid [bmim]FeCl₄. *Chemistry Letters* **2004**, *33* (12), 1590-1591.
47. Sitze, M. S.; Schreiter, E. R.; Patterson, E. V.; Freeman, R. G., Ionic Liquids Based on FeCl₃ and FeCl₂. Raman Scattering and ab Initio Calculations. *Inorganic Chemistry* **2001**, *40* (10), 2298-2304.
48. Yoshida, Y.; Otsuka, A.; Saito, G.; Natsume, S.; Nishibori, E.; Takata, M.; Sakata, M.; Takahashi, M.; Yoko, T., Conducting and Magnetic Properties of 1-Ethyl-3-methylimidazolium (EMI) Salts Containing Paramagnetic Irons: Liquids [EMI][M^{III}Cl₄] (M = Fe and Fe_{0.5}Ga_{0.5}) and Solid [EMI]₂[Fe^{II}Cl₄]. *Bulletin of the Chemical Society of Japan* **2005**, *78* (11), 1921-1928.

49. Del Sesto, R. E.; McCleskey, T. M.; Burrell, A. K.; Baker, G. A.; Thompson, J. D.; Scott, B. L.; Wilkes, J. S.; Williams, P., Structure and magnetic behavior of transition metal based ionic liquids. *Chemical Communications* **2008**, (4), 447-449.
50. Mallick, B.; Balke, B.; Felser, C.; Mudring, A. V., Dysprosium room-temperature ionic liquids with strong luminescence and response to magnetic fields. *Angew Chem Int Ed Engl* **2008**, 47 (40), 7635-8.
51. Kogelnig, D.; Stojanovic, A.; v.d. Kammer, F.; Terzieff, P.; Galanski, M.; Jirsa, F.; Krachler, R.; Hofmann, T.; Keppler, B. K., Tetrachloroferrate containing ionic liquids: Magnetic- and aggregation behavior. *Inorganic Chemistry Communications* **2010**, 13 (12), 1485-1488.
52. Peppel, T.; Kockerling, M.; Geppert-Rybczynska, M.; Ralys, R. V.; Lehmann, J. K.; Verevkin, S. P.; Heintz, A., Low-viscosity paramagnetic ionic liquids with doubly charged [Co(NCS)₄]²⁻ ions. *Angew Chem Int Ed Engl* **2010**, 49 (39), 7116-9.
53. Funasako, Y.; Mochida, T.; Inagaki, T.; Sakurai, T.; Ohta, H.; Furukawa, K.; Nakamura, T., Magnetic memory based on magnetic alignment of a paramagnetic ionic liquid near room temperature. *Chem Commun (Camb)* **2011**, 47 (15), 4475-7.
54. Nie, L.-r.; Yao, S.; Dong, B.; Li, X.-l.; Song, H., Synthesis, characterization and physical properties of novel cholinium-based organic magnetic ionic liquids. *Journal of Molecular Liquids* **2017**, 240, 152-161.
55. Yoshida, Y.; Tanaka, H.; Saito, G., Organic Paramagnetic Ionic Liquids Based on Anion Containing 2,2,6,6-Tetramethyl-1-piperidinyloxy Radical Moiety. *Chemistry Letters* **2007**, 36 (9), 1096-1097.
56. Olivier-Bourbigou, H.; Magna, L.; Morvan, D., Ionic liquids and catalysis: Recent progress from knowledge to applications. *Applied Catalysis A: General* **2010**, 373 (1-2), 1-56.
57. Clark, K. D.; Nacham, O.; Yu, H.; Li, T.; Yamsek, M. M.; Ronning, D. R.; Anderson, J. L., Extraction of DNA by magnetic ionic liquids: tunable solvents for rapid and selective DNA analysis. *Anal Chem* **2015**, 87 (3), 1552-9.
58. Santra, K.; Clark, K. D.; Maity, N.; Petrich, J. W.; Anderson, J. L., Exploiting Fluorescence Spectroscopy To Identify Magnetic Ionic Liquids Suitable for the Isolation of Oligonucleotides. *J Phys Chem B* **2018**, 122 (31), 7747-7756.
59. Clark, K. D.; Yamsek, M. M.; Nacham, O.; Anderson, J. L., Magnetic ionic liquids as PCR-compatible solvents for DNA extraction from biological samples. *Chem Commun (Camb)* **2015**, 51 (94), 16771-3.
60. Panja, S. K.; Saha, S., Recyclable, magnetic ionic liquid bmim[FeCl₄]-catalyzed, multicomponent, solvent-free, green synthesis of quinazolines. *RSC Advances* **2013**, 3 (34).

61. Bwambok, D. K.; Thuo, M. M.; Atkinson, M. B. J.; Mirica, K. A.; Shapiro, N. D.; Whitesides, G. M., Paramagnetic Ionic Liquids for Measurements of Density Using Magnetic Levitation. *Analytical Chemistry* **2013**, *85* (17), 8442-8447.
62. Kim, J.-Y.; Kim, J.-T.; Song, E.-A.; Min, Y.-K.; Hamaguchi, H.-o., Polypyrrole Nanostructures Self-Assembled in Magnetic Ionic Liquid as a Template. *Macromolecules* **2008**, *41* (8), 2886-2889.
63. Muraoka, J.; Kamiya, N.; Ito, Y., Preparation and evaluation of cellulose-dissolving magnetic ionic liquid. *Journal of Molecular Liquids* **2013**, *182*, 76-78.
64. Rabinow, J., The Magnetic Fluid Clutch. *Transactions of the American Institute of Electrical Engineers* **1948**, *67* (2), 1308-1315.
65. Evans, D. F., The determination of the paramagnetic susceptibility of substances in solution by nuclear magnetic resonance. *Journal of the Chemical Society (Resumed)* **1959**.
66. Loliger, J.; Scheffold, R., Paramagnetic moment measurements by nmr. A micro technique. *Journal of Chemical Education* **1972**, *49* (9).
67. Schubert, E. M., Utilizing the Evans method with a superconducting NMR spectrometer in the undergraduate laboratory. *Journal of Chemical Education* **1992**, *69* (1).
68. Deutsch, J. L.; Poling, S. M., The determination of paramagnetic susceptibility by NMR: A physical chemistry experiment. *Journal of Chemical Education* **1969**, *46* (3).
69. Yoshida, Y.; Saito, G., Influence of structural variations in 1-alkyl-3-methylimidazolium cation and tetrahalogenoferrate(iii) anion on the physical properties of the paramagnetic ionic liquids. *Journal of Materials Chemistry* **2006**, *16* (13), 1254-1262.
70. Hayashi, S.; Saha, S.; Hamaguchi, H., A new class of magnetic fluids: bmim[FeCl₄] and nbmim[FeCl₄] ionic liquids. *IEEE Transactions on Magnetics* **2006**, *42* (1), 12-14.